M 2023

U.PORTO
FEUP FACULDADE DE ENGENHARIA
UNIVERSIDADE DO PORTO

PARTITIONING OF PHARMACEUTICAL POLLUTANTS USING AQUEOUS TWO-PHASE SYSTEMS BASED ON CHOLINE

LEONOR CARDIELOS DOS REIS BARROCA
MASTER'S THESIS IN CHEMICAL ENGINEERING
PRESENTED TO THE FACULTY OF ENGINEERING
OF THE UNIVERSITY OF PORTO

Master of Science in Chemical Engineering

Partitioning of pharmaceutical pollutants using Aqueous Two-Phase Systems based on choline

Master's Dissertation of

Leonor Cardielos dos Reis Barroca

Developed within the course of Dissertation (M.EQ013) and held at

Supervisor:

Prof. Maria Eugénia Macedo

July 2023

Acknowledgements

There are many people who, in one way or another, have marked my journey.

My first thanks goes to my supervisor, Professor Maria Eugénia Macedo, for believing in me and having accepted me in the Thermodynamics Group of LSRE-LCM. I also thank all the wisdom transmitted, the given advice, and for having encouraged me during these months of work. I would also like to thank Pedro Velho, for the invaluable guidance and support, for helping me to laugh at my mistakes, while encouraging me to go further in this work! To Cati, companion of this adventure in Thermodynamics, thank you so much for all the support and company in the lab. All the experience and knowledge, as well as the laughs and coffee breaks shared by the Thermo Group were crucial for my work, and for that I am grateful.

I am also thankful for the help of Professor Natália Cordeiro, from the Faculty of Sciences of the University of Porto. Thank you for being so available to discuss DFT calculations.

To all Professors who have shaped helped me get here, to those who made me learn to love science and to those who have contributed directly or indirectly to this work: thank you.

On a more personal note, I am very grateful for my friends: Ana, Ana, Bia, Inês, Laura, Mariana, thank you for always being available to chat and have a coffee. You have helped me when I needed it the most, always with good advice, and I am truly thankful for that.

Last but not least, an especial thanks to my family. I am eternally grateful for your love and support. Without you and your encouragement, this would not have been possible. To my father and sister, thank you for believing in me and putting up with me, especially during these hectic months!

I would not be who I am today without my Parents and Grandparents, my greatest examples of resilience and strength, who showed me that everything could be achieved.

I also thank financial support from a scientific grant under the project 2SMART (NORTE-01-0145-FEDER-000054), supported by Norte Portugal Regional Operational Programme (NORTE 2020), under the PORTUGAL 2020 Partnership Agreement, through the European Regional Development Fund (ERDF).

Abstract

The intensive use and disposal of pharmaceuticals and their packaging have led to the detection of active pharmaceutical ingredients (APIs) in soil and in water bodies. Therefore, it is vital to develop effective and sustainable methodologies to remove pharmaceutical pollutants from water.

Aqueous Two-Phase Systems (ATPS) are biocompatible extractive media with applicability at industrial scale which present a low environmental impact. In this work, ATPS containing salts or ionic liquids based on choline, as well as green solvents (ethyl lactate (EL) or Choline Amino Acid Ionic Liquids (CAAILs)) were studied, so as to assess their potential to remove three APIs commonly found in water: acetaminophen (Ac), amoxicillin (Amox) and salicylic acid (SA).

The CAAILs cholinium L-alaninate ([Ch][Ala]), cholinium glycinate ([Ch][Gly]), cholinium leucinate ([Ch][Leu]) and cholinium L-serinate ([Ch][Ser]) were successfully synthesised and used in ATPS. The syntheses were confirmed by infrared spectroscopy (comparing experimental spectra with predictions from Density Functional Theory) and by density measurements.

Following a thorough study of the stability of the APIs, a total of 15 partitions in 7 different ATPS were carried out at 298.15 K and 0.1 MPa, including an ATPS determined in this work, {EL (1) + choline bitartrate (2) + water (3)}. Low solute losses ($< 5\ \%$) were obtained in all cases. In systems containing CAAILs, salicylic acid (SA) could not be extracted, due to a chemical reaction that produced cholinium salicylate. For acetaminophen (Ac) and amoxicillin (Amox), systems {[Ch][Ala] or [Ch][Gly] (1) + K_2HPO_4 (2) + water (3)} and {[Ch][Leu] (1) + K_3PO_4 (2) + water (3)} were identified as the most promising to remove these components from polluted water streams. Partitions with the novel ATPS showed the best results for SA: the highest partition coefficients (K) and extraction efficiencies (E) were obtained for the longest tie-line, which had a length of 115.1 % ($K = 9 \pm 2$ and $E \geq 95\ \%$).

Additionally, this work sought testing novel methodologies with the objective of enhancing the predictability of the thermodynamic modelling parameters, whilst keeping their physical meaning. An innovative methodology to calculate the non-randomness factor (α), a parameter closely related to the lattice coordination number (Z), was developed. For this, after optimising the cartesian coordinates of the molecules using DFT, the non-randomness factors were calculated based on a novel geometric approach based on the dipole moment and the polarity of the species.

This new methodology was validated using UNIQUAC, a widely used thermodynamic model, for 6 ternary systems. For systems containing electrolytes, an additional term (Pitzer-Debye-Hückel, PDH) was considered to account for long-range interactions. The novel ATPS was modelled using PDH+UNIQUAC in its classical version and adapted version (with Z as a function of α). This innovative approach allowed to obtain very satisfactory results as well as to maintain the physical meaning of Z.

Nonetheless, seeing that the calculated non-randomness factor is closely related to the species' polarity, it was used to predict and compare the relative position of solubility curves, leaving the door open to other applications of this pioneering methodology.

Keywords: Pharmaceutical pollutants; ATPS; PDH+UNIQUAC; Non-randomness factor; Density Functional Theory.

Resumo

A utilização e eliminação intensivas de fármacos e das suas embalagens levaram à deteção de ingredientes farmacêuticos ativos (API) no solo e em massas de água. Logo, é crucial desenvolver metodologias eficazes e sustentáveis para remover os poluentes farmacêuticos da água.

Os Sistemas Bifásicos Aquosos (SBA) são meios extrativos biocompatíveis com aplicabilidade à escala industrial e que apresentam um baixo impacto ambiental. Neste trabalho, foram estudados SBAs contendo sais ou líquidos iónicos à base de colina, bem como solventes verdes (lactato de etilo (EL) ou líquidos iónicos de colina e aminoácidos (CAAILs)), de modo a avaliar o seu potencial para remover três APIs geralmente encontrados em água: acetaminofeno (Ac), amoxicilina (Amox) e ácido salicílico (SA).

Os CAAILs alaninato de colina ([Ch][Ala]), glicinato de colina ([Ch][Gly]), leucinato de colina ([Ch][Leu]) e serinato de colina ([Ch][Ser]) foram sintetizados com sucesso e aplicados em extrações líquido-líquido. As sínteses foram confirmadas por espetroscopia de infravermelho (comparando espetros experimentais com previsões pela Teoria do Funcional da Densidade (DFT)) e por medições de densidade.

Após um estudo aprofundado da estabilidade dos APIs, foram efetuadas 15 extrações (partições) em 7 SBA diferentes a 298,15 K e 0,1 MPa, incluindo num SBA determinado neste trabalho, {EL (1) + bitartarato de colina (2) + água (3)}. Foram obtidas baixas perdas de soluto ($< 5\ \%$) em todos os casos. Nos sistemas que contêm CAAILs, não foi possível extrair o ácido salicílico (SA), devido a uma reação química em que se produzia salicilato de colina. Relativamente à amoxicilina (Amox) e ao acetaminofeno (Ac), os sistemas {[Ch][Ala] ou [Ch][Gly] (1) + K_2HPO_4 (2) + água (3)} e {[Ch][Leu] (1) + K_3PO_4 (2) + água (3)} foram identificados como os mais promissores para remover estes componentes de correntes de água poluídas. As partições com o novo SBA apresentaram os melhores resultados para o SA: os coeficientes de partição (K) e as eficiências de extração (E) mais elevados foram obtidos para a linha de equilíbrio mais longa, com comprimento de 115,1 % ($K = 9 \pm 2$ e $E \geq 95\ \%$).

Adicionalmente, este trabalho procurou testar novas metodologias para melhorar a capacidade de previsão dos parâmetros de modelação termodinâmica, conservando o seu significado físico. Foi desenvolvida uma forma inovadora de calcular o fator de não-aleatoriedade (α), um parâmetro intimamente relacionado com o número de coordenação (Z). Para tal, após a otimização das coordenadas cartesianas das moléculas utilizando DFT, os fatores de não-aleatoriedade foram calculados com base numa abordagem geométrica, na qual este fator se considerou relacionado com o momento de dipolo e a polaridade das espécies.

Esta nova metodologia foi validada utilizando a equação UNIQUAC, um modelo termodinâmico amplamente utilizado, para 6 sistemas ternários. Para os sistemas que continham eletrólitos, foi considerado um termo adicional (Pitzer-Debye-Hückel, PDH) de modo a ter em conta as interações de longo alcance. O novo SBA foi modelado utilizando PDH+UNIQUAC na sua versão clássica e na sua versão adaptada (com Z em função de α). Esta abordagem inovadora permitiu obter resultados bastante satisfatórios, preservando o significado físico de Z.

Por outro lado, uma vez que o fator de não-aleatoriedade calculado estava correlacionado com a polaridade das espécies, foi utilizado para prever e comparar a posição relativa de curvas de solubilidade, deixando em aberto outras aplicações deste método pioneiro.

Palavras-chave: Poluentes farmacêuticos; SBA; PDH+UNIQUAC; Fator de não-aleatoriedade; Teoria do Funcional da Densidade.

Declaration

I hereby declare, under word of honour, that this work is original and that all non-original contributions were properly referenced with source identification.

Leonor Cardielos dos Reis Barroca

3rd July 2023

Index

1 Introduction 1

1.1 Problem statement 1

1.2 Presentation of LSRE-LCM and ALiCE 2

1.3 Author's contribution 2

1.4 Document's structure 2

2 State of the art 3

2.1 Pharmaceutical pollutants in water 3

2.2 Ionic liquids 4

2.2.1 Choline Amino Acid Ionic Liquids (CAAILs) 6

2.3 Aqueous Two-Phase Systems (ATPS) 7

2.4 Thermodynamic modelling 8

2.4.1 UNIQUAC 10

2.4.2 PDH equation 11

2.5 Density Functional Theory (DFT) 13

3 Materials and methods 15

3.1 Chemicals 15

3.2 Computational tools 16

3.3 Experimental methodology 17

3.3.1 Ionic liquid synthesis 17

3.3.2 Theoretical infrared spectra determination 18

3.3.3 LLE determination 19

3.3.4 Partition of pharmaceuticals in ATPS 21

3.4 Thermodynamic modelling 23

3.4.1 A novel approach for the lattice coordination number 24

3.4.2 Application of PDH+UNIQUAC 25

4 Liquid-liquid equilibria 27

4.1 Liquid-Liquid Equilibria (LLE) of ternary systems 27

4.2 Thermodynamic modelling 30

4.2.1 Validation 30

4.2.2 Application to the novel ATPS 31
4.2.3 Additional applications 32
5 Partitions of pharmaceuticals in ATPS 33
5.1 Ionic liquid synthesis 33
5.2 Effect of pH in the mean electrical charge 34
5.3 Effect of pH in the absorbance spectra 35
5.4 Ultraviolet–Visible (UV-Vis) absorbance calibration curves 35
5.5 Partition coefficients and extraction efficiencies 36
6 Conclusions 41
7 Project assessment 43
7.1 Degree of completion 43
7.2 Future work 43
7.3 Final assessment 44
8 References 45
Annexes and Appendices 51
Annex A - Chemicals 53
A.1 Two-dimensional structures 53
A.2 Molar masses and solubilities 55
Annex B - Data used for the modelling approach validation 57
B.1 Ternary systems used for the modelling approach validation 57
B.2 How to define new solvents for PCM in Gaussian 59
B.3 Physical properties of pure species 60
Annex C - Liquid-liquid equilibria (LLE) data of used systems 63
Appendix A - Liquid-liquid equilibria (LLE) data of new systems 65
A.1 Experimental 65
A.2 Binodal data 65
A.3 LLE fitting 67
A.4 {EL (1) + [Ch]Bit (2) + water (3)} 68
A.4.1 Isolines 68
A.4.2 Critical point 70
Appendix B - Thermodynamic modelling 73
B.1 Calculated van der Waals volumes and surface areas 73

B.2 Calculated non-randomness factors 73
B.3 Validation of the novel approach for the non-randomness factor 74
B.4 Modelling with PDH-UNIQUAC 76
Appendix C - Ionic Liquid synthesis 77
C.1 Experimental apparatus 77
C.2 FTIR spectra 78
C.3 Density measurements 81
Appendix D - Ultraviolet-visible (UV-Vis) absorbance spectra of pure compounds 85
Appendix E - Variation of mean charge with pH 87
E.1 Acetaminophen 87
E.2 Amoxicillin 88
E.3 Salicylic acid 90
Appendix F - Stability of Ultraviolet-Visible (UV-Vis) absorbance spectra 93
F.1 Acetaminophen 93
F.2 Amoxicillin 96
F.3 Salicylic acid 98
Appendix G - Calibration curves 101
G.1 Acetaminophen 101
G.2 Amoxicillin 102
G.3 Salicylic acid 103
Appendix H - Partition coefficients and extraction efficiencies 105
H.1 {[Ch][Ala] (1) + K_2HPO_4 (2) + water (3)} 105
H.2 {[Ch][Ala] (1) + K_3PO_4 (2) + water (3)} 107
H.3 {[Ch][Gly] (1) + K_2HPO_4 (2) + water (3)} 109
H.4 {[Ch][Ser] (1) + K_2HPO_4 (2) + water (3)} 111
H.5 {[Ch][Leu] (1) + K_3PO_4 (2) + water (3)} 113
H.6 {PEG600 (1) + [Ch]Bic (2) + water (3)} 115
H.7 {EL (1) + [Ch]Bit (2) + water (3)} 117

List of Figures

Fig. 2.1. Solubility curve and tie-lines for the system {PEG6000 (1) + sodium citrate (2) + water (3)}, at 298.15 K and 0.1 MPa (represented with data from literature). 8

Fig. 3.1. Reaction route for the synthesis of cholinium alaninate ([Ch][Ala]). 18

Fig. 3.2. Flowchart of the procedure for partition studies in ATPS. 21

Fig. 3.3. Validation algorithm of the novel non-randomness calculation method. 26

Fig. 3.4. Algorithm for the application of the new non-randomness calculation method in thermodynamic modelling. 26

Fig. 4.1. Solubility curves determined in this work at 298.15 K and 0.1 MPa. 27

Fig. 4.2. Comparison between solubility curves of ternary systems composed of PEG with different molar masses and choline bitartrate, at 298.15 K and 0.1 MPa. 28

Fig. 4.3. Comparison between solubility curves of ternary systems composed of {PEG4000 (1) + choline salts or ILs (2) + water (3)} at 298.15 K and 0.1 MPa 28

Fig. 4.4. Solubility curve and tie-lines of the novel system {EL (1) + [Ch]Bit (2) + water (3)}, at 298.15 K and 0.1 MPa. 29

Fig. 4.5. Tie-lines for the ternary system {ethyl lactate (1) + [Ch]Bit (2) + water (3)} at 298.15 K and 0.1 MPa: traditional PDH+UNIQUAC modelling and novel PDH+UNIQUAC modelling. 31

Fig. 5.1. [Ch][Ala] density measurements as a function of temperature and comparison with literature data 33

Fig. 5.2. Experimental Fourier Transform Infrared Spectra (FTIR) for cholinium L-alaninate ([Ch][Ala]) and predicted infrared absorption spectra. 33

Fig. 5.3. Calculated mean electrical charge for acetaminophen, amoxicillin, and salicylic acid, expressed in terms of the elementary charge 34

Fig. 5.4. UV–vis absorbance spectra at pH = 3, from 200 to 600 nm, for acetaminophen, amoxicillin and salicylic acid. 35

Fig. 5.5. UV–vis absorbance spectra at pH = 12, from 200 to 600 nm, for acetaminophen, amoxicillin and salicylic acid 35

Fig. 5.6. UV-Vis absorbance calibration curves at pH 3 for acetaminophen, amoxicillin and salicylic acid. 36

Fig. 5.7. UV-Vis absorbance calibration curves at pH 12 for acetaminophen, amoxicillin and salicylic acid 36

Fig. 5.8. Relation of the tie-line length with the natural logarithm of the partition coefficients for acetaminophen, in the studied ATPS, at 298.15 K and 0.1 MPa. 37

Fig. 5.9. Relation of the tie-line length with the extraction efficiencies for acetaminophen, in the studied ATPS, at 298.15 K and 0.1 MPa. 37

Fig. 5.10. Relation of the tie-line length with the natural logarithm of the partition coefficients for amoxicillin, in the studied ATPS, at 298.15 K and 0.1 MPa. 38

Fig. 5.11. Relation of the tie-line length with the extraction efficiencies for amoxicillin, in the studied ATPS, at 298.15 K and 0.1 MPa. 38

Fig. 5.12. Relation of the tie-line length with the natural logarithm of the experimental partition coefficients for acetaminophen, amoxicillin and salicylic acid, in the system {EL (1) + [Ch]Bit (2) + water (3)} at 298.15 K and 0.1 MPa. 39

Fig. 5.13. Relation of the tie-line length with the extraction efficiencies for acetaminophen, amoxicillin and salicylic acid, in the system {EL (1) + [Ch]Bit (2) + water (3)} at 298.15 K and 0.1 MPa. 39

Fig. 5.14. Influence of the tie-line compositions in the relative abundance of the stages of the studied pharmaceuticals, in the ATPS {EL (1) + [Ch]Bit (2) + water (3)} at 298.15 K and 0.1 MPa. 40

Fig. A1.1. Example of a cloud point. 65

Fig. A1.2. Example of a clear mixture, not in cloud point 65

Fig. A4.1. Three-dimensional ternary plot of the density (ρ) as a function of the mass fraction of ethyl lactate (EL) and choline bitartrate ([Ch]Bit). 68

Fig. A4.2. Three-dimensional ternary plot of the electrical conductivity (μ) as a function of the mass fraction of ethyl lactate (EL) and choline bitartrate ([Ch]Bit). 69

Fig. A4.3. Phase diagram of the system {EL (1) + [Ch]Bit (2) + water (3)} used for the critical point determination. 70

Fig. C1.1. Experimental setup of the ionic liquid synthesis. 77

Fig. C1.2. Drying of the ionic liquid by reduced-pression distillation, at 323.15 K, in a rotary evaporator. 77

Fig. C1.3. Drying of the ionic liquid by reduced-pression filtration. 77

Fig. C1.4. Aspect of the ionic liquid [Ch][Ala] (cholinium alaninate) after purification. 78

Fig. C2.1. Experimental and predicted infrared spectra of cholinium glycinate ([Ch][Gly]). 78

Fig. C2.2. Experimental and predicted infrared spectra of cholinium leucinate ([Ch][Leu]). 78

Fig. C2.3. Experimental and predicted infrared spectra of cholinium serinate ([Ch][Ser]). 79

Fig. C3.1. Measured and literature density of cholinium glycinate ([Ch][Gly]) 81

Fig. C3.2. Measured and literature density of cholinium leucinate ([Ch][Leu]). 82

Fig. C3.3. Measured and literature density of cholinium serinate ([Ch][Ser]) 82

Fig. D.1. UV-Vis absorbance spectra of the four Choline Amino Acid Ionic Liquids (CAAILs) used: cholinium alaninate ([Ch][Ala]), cholinium glycinate ([Ch][Gly]), cholinium leucinate ([Ch][Leu]) and cholinium serinate ([Ch][Ser]). 85

Fig. D.2. UV-Vis absorbance spectra of aqueous solutions of the choline salts used: choline bicarbonate ([Ch]Bic) and choline bitartrate ([Ch]Bit). 85

Fig. D.3. UV-Vis absorbance spectra of aqueous solutions of the other salts used: K_2HPO_4 and K_3PO_4 ... 86

Fig. D.4. UV-Vis absorbance spectra of pure polyethylene glycol 600 (PEG600) and aqueous solutions of polyethylene glycol 4000 (PEG4000). 86

Fig. D.5. UV-Vis absorbance spectra of pure solvents: water and ethyl lactate. 86

Fig. F1.1. Influence of pH on the UV-Vis absorbance spectra of an aqueous solution of acetaminophen at 298.15 K and 0.1 MPa. 93

Fig. F1.2. UV-Vis absorbance spectra of an aqueous solution of acetaminophen (pH = 3) in the moment of preparation and after 72 h of settling, at 298.15 K and 0.1 MPa. 93

Fig. F1.3. UV-Vis absorbance spectra of an aqueous solution of acetaminophen (pH = 6) in the moment of preparation and after 72 h of settling, at 298.15 K and 0.1 MPa. 94

Fig. F1.4. UV-Vis absorbance spectra of an aqueous solution of acetaminophen (pH = 7) in the moment of preparation and after 72 h of settling, at 298.15 K and 0.1 MPa. 94

Fig. F1.5. UV-Vis absorbance spectra of an aqueous solution of acetaminophen (pH = 9) in the moment of preparation and after 72 h of settling, at 298.15 K and 0.1 MPa. 94

Fig. F1.6. UV-Vis absorbance spectra of an aqueous solution of acetaminophen (pH = 12) in the moment of preparation and after 72 h of settling, at 298.15 K and 0.1 MPa. 95

Fig. F2.1. Influence of pH on the UV-Vis absorbance spectra of an aqueous solution of amoxicillin at 298.15 K and 0.1 MPa. 96

Fig. F2.2. UV-Vis absorbance spectra of an aqueous solution of amoxicillin (pH = 3) in the moment of preparation and after 72 h of settling, at 298.15 K and 0.1 MPa. 96

Fig. F2.3. UV-Vis absorbance spectra of an aqueous solution of amoxicillin (pH = 5) in the moment of preparation and after 72 h of settling, at 298.15 K and 0.1 MPa. 97

Fig. F2.4. UV-Vis absorbance spectra of an aqueous solution of amoxicillin (pH = 7) in the moment of preparation and after 72 h of settling, at 298.15 K and 0.1 MPa. 97

Fig. F2.5. UV-Vis absorbance spectra of an aqueous solution of amoxicillin (pH = 12) in the moment of preparation and after 72 h of settling, at 298.15 K and 0.1 MPa. 98

Fig. F3.1. Influence of pH on the UV-Vis absorbance spectra of an aqueous solution of salicylic acid at 298.15 K and 0.1 MPa. 98

Fig. F3.2. UV-Vis absorbance spectra of an aqueous solution of salicylic acid (pH = 3) in the moment of preparation and after 72 h of settling, at 298.15 K and 0.1 MPa. 99

Fig. F3.3. UV-Vis absorbance spectra of an aqueous solution of salicylic acid (pH = 10) in the moment of preparation and after 72 h of settling, at 298.15 K and 0.1 MPa. 99

Fig. F3.4. UV-Vis absorbance spectra of an aqueous solution of salicylic acid (pH = 12) in the moment of preparation and after 72 h of settling, at 298.15 K and 0.1 MPa. 99

Fig. H1.1. Relation of the tie-line length with the natural logarithm of the experimental partition coefficients for acetaminophen and amoxicillin, in the system {[Ch][Ala] (1) + K_2HPO_4 (2) + water (3)} at 298.15 K and 0.1 MPa. 105

Fig. H1.2. Relation of the tie-line length with the extraction efficiencies for acetaminophen and amoxicillin, in the system {[Ch][Ala] (1) + K_2HPO_4 (2) + water (3)} at 298.15 K and 0.1 MPa. 105

Fig. H1.3. Influence of the tie-line compositions in the relative abundance of the stages of the studied pharmaceuticals, in the ATPS {[Ch][Ala] (1) + K_2HPO_4 (2) + water (3)} at 298.15 K and 0.1 MPa.. 106

Fig. H2.1. Relation of the tie-line length with the natural logarithm of the experimental partition coefficients for acetaminophen, in the system {[Ch][Ala] (1) + K_3PO_4 (2) + water (3)} at 298.15 K and 0.1 MPa. 107

Fig. H2.2. Relation of the tie-line length with the extraction efficiencies for acetaminophen, in the system {[Ch][Ala] (1) + K_3PO_4 (2) + water (3)} at 298.15 K and 0.1 MPa. 108

Fig. H2.3. Influence of the tie-line compositions in the relative abundance of the stages of the studied pharmaceuticals, in the ATPS {[Ch][Ala] (1) + K_3PO_4 (2) + water (3)} at 298.15 K and 0.1 MPa 108

Fig. H3.1. Relation of the tie-line length with the natural logarithm of the experimental partition coefficients for acetaminophen and amoxicillin, in the system {[Ch][Gly] (1) + K_2HPO_4 (2) + water (3)} at 298.15 K and 0.1 MPa. 109

Fig. H3.2. Relation of the tie-line length with the extraction efficiencies for acetaminophen and amoxicillin, in the system {[Ch][Gly] (1) + K_2HPO_4 (2) + water (3)} at 298.15 K and 0.1 MPa. 109

Fig. H3.3. Influence of the tie-line compositions in the relative abundance of the stages of the studied pharmaceuticals, in the ATPS {[Ch][Gly] (1) + K_2HPO_4 (2) + water (3)} at 298.15 K and 0.1 MPa 110

Fig. H4.1. Blank (left) and partition of salicylic acid (right) in the system {[Ch][Ser] (1) + K_2HPO_4 (2) + water (3)}, where a difference in colour of the top phases can be observed. 111

Fig. H4.2. Relation of the tie-line length with the natural logarithm of the experimental partition coefficients for acetaminophen, in the system {[Ch][Ser] (1) + K_2HPO_4 (2) + water (3)} at 298.15 K and 0.1 MPa. 111

Fig. H4.3. Relation of the tie-line length with the extraction efficiencies for acetaminophen, in the system {[Ch][Ser] (1) + K_2HPO_4 (2) + water (3)} at 298.15 K and 0.1 MPa. 112

Fig. H5.1. Relation of the tie-line length with the natural logarithm of the experimental partition coefficients for acetaminophen and amoxicillin, in the system {[Ch][Leu] (1) + K_3PO_4 (2) + water (3)} at 298.15 K and 0.1 MPa. 113

Fig. H5.2. Relation of the tie-line length with the extraction efficiencies for acetaminophen and amoxicillin, in the system {[Ch][Leu] (1) + K_3PO_4 (2) + water (3)} at 298.15 K and 0.1 MPa. 113

Fig. H5.3. Influence of the tie-line compositions in the relative abundance of the stages of the studied pharmaceuticals, in the ATPS {[Ch][Leu] (1) + K_3PO_4 (2) + water (3)} at 298.15 K and 0.1 MPa..... 114

Fig. H6.1. Relation of the tie-line length with the natural logarithm of the experimental partition coefficientsfor acetaminophen and amoxicillin, in the system {PEG600 (1) + [Ch]Bic (2) + water (3)} at 298.15 K and 0.1 MPa. 115

Fig. H6.2. Relation of the tie-line length with the extraction efficiencies for acetaminophen and amoxicillin, in the system {PEG600 (1) + [Ch]Bic (2) + water (3)} at 298.15 K and 0.1 MPa. 116

Fig. H6.3. Influence of the tie-line compositions in the relative abundance of the stages of the studied pharmaceuticals, in the ATPS {PEG600 (1) + [Ch]Bic (2) + water (3)} at 298.15 K and 0.1 MPa..... 116

List of Tables

Table 3.1. List of chemicals used, with chemical formula, suppliers, purities, CAS numbers and abbreviations. **15**

Table 4.1. Ternary systems studied in this work, at 298.15 K and 0.1 MPa. **27**

Table 4.2. Polynomial expressions (isolines) for density and electric conductivity as a function of the composition for the ternary system {EL (1) + [Ch]Bit (2) + water (3)} at 298.15 K and 0.1 MPa..... ..... **29**

Table 4.3. Phase equilibrium compositions (mass fractions), tie-line lengths and slopes for the system {EL (1) + [Ch]Bit (2) + water (3)} at 298.15 K and 0.1 MPa..... **29**

Table 4.4. Parameters obtained using Othmer–Tobias and Bancroft-Hubbard equations for the system {EL (1) + [Ch]Bit (2) + water (3)} at 298.15 K and 0.1 MPa..... **30**

Table 5.1. Stability of the UV-Vis absorbance spectra of acetaminophen, amoxicillin and salicylic acid after settling for 3 days at 298.15 K and 0.1 MPa. **35**

Table 5.2. Liquid-liquid extractions (partitions) performed in this work. **37**

Table AA.1. Two dimensional structures of chemicals used in this work. **53**

Table AA.2. Molar mass of chemicals used in this work **55**

Table AA.3. Solubility of studied pharmaceutical compounds in water, at 298.15 K and 0.1 MPa..... **55**

Table BB1.1. Liquid-liquid equilibria (LLE) data of ternary systems with only neutral species, at 298.15 K and 0.1 MPa, collected from literature. **57**

Table CC.1. Liquid-liquid equilibria (LLE) data, tie-line slope and length for studied ternary systems, at 298.15 K and 0.1 MPa. **63**

Table A2.1. List of tested systems and respective range of compositions. **65**

Table A2.2. Experimental LLE data for studied ternary systems, at 298.15 K and 0.1 MPa. **66**

Table A3.1. Parameters of the Merchuk, Li and Yu correlations, for the new ternary systems, at 298.15 K and 0.1 MPa **67**

Table A4.1. Experimental mass fractions and measured density at 298.15 K. **68**

Table A4.2. Experimental mass fractions and measured electrical conductivity at 298.15 K. **69**

Table A4.3. Results of the *F*-test performed to the density and electrical conductivity isolines. **70**

Table B1.1. van der Waals volumes and surface areas calculated using Bondi's method for pure neutral compounds. **73**

Table B1.2. van der Waals volumes and surface areas calculated using Bondi's method for ions. **73**

Table B2.1. Non-randomness factors calculated for pure neutral compounds **73**

Table B2.2. Non-randomness factors calculated for ions. **73**

Table B3.1. Average value of the non-randomness factor in phases **I** and **II**, and overall in each system, at 298.15 K and 0.1 MPa. **74**

Table B3.2. Optimised interaction energies with UNIQUAC, for the system {methanol (1) + toluene (2) + *n*-decane (3)}, at 298.15 K and 0.1 MPa, and standard deviation from the tie-line data. **74**

Table B3.3. Optimised interaction energies with UNIQUAC, for the system {water (1) + *n*-hexane (2) + methanol (3)}, at 298.15 K and 0.1 MPa, and standard deviation from the tie-line data. **74**

Table B3.4. Optimised interaction energies with UNIQUAC, for the system {butan-1-ol (1) + ethanol (2) + water (3)}, at 298.15 K and 0.1 MPa, and standard deviation from the tie-line data..... **75**

Table B3.5. Optimised interaction energies with UNIQUAC, for the system {water (1) + isopropanol (2) + heptan-1-ol (3)}, at 298.15 K and 0.1 MPa, and standard deviation from the tie-line data..... **75**

Table B3.6. Optimised interaction energies with UNIQUAC, for the system {dibutyl ether (1) + methanol (2) + water (3)}, at 298.15 K and 0.1 MPa, and standard deviation from the tie-line data..... **75**

Table B3.7. Optimised interaction energies with UNIQUAC, for the system {dibutyl ether (1) + propan-1-ol (2) + water (3)}, at 298.15 K and 0.1 MPa, and standard deviation from the tie-line data..... **75**

Table B4.1. Average value of the non-randomness factor in phases **I** and **II**, and overall for the system {ethyl lactate (1) + [Ch]Bit (2) + water (3)}, at 298.15 K and 0.1 MPa. **76**

Table B4.2. Optimised interaction energies with PDH+UNIQUAC, for the system {EL (1) + [Ch]Bit (2) + water (3)}, at 298.15 K and 0.1 MPa, and standard deviation from the tie-line data..... **76**

Table C2.1. Predicted wavenumbers and normalised intensities of absorption for [Ch][Ala]. **79**

Table C2.2. Predicted wavenumbers and normalised intensities of absorption for [Ch][Gly]. **80**

Table C2.3. Predicted wavenumbers and normalised intensities of absorption for [Ch][Leu]. **80**

Table C2.4. Predicted wavenumbers and normalised intensities of absorption for [Ch][Ser]. **81**

Table E1.1. Calculated fractions of each stage and mean charge for acetaminophen at different pH values..... **87**

Table E2.1. Calculated fractions of each stage and mean charge for amoxicillin at different pH values..... **88**

Table E3.1. Calculated fractions of each stage and mean charge for salicylic acid at different pH values..... **90**

Table G1.1. Concentration and UV-Vis absorbances of the solutions prepared for the calibration curves of acetaminophen, at pH = 3 and 12. ..... **101**

Table G1.2. Calculated detection and quantification limits for the calibration curves of acetaminophen..... **101**

Table G2.1. Concentration and UV-Vis absorbances of the solutions prepared for the calibration curves of amoxicillin, at pH = 3 and 12..... **102**

Table G2.2. Calculated detection and quantification limits for the calibration curves of amoxicillin..... **102**

Table G3.1. Concentration and UV-Vis absorbances of the solutions prepared for the calibration curves of salicylic acid, at pH = 3 and 12. **103**

Table G3.2. Calculated detection and quantification limits for the calibration curves of salicylic acid..... **103**

Table H1.1. Experimental mass of each phase, mass losses in the phase separation, solute concentration, phase density and phase pH for the top and bottom phases in the extraction of acetaminophen and amoxicillin in the ATPS {[Ch][Ala] (1) + K_2HPO_4 (2) + water (3)}, at 298.15 K and 0.1 MPa. **106**

Table H1.2. Calculated solute losses, extraction efficiency intervals, partition coefficients and literature values of tie-line lengths for the partition of acetaminophen and amoxicillin in the ATPS {[Ch][Ala] (1) + K_2HPO_4 (2) + water (3)}, at 298.15 K and 0.1 MPa. **107**

Table H2.1. Experimental mass of each phase, mass losses in the phase separation, solute concentration, phase density and phase pH for the top and bottom phases in the extraction of acetaminophen and amoxicillin in the ATPS {[Ch][Ala] (1) + K_3PO_4 (2) + water (3)}, at 298.15 K and 0.1 MPa. **108**

Table H3.2. Calculated solute losses, extraction efficiency intervals, partition coefficients and literature values of tie-line lengths for the partition of acetaminophen and amoxicillin in the ATPS {[Ch][Gly] (1) + K_2HPO_4 (2) + water (3)}, at 298.15 K and 0.1 MPa. **109**

Table H3.1. Experimental mass of each phase, mass losses in the phase separation, solute concentration, phase density and phase pH for the top and bottom phases in the extraction of acetaminophen and amoxicillin in the ATPS {[Ch][Gly] (1) + K_2HPO_4 (2) + water (3)} at 298.15 K and 0.1 MPa. **110**

Table H3.2. Calculated solute losses, extraction efficiency intervals, partition coefficients and literature values of tie-line lengths for the partition of acetaminophen and amoxicillin in the ATPS {[Ch][Gly] (1) + K_2HPO_4 (2) + water (3)}, at 298.15 K and 0.1 MPa. **111**

Table H4.1. Experimental mass of each phase, mass losses in the phase separation, solute concentration, phase density and phase pH for the top and bottom phases in the extraction of acetaminophen in the ATPS {[Ch][Ser] (1) + K_2HPO_4 (2) + water (3)} at 298.15 K and 0.1 MPa. **112**

Table H4.2. Calculated solute losses, extraction efficiency intervals, partition coefficients and literature values of tie-line lengths for the partition of acetaminophen in the ATPS {[Ch][Ser] (1) + K_2HPO_4 (2) + water (3)}, at 298.15 K and 0.1 MPa. **113**

Table H5.1. Experimental mass of each phase, mass losses in the phase separation, solute concentration, phase density and phase pH for the top and bottom phases in the extraction of acetaminophen and amoxicillin in the ATPS {[Ch][Leu] (1) + K_3PO_4 (2) + water (3)} at 298.15 K and 0.1 MPa. **114**

Table H5.2. Calculated solute losses, extraction efficiency intervals, partition coefficients and literature values of tie-line lengths for the partition of acetaminophen and amoxicillin in the ATPS {[Ch][Leu] (1) + K_3PO_4 (2) + water (3)}, at 298.15 K and 0.1 MPa. **115**

Table H6.1. Experimental mass of each phase, mass losses in the phase separation, solute concentration, phase density and phase pH for the top and bottom phases in the extraction of acetaminophen and amoxicillin in the ATPS {PEG600 (1) + [Ch]Bic (2) + water (3)} at 298.15 K and 0.1 MPa. **116**

Table H6.2. Calculated solute losses, extraction efficiency intervals, partition coefficients and literature values of tie-line lengths for the partition of acetaminophen and amoxicillin in the ATPS {PEG600 (1) + [Ch]Bic (2) + water (3)}, at 298.15 K and 0.1 MPa. **117**

Table H7.1. Experimental mass of each phase, mass losses in the phase separation, solute concentration, phase density and phase pH for the top and bottom phases in the extraction of acetaminophen, amoxicillin and salicylic acid in the ATPS {EL (1) + [Ch]Bit (2) + water (3)}, at 298.15 K and 0.1 MPa..... **117**

Table H7.2. Calculated solute losses, extraction efficiency intervals, partition coefficients and values of tie-line lengths for the partition of acetaminophen, amoxicillin and salicylic acid in the ATPS {EL (1) + [Ch]Bit (2) + water (3)}, at 298.15 K and 0.1 MPa..... **118**

Notation and Glossary

$\vec{A}$	Asymmetry	C·m
A	Absorbance	
a	Hard-core collision diameter	m
A_1, B_1, C_1, D_1	Adjustable parameters of correlations	
a, b, c	Components of the asymmetry vector along the x, y and z axes	
$A_{\mathrm{DH},x}$	Debye-Hückel parameter	
$\vec{A}_{\mathrm{max},x}$	Maximum value of the asymmetry along the x axis	C·m
$\vec{A}_{\mathrm{max},y}$	Maximum value of the asymmetry along the y axis	C·m
$\vec{A}_{\mathrm{max},z}$	Maximum value of the asymmetry along the z axis	C·m
A_{w}	van der Waals area	$\mathrm{m}^2 \cdot \mathrm{mol}^{-1}$
C	Concentration	$\mathrm{kg} \cdot \mathrm{m}^{-3}$
$\vec{d}_{ij}$	Distance vector between atoms i and j	m
E	Extraction efficiency	%
e	Elementary charge	C
E_{RMSE}	Root mean square error	-
F	Statistical *F*-values	
G^{E}	Excess Gibbs free energy	J
I	Intensity	
I_x	Molar ionic strength of the solution	e^2
K	Partition coefficient	
k_{B}	Boltzmann's constant	$\mathrm{J} \cdot \mathrm{K}^{-1}$
k_{BH}, r_{BH}	Adjustable parameters of the Bancroft and Hubbard model	
k_{ij}	Coefficient of the polynomial fitting for the isolines	
k_{OT}, n_{OT}	Adjustable parameters of the Othmer-Tobias model	
l_i	Auxiliary term of the UNIQUAC model	
L_{m}	Mass losses in phase separation	%
L_{s}	Solute losses	%
M	Molar mass	$\mathrm{kg} \cdot \mathrm{mol}^{-1}$
M_{ms}	Molar mass of the mixed solvent	$\mathrm{kg} \cdot \mathrm{mol}^{-1}$
m	Mass	kg
N_{A}	Avogadro's constant	mol^{-1}
n_{D}	Refractive index	
n_i	Number of moles of species i	mol
n_{bonds}	Number of bonds	
n_{ions}	Number of ions in solution	
n_{points}	Number of points	
n_{species}	Number of species in solution	
P	Total pressure	Pa
pH	Negative base-10 logarithm of the equilibrium molar concentration of H^+ in solution	
$\mathrm{p}K_{\mathrm{a}}$	Negative base-10 logarithm of the acid dissociation constant	
Q	Relative surface area of each functional group	
$\bar{q}$	Mean electrical charge of the solution	e
q_0	Initial electrical charge, at $\mathrm{pH} = 0$	e
q_i	van der Waals surface area	
R	Volume of each functional group	
R^2	Determination coefficient	

R_g	Universal gas constant	$J \cdot K^{-1} \cdot mol^{-1}$
r_i	van der Waals molecular volume	
$[S^{q_0-i}]$	Mole concentrations of the solute S with electrical charges equal to $(q_0 - i)$ e	
STL	Tie-line slope	
T	Temperature	K
T_{gt}	Glass transition temperature	K
TLL	Tie-line length	m%
T_m	Melting temperature	K
U_{ij}, u_{ij}	Interaction energy between i and j	$J \cdot mol^{-1}$
V_w	van der Waals volume	$m^3 \cdot mol^{-1}$
V_j^{φ}	Volume of the phase φ in tie-line j	m^3
w_i	Mass fraction of component i	
w_i'	Salt-free mass fraction of component i	
WN	Wavenumber	m^{-1}
$x_{S^{q_0-(i-1)}}$	Fraction of molecules of species S with an electrical charge of $q_0 - (i-1)$ e	
X	Independent variable	-
x_i	Mole fraction of component i	
x_i'	Salt-free mole fraction of component i	
Y	Measured dependent variable	-
$\hat{Y}$	Calculated dependent variable	-
z_i	Electrical charge of species i	e
Z	Lattice coordination number	

Greek Letters

α	Non-randomness factor	
α_{ij}	Non-randomness factor of the binary pair ij	
$\alpha_{mixture}$	Non-randomness factor of the mixture	
γ_i	Activity coefficient of species i	
δq_i	Partial charge of the atoms	e
ε	Dielectric constant	
ε_0	Vacuum permittivity	$F \cdot m^{-1}$
ε_{ms}	Mixed solvent's dielectric constant	
θ_i	Average surface area fraction of component i	
λ_{max}	Wavelength of the local maximum of ultraviolet-visible absorbance spectrum	m
μ	Electrical conductivity	$S \cdot m^{-1}$
$\nu_k^{(i)}$	Number of functional groups k found in molecule i	
ρ_{CA}	Closest approach parameter	
ρ	Density	$kg \cdot m^{-3}$
$\rho_{ms,m}$	Mass density of the mixed solvent	$kg \cdot m^{-3}$
$\rho_{ms,x}$	Molar density of the mixed solvent	$mol \cdot m^{-3}$
σ	Standard deviation	-
τ_{ij}	UNIQUAC binary interaction energy parameter of the pair ij	
ϕ_i	Average volume fraction of component i	

Indices

′	Salt-free
Ac	Acetaminophen
Amox	Amoxicillin
B	Bottom phase

BH	Bancroft and Hubbard
C	Combinatorial contribution
calc	Calculated value
DH	Debye-Hückel
E	Excess property
exp	Experimental value
F, feed	Feed mixture
g	Ideal gas
gt	Glass transition
I, II	Phase number
i	Index or counter
j	Index or counter
k	Index or counter
m	Mass property
m	Melting point
max	Maximum
ms	Mixed solvent
PDH	Pitzer-Debye-Hückel contribution
R	Residual contribution
RMSE	Root mean square error
s, S	Solute
SA	Salicylic acid
T	Top phase
UNIQUAC	UNIQUAC contribution
x	Molar property
φ	Phase

List of Abbreviations

AAILs	Amino Acid Ionic liquids
ABS	Aqueous Biphasic System
ALiCE	Associate Laboratory in Chemical Engineering
AOP	Advanced Oxidation Processes
API	Active Pharmaceutical Ingredient
ATPS	Aqueous Two-Phase System
B3LYP	Becke, 3-parameter, Lee–Yang–Parr hybrid functional
CAAILs	Choline Amino Acid Ionic Liquids
CAS	Chemical Abstracts Service
CPA	Cubic Plus Association
DES	Deep Eutectic Solvents
DFT	Density Functional Theory
ECP	Emerging Concern Pollutants
EoS	Equations of State
ePC-SAFT	Electrolyte Perturbed Chain Statistical Associating Fluid Theory
EU	European Union
FEUP	Faculty of Engineering of the University of Porto
FIL	Fluorinated Ionic Liquids
FTIR	Fourier Transform Infrared
GC	Group contribution
HPLC	High Performance Liquid Chromatography
ILs	Ionic liquids
IR	Infrared

L	Liquid phase
LC	Local composition
LLE	Liquid-Liquid Equilibrium/Equilibria
LSRE-LCM	Laboratory of Separation and Reaction Engineering - Laboratory of Catalysis and Materials
NBO	Natural Bond Orbital
NRTL	Non-Random Two-Liquid
NSAID	Nonsteroidal anti-inflammatory drug
PCB	Polychlorinated Biphenyl
PCM	Polarizable Continuum Model
PC-SAFT	Perturbed Chain Statistical Associating Fluid Theory
PDH	Pitzer-Debye-Hückel
PHCT	Perturbed Hard-Chain Theory
PILs	Polymerized Ionic Liquids
R&D	Research and Development
REACH	Registration, Evaluation, Authorisation and Restriction of CHemicals
RTILs	Room-Temperature Ionic Liquids
SAFT	Statistical Associating Fluid Theory
SAILs	Surface-Active Ionic Liquids
SDG	Sustainable Development Goals
STL	Tie-line slope
TL	Tie-line
TLL	Tie-line length
TSILs	Task Specific Ionic Liquids
UNIQUAC	UNIversal QUAsi-Chemical
VABC	Atomic and Bond Contributions of van der Waals volume
VLE	Vapor-Liquid Equilibria
VOC	Volatile Organic Compounds

Cations

$[Ch]^+$	Cholinium
$[EtNH_3]^+$	Ethylammonium

Anions

$[Ala]^-$	Alaninate
$[DCA]^-$	Dicyanamide
$[Gly]^-$	Glycinate
$[Leu]^-$	Leucinate
$[NTf_2]^-$	Bis(trifluoromethyl)sulfonylimide
$[Ser]^-$	Serinate
Bic^-	Bicarbonate
Bit^-	Bitartrate
$DHCit^-$	Di-hydrogen citrate

Other Chemicals

Ac	Acetaminophen
Amox	Amoxicillin
EL	Ethyl lactate
EtOH	Ethanol
PEG	Polyethylene glycol
PVP	Polyvinylpyrrolidone
SA	Salicylic Acid

1 Introduction

The pharmaceutical industry is a key sector of the economy of the European Union (EU): its market was estimated in 300 billion euros in 2021, attaining a trade balance of 175 billion euros [1]. It created around 840 000 employments, and its research and development (R&D) activity generated over 41.5 billion euros, while the Portuguese market represented 3.524 billion euros [1].

According to Valormed, a non-profit entity responsible for the management of empty packaging waste and expired medicines of domestic origin in Portugal, there were 18.3 t of pharmaceutical residues and packaging discarded in Portugal in 2021 [2]. In fact, worldwide, the intensive use and disposal of pharmaceuticals and their packaging have led to their detection in water bodies and soil. It has been found that active pharmaceutical ingredients (APIs), excipients and additives can enter the environment from different routes, such as manufacturing plants, effluents of sewage treatment plants, and hospital or household waste [3]. This problem is worsened given that some pharmaceuticals are not fully metabolised by the organism after their ingestion, being excreted as functional APIs [3].

The presence of antimicrobials (a class of drugs that comprises antibiotics, antivirals, antifungals and antiparasitics) in soil and water bodies can cause the rise of multi-resistant strains of bacteria. Antimicrobial resistance is considered by the World Health Organisation as one of the most urgent health problems for the forthcoming years, as currently used antibiotics could become ineffective [4].

Since avoiding antimicrobial resistance, reducing water pollution and freshwater shortage are targeted by the United Nations' Sustainable Development Goals (SDG) [5], it is of the utmost importance to develop effective and sustainable methodologies to remove pharmaceutical pollutants from water.

1.1 Problem statement

Techniques such as electrochemical advanced oxidation processes (AOPs) have been recently studied for the removal of pharmaceutical compounds from water bodies [6]. AOPs are processes that involve degradation of organic compounds using highly reactive radicals, such as the hydroxyl free radical, $^{\bullet}OH$. Therefore, these are highly destructive processes, with disinfecting capabilities and that are effective in water treatments. Nonetheless, AOPs are associated with high costs and high consumption of electricity, and there is a tendency for an accumulation of organic and inorganic oxidation by-products, often more toxic than the original pollutant [7].

More sustainable alternatives include liquid-liquid extractions, using green solvents such as ethyl lactate [8] or ionic liquids (ILs) [9,10]. These solvents are promising replacements to the commonly used volatile organic solvents (or volatile organic compounds, VOCs), which are harmful to the environment. In particular, Aqueous Two-Phase Systems (ATPS) are a biocompatible extractive media with applicability to an industrial scale, due to their good scale-up potential. ATPS are composed by two solutes with high solubility in water (such as two salts, a salt and a solvent, or a salt and a polymer) and low environmental impact. Therefore, these systems could be used to extract pharmaceuticals from water bodies. Specifically, systems based on choline salts, an essential micronutrient of the class of B vitamins, as well as systems with Choline Amino Acid Ionic Liquids (CAAILs, a class of ILs composed of the choline cation and an amino acid anion), could be used.

Therefore, the main goal of this work was the study the partitioning of pharmaceutical compounds in ATPS containing salts or solvents based on choline, in order to evaluate the potential of these systems in the removal of contaminants from water bodies. For this, the Liquid-Liquid Equilibria (LLE) of choline-based ATPS will be determined and described using thermodynamic models developed for electrolytes. Finally, novel methodologies will be tested, so as to enhance the predictability of the modelling parameters.

1.2 Presentation of LSRE-LCM and ALiCE

This work was carried out at the Laboratory of Separation and Reaction Engineering – Laboratory of Catalysis and Materials (LSRE-LCM), set in the Chemical Engineering Department of the Faculty of Engineering of the University of Porto (FEUP). The research done at this laboratory is focused on the development of sustainable processes for the chemical and biochemical industry, with emphasis on separation and reaction engineering, catalysis, thermodynamics, and materials science. LSRE–LCM is a leading national research and development (R&D) unit and one of the three that compose the Associate Laboratory in Chemical Engineering (ALiCE).

ALiCE is a consortium formed between three research units based at the Chemical Engineering Department of FEUP, including LSRE-LCM. Created in 2021, ALiCE is the largest Portuguese associate laboratory in the field of chemical engineering and aims to promote R&D in the field of chemical engineering, with emphasis on sustainability and innovation.

1.3 Author's contribution

All the work presented in this document was performed by the author at the Chemical Engineering Department of FEUP, under the supervisor's guidance. All the experimental procedures, MATLAB codes required for the thermodynamic modelling of electrolytes and Density Functional Theory (DFT) calculations were performed by the author. All sourced data is properly referenced.

1.4 Document's structure

After having an overview of the work in the **Introduction**, the following topics will be addressed.

In chapter 2, **State of the art**, a review of literature is performed, comprising theoretical notions about ionic liquids (ILs), Aqueous Two-Phase Systems (ATPSs), thermodynamic modelling and Density Functional Theory (DFT), as well as the need for the removal of pharmaceutical pollutants from water bodies.

Chapter 3, **Materials and methods,** presents a list of the chemicals used, as well as a brief description of all computational tools. Additionally, the followed experimental procedures are explained, and the approach for the thermodynamic modelling is detailed.

Results are discussed in chapters 4 and 5. In chapter 4**, Liquid-liquid equilibria**, the obtained data for Liquid-Liquid Equilibria (LLE) of new ternary systems are presented and fitted to correlations found in literature, followed by the results of thermodynamic modelling. The curation of the partition results of pharmaceutical compounds in ATPS are shown and discussed in chapter 5, **Partitions of pharmaceuticals in ATPS.**

In chapters 6 and 7, **Conclusions** and **Project assessment**, the main findings of this work are assessed, and a short critique of the performed work, together with some suggestions for future work, are presented.

2 State of the art

Throughout this chapter, a literature review will be performed, so as to explain the core concepts related to the scope of this work and explore recent advances.

2.1 Pharmaceutical pollutants in water

Environmental pollution has been a constant issue for centuries, with its magnitude increasing after the industrial revolution in the 19th century, causing damage to the environment and posing a threat to humans and other living species. Pollution occurs when contaminants, such as polychlorinated biphenyls (PCBs), pesticides or heavy metals, are introduced into the natural environment. In recent years, this class has been extended to include pharmaceutical compounds, illicit drugs, antibacterials, hormones and nanomaterials [11]. Moreover, freshwater shortage has become a major concern, so providing an equal access to clean drinking water and sanitation is considered as one of the United Nations' main Sustainable Development Goals (SDG) [5].

Pharmaceuticals, which are used in the treatment of diseases, are composed of active pharmaceutical ingredients (APIs) with different physicochemical and biological properties, and can be classified according to their functionality [3]. For instance, antibiotics are chemical compounds, totally or partly synthesised by living microorganisms, that present antibacterial activity, *i.e.*, they either inhibit the growth or kill bacteria. On the other hand, analgesics are used to minimise pain, while antipyretics reduce fever [3].

Globally, the intensive use and disposal of these pharmaceutical substances result in their occurrence in natural environments, such as water bodies and soil. In addition to APIs, excipients and additives can also enter the environment from different routes, such as manufacturing plants, effluents of sewage treatment plants, and hospital or household waste [3].

Furthermore, some pharmaceuticals are not metabolised by the human body after being ingested, so they are excreted as functional APIs [3]. Besides the insufficient metabolisation of ingested pharmaceuticals, their industrial effluents and inadequate disposal of unused and expired drugs play an important role in the introduction of these drugs into the environment. Their significant presence in environmental waters leads to the contamination of drinking water [3]. In fact, many of these emerging contaminants, or emerging concern pollutants (ECPs), are bioaccumulative, meaning that there is a higher concentration of these compounds in organisms when compared to that in their environment, due to a resistance to degradation [3]. Moreover, it has been shown that these compounds negatively affect aquatic organisms, as will be further discussed [3].

Antibiotics, antivirals, antifungals and antiparasitics – a class of pharmaceutical compounds often grouped as antimicrobials – are of special interest due to the possible promotion of antimicrobial resistance, which is the ability of microorganisms to counteract the drugs designed to neutralise them. The appearance of multi-resistant bacteria strains is a rising problem of the utmost importance concerning public health, given that resistant bacteria can enter the food chain if contaminated waters

are ingested or used for irrigation [12]. Moreover, if antimicrobial resistance to currently used antibiotics rises, these drugs can become ineffective [4].

The most commonly prescribed pharmaceuticals include acetaminophen, amoxicillin, and salicylic acid, which will be further detailed. These are also amongst the pharmaceuticals most commonly found in water bodies and targeted on monitoring programmes due to the risks they present [13].

Acetaminophen, also known as N-(4-hydroxyphenyl)acetamide or paracetamol, is one of the most widespread pain killers and antipyretic pharmaceuticals and is sold worldwide without the need for a medical prescription. Studies have shown that, when found in high concentrations in water bodies, acetaminophen may interfere with normal embryonic development, normal growth, reproductive and endocrine systems of fish [14].

Amoxicillin is an antibiotic pertaining to the class of aminopenicillins and is administered orally in tablets or liquid forms, intravenously or via intramuscular injection. Amoxicillin has a wide range of therapeutic uses, including infections of the chest, nose, ear, and throat. A typical dose of amoxicillin (ranging from fewer than 1000 to 4000 mg per day) varies with the dosing method, which in turn will affect the concentration of this drug in urine: in fact, the majority of ingested amoxicillin is excreted unaltered and unmetabolised [15].

Salicylic acid (2-hydroxybenzoic acid) is essentially used for the synthesis of acetylsalicylic acid (aspirin), the most commonly distributed pharmaceutical product. However, salicylic acid itself presents bacteriostatic properties, for which it is used as a disinfectant and preservative [16]. Salicylic acid is a nonsteroidal anti-inflammatory drug (NSAID), alongside acetylsalicylic acid. Its elimination by the human body has a slower rate than its resorption by the skin and mucous membranes, so there is a risk of accumulation in the organism. In this case, intoxication may occur, with symptoms such as gastric and intestinal pain [16].

Techniques for the removal of pharmaceutical compounds from water bodies have been recently studied, and include membrane separation [17] and electrochemical advanced oxidation processes (AOPs) [6]. Notwithstanding the disinfecting capabilities and great effectiveness in water treatments, AOPs involve high costs and a high consumption of electricity. Besides, both organic and inorganic by-products (such as bromates) can be formed, some of which more toxic than the original pollutant [7]. Less harsh alternatives are liquid-liquid extractions using green polymers [15] or green solvents, such as ethyl lactate [8] or ionic liquids [9,10].

2.2 Ionic liquids

Ionic liquids (ILs) are a class of ionic compounds with a low melting temperature (T_{m}), often below 100 °C, or low glass transition temperature (T_{gt}) at atmospheric pressure [18], and are generally liquid at room temperature. In particular, Room-Temperature Ionic Liquids (RTILs) are also called first-generation ILs, the first reported RTIL being ethylammonium nitrate, $[EtNH_3][NO_3]$ in 1914 [19], though the first patent regarding ILs dates from 1934 [20]. Second-generation ILs, *i.e.*, air- and water-stable ILs have only been synthesised since 1992 [21,22].

Nonetheless, in recent years, ILs have emerged as an eco-friendlier alternative to volatile organic solvents. As opposed to organic solvents, ILs present good chemical and thermal stability and have high solvation capability, with many of them being soluble in water [23,24]. ILs also have high electrical conductivity, high viscosity (typically ranging from 30 to 600 mPa·s at 25 °C, higher than water's viscosity, 0.1 mPa·s [18]), and are non-flammable [25]. Traditionally, ILs are reported to have negligible volatility, although certain ILs can be vaporised at low pressures [26]. As mentioned before, ILs have low melting and glass transition temperatures, the former being explained by their lack of a well-defined crystalline structure [27].

Most ILs can be considered green solvents, mainly due to their chemical properties (such as low vapour pressure), which lower their environmental impacts. Yet, to be truly classed as green solvents, toxicological impacts must be assessed. Since this class of compounds has only been intensively studied in recent years, it still lacks scientific maturity, so it is necessary to evaluate their manufacturing, utilisation and disposal, and determine IL toxicity according to criteria defined in the Registration, Evaluation, Authorisation and Restriction of CHemicals (REACH) regulation [24].

A wide range of applications for ILs have been presented in literature, such as electrolytes in batteries [28], extraction agents [29,30], solvents [31], or catalysts [32]. ILs have been used in areas as diverse as carbon capture [33,34] or liquid mirrors for lunar telescopes [35]. In recent years, considerable attention has been paid to applications of ILs in drug solubility: if one of the ions has therapeutic activity, this new IL could be employed in formulation of pharmaceuticals, as an API, or play a role in drug release [36]. Furthermore, ILs have been employed in wastewater treatment [9], as seen in section 2.1. However, the low economic efficiency and high viscosity of ILs currently hinders their use at industrial scale. Nevertheless, IL recovery can be performed by numerous means (low pressure or molecular distillation [37], adsorption [38], induced phase separation [39], membrane separation [40], among others) which could allow for recycling ILs.

Generally, ILs are composed of monocharged cations and anions, as ions with double charges can usually lead to the formation of "classical" salts with high melting temperatures [41]. Common cations are organic and include imidazolium ($[C_3H_5N_2]^+$), pyridinium ($[C_5H_6N]^+$), pyrrolidinium ($[C_4H_{10}N]^+$), phosphonium ($[H_4P]^+$) or ammonium ($[H_4N]^+$) [22]. Anions, on the other hand, can either be organic (trifluoromethylsulfonate ($[CF_3SO_3]^-$), bis(trifluoromethyl)sulfonylimide ($[(CF_3SO_2)_2N]^-$ or $[NTf_2]^-$), trifluoroethanoate ($[CF_3CO_2]^-$) or dicyanamide ($[C_2N_3]^-$ or $[DCA]^-$)) or inorganic (such as chloride ($[Cl]^-$), hexafluorophosphate ($[PF_6]^-$) and tetrafluoroborate ($[BF_4]^-$)) [22].

Because of the high number of existing cations and of anion/cation combinations, it is estimated that the number of ILs surpasses 10^6 [42]. Alongside Deep Eutectic Solvents (DES, a class of ionic mixtures composed of 2 or more components forming an eutectic mixture with a lower melting point than each pure constituent [43]), ILs present a flexibility of synthesis: they are known as "designer solvents" [31]. It is possible to tune their physical and chemical properties by selecting the correct anion and cation combination [31]. For instance, IL hydrophobicity is closely related to the cation's alkyl chain length, which can be modified to tailor their properties [44]. This has led to the third-generation of ILs: Task Specific Ionic Liquids (TSILs), which are ILs with a functional group bonded to one of the ions, so that structure-dependent physical properties can be enhanced [45]. For example, the water solubility of the

ionic liquid 1-alkyl-3-methylimidazolium hexafluorophosphate was increased by functionalising the anion ($[PF_6]^-$) with an ether group [46].

ILs can also be classified as protic or aprotic. Protic ILs are synthesised via a neutralisation reaction between a Brønsted acid and a Brønsted base [47]. On the other hand, aprotic ILs are formed by an alkylation followed by an anion exchange reaction [48]. There are other classes of ILs worth mentioning, such as:

- Polyionic liquids or polymerised ionic liquids (PILs) are composed of a polymeric structure coupled to IL species in each repeating unit [49]. PILs have various applications as thermoresponsive materials, in catalysis and in electrochemical devices [50]. However, at high temperatures, PILs can suffer thermal degradation, leading to depolymerisation and scission [50].
- Surface-Active Ionic Liquids (SAILs) are ILs with their longer alkyl chain attached to any of their structural parts, thus conferring surface activity to the ILs [51]. SAILs have been used in place of conventional surfactants in paints, cleansing agents and lubricants [51].
- Fluorinated Ionic Liquids (FILs) are ILs with fluorine chains of variable length in the cation or in the anion. ILs containing anions such as $[NTf_2]^-$, $[BF_4]^-$ and $[PF_6]^-$ have been extensively characterised and possess several applications [52].
- Amino Acid ILs (AAILs) are ILs in which the anion is an amino acid [53]. This emerging group of ILs is considered greener than their classical counterparts, and include, for example, Choline Amino Acid Ionic Liquids (CAAILs).

2.2.1 Choline Amino Acid Ionic Liquids (CAAILs)

Choline Amino Acid Ionic Liquids (CAAILs) are AAILs in which the cation is the cholinium ion, commonly called choline: an essential micronutrient that belongs to the class of B vitamins, found in eggs, peanuts, meat and vegetables [54]. Choline salts consist of the quaternary ammonium cation $[N(CH_3)_3(CH_2CH_2OH)]^+$ (or $[Ch]^+$) combined with diverse anions, either organic (such as tartrate or citrate) or inorganic (such as bicarbonate or chloride). Additionally, extensive research has been performed on choline-based Deep Eutectic Solvents (DES), the most recurrent and widely applied being choline chloride ([Ch]Cl)/urea (in proportions 1:2), [Ch]Cl/phenol (1:2) and [Ch]Cl /ethylene glycol (1:2) [55].

Due to the two ions that compose these ILs, CAAILs can be classed as amphiphilic. Nonetheless, CAAILs have tuneable hydrophobicity, hydrogen bonding ability and acid-base characteristics, similarly to other ILs. Moreover, since they are formed by two natural and non-toxic compounds (an amino acid and the choline ion), CAAILs are considered promising alternatives to other ILs. As opposed to imidazolium- and pyridinium-based ILs, CAAILs are biodegradable, non-toxic and highly biocompatible [30,56]. Their synthesis can be performed in fewer steps, and the raw materials (amino acids and choline) are available from renewable sources thus aligning with the principles of green chemistry.

CAAILs could be employed as lubricants [57] and have been successfully employed in liquid-liquid extractions of bioactive molecules [30] and pollutants [58,59].

2.3 Aqueous Two-Phase Systems (ATPS)

In bioprocesses at industrial scale, such as fermentation, the recovery and purification of biomolecules has proven to be a hurdle, limiting the overall efficiency of the process. Hence, purification techniques must be carefully chosen, as the desired biomolecules are sensitive to the operating conditions (temperature, pH, ionic strength), and choosing an inadequate purification technique could damage their bioactivity and/or cause degradation. Separation and recovery processes often contribute to the greatest fraction of the product cost, in which this cost can be as high as 80 % of the total manufacturing costs [60].

Liquid-liquid extractions traditionally use volatile organic solvents (or volatile organic compounds, VOCs), which are harmful to the environment. On the other hand, the high temperatures needed in distillation processes could hamper biomolecules' activity. Therefore, the need for less harsh and more sustainable purification processes arises.

Following the discovery of a gelatine/agar biphasic system in 1896 by Beijerinck [61], Per-Åke Albertson's work found an application in biotechnology for Aqueous Two-Phase Systems (ATPS), also known as Aqueous Biphasic Systems (ABS) [62,63]. In fact, as ATPS are composed of two aqueous phases, they constitute biocompatible media for the separation or purification of cells, viruses, proteins, enzymes, vitamins, antioxidants, and other biologically active molecules [8,53,64-70]. In recent years, ATPS have been applied in the removal of pharmaceuticals from aqueous media [9,10,71,72]. Furthermore, ATPS show prospects of being applied to an industrial scale, due to their good scale-up potential.

Most of the reported ATPS are ternary systems, but exceptions include DES-based ATPS [73]. ATPS are composed by two species with a considerable solubility in water, for example two polymers, two salts, a salt and a solvent, or a salt and a polymer. Concerning polymers, polyethylene glycol (PEG) with various molar masses is often used, due to its low ecological impact and phase separation ability [15,74]. Another substance applied to ATPS in recent years is ethyl lactate [8,67,70,75,76], a green solvent derived from lactic acid. Regarding salts, both organic and inorganic salts have been used, such as phosphates, sulphates, tartrates, or citrates [29,30,69,74,76]. Furthermore, since the 1980s, IL-based ATPS have been studied as promising extraction media [30].

Each ATPS has a ternary phase diagram, which is specific to each system at a certain temperature and pressure. Before applying these systems to extraction and purification processes, it is crucial to determine the system's phase diagram, in order to gather information about its biphasic region, in which the extraction will be feasible. The solubility curve limits the monophasic and biphasic areas on a phase diagram, as can be seen in Fig. 2.1: the biphasic region, in which two liquid phases are in equilibrium (L+L), is situated above the solubility curve, whereas only one liquid phase (L) exists under the solubility curve.

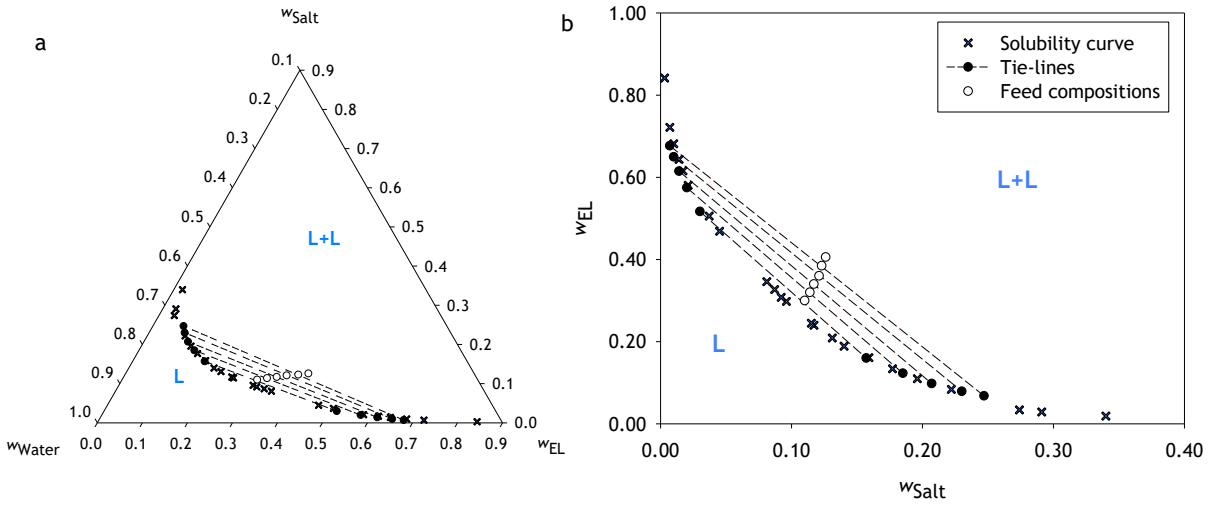

Fig. 2.1. Solubility curve and tie-lines for the system {PEG6000 (1) + sodium citrate (2) + water (3)}, at 298.15 K and 0.1 MPa, represented with data from [76], in: (a) a triangular plot and (b) a rectangular plot.

In Fig. 2.1, below the solubility curve, solutions can exist in a single homogenous phase, though mixtures above the solubility curve do not exist in that range of concentrations, at the reported temperature and pressure. Instead, they split into a top (with a lower density) and a bottom phase (with a higher density). This is caused by a salting-out agent, which leads to the formation of two phases in equilibrium, at the same temperature and pressure. In ternary diagrams, the composition of these two phases can be joined by a line, called a tie-line. The system's binodal curve is obtained by joining the ends of tie-lines, and not by a visual method (such as the cloud point method), as commonly described in literature [77].

The salting-out effect occurs when the addition of high charge-density salts to aqueous solutions leads to liquid-liquid demixing. This happens due to a preferential hydration of the high charge density salt over the third component (IL, polymer or solvent), leading to the salting-out, or the exclusion, of that third component to one of the phases [65].

The migration of each component to either phase is promoted by a difference in physical properties, such as polarity, density, hydrophobicity, and viscosity. Additionally, a solute can be introduced in an ATPS, and will migrate preferentially to one of the phases, thus allowing for its extraction. The extraction of solutes is promoted by a difference in affinities between the solute and the composition of the ATPS's each phase.

The longer the tie-line, the more distinct the phases' compositions, so, in literature, tie-lines are often sorted by their lengths [76]. The behaviour of solute partitioning follows a trend according to the tie-line length (TLL), as solutes typically have a preferential affinity to the ATPS components.

Finally, a critical point can also be defined, as the point of the solubility curve in which $\mathrm{TLL} = 0\ \%$, a theoretical point where the composition and volume of the two phases become equal.

2.4 Thermodynamic modelling

In order to reduce the need for time-consuming experiments, some of which requires the usage of expensive equipment, it is important to model binary or ternary mixtures' properties and their phase equilibria. Hence, the development of thermodynamic models is vital. Thermodynamic models fall into one of two classes: equations of state (EoS) and models for the excess Gibbs free energy [78].

Equations of state (EoS) are equations which relate state variables (such as temperature, pressure, or volume). Widely used in industry and academia, EoS allow for the calculation of thermodynamic properties of mixtures (fugacity coefficients) in liquid and vapour phases at high pressures [79]. Most well-known cubic EoS are the van der Waals EoS [80], the Redlich-Kwong EoS [81], the Soave-Redlich-Kwong EoS [82] and the Peng-Robinson EoS [83]. Moreover, several other have been developed by modifying these existing EoS [84,85].

Some of these EoS are the Statistical Associating Fluid Theory (SAFT, a model based on statistical thermodynamics developed in 1988 by Chapman *et al.* [86]) and the Perturbed Hard-Chain Theory (PHCT, developed by Beret and Prausnitz [87] and Donohue and Prausnitz [88]). In order to improve these thermodynamic models, a novel approach was developed, combining both models, which is called PC-SAFT (Perturbed Chain SAFT). This EoS was first developed by Gross and Sadowski [89] in 2001, and has since been modified to describe mixtures with ionic compounds [89] (electrolyte PC-SAFT or ePC-SAFT), to model physical properties of ionic mixtures [90], Liquid-Liquid Equilibria (LLE) data [91], and partitioning of biomolecules in ATPS [92].

Another EoS with high accuracy in predicting the properties of complex mixtures is the Cubic Plus Association (CPA) EoS, developed by Kontogeorgis *et al.* [93] and commonly applied in petrochemical and pharmaceutical industries [94-96]. It is based on the Soave–Redlich–Kwong EoS, with the addition of a term to account for hydrogen bonding (association) [93,94]. One of its disadvantages, common to other EoS (such as PC-SAFT), is the high number of parameters (5 per pure associating compound, 3 per pure non-associating compound); however, its predictive capacity has been enhanced in recent years by establishing correlations between the parameters and the properties of the pure components [97]. The CPA EoS has also been extended to electrolyte solutions and applied in the modelling of systems containing ILs [98].

On the other hand, excess Gibbs free energy models, or activity coefficient models, are divided into 2 groups: 'random-mixing models' (like the Margules and van Laar models) and local composition (LC) models (such as the Wilson equation [99], the Non-Random Two-Liquid model (NRTL, [100]) or the UNIversal QUAsi-Chemical model, commonly called UNIQUAC [101]) [102,103].

Excess Gibbs free energy (G^{E}) models relate the excess Gibbs free energy with activity coefficients (γ_i):

$$R_{\mathrm{g}} T \ln \gamma_i = \left(\frac{\partial G^{\mathrm{E}}}{\partial n_i} \right)_{T,P,n_{j \neq i}} \tag{2.1}$$

In equation (2.1), R_{g} is the universal gas constant ($8.314\ \mathrm{J \cdot K^{-1} \cdot mol^{-1}}$), T is temperature, n_i is the number of moles of component i and P is the total pressure.

LC models are based on the LC concept developed by Grant Wilson in the 1960s and assume that the local composition is different than the global composition. These models account for short-range interactions between particles [99]. The aforementioned Wilson equation is used to model and predict Vapor-Liquid Equilibria (VLE), whilst NRTL is valid for both Liquid-Liquid Equilibria (LLE) and VLE [103].

The next section delves into UNIQUAC, a thermodynamic model with which the research group has long-term experience [76,104-107].

2.4.1 UNIQUAC

The UNIversal QUAsi-Chemical (UNIQUAC) equation is a thermodynamic model, first developed in 1975 by Abrams and Prausnitz [101]. UNIQUAC is a local composition model based on the two-fluid theory, capable of representing both VLE and LLE in mixtures [101,103]. UNIQUAC was deduced from a statistical mechanics basis, extending Guggenheim's quasi-chemical theory [101].

According to UNIQUAC, the excess Gibbs free energy, G^{E}, is the sum of a combinatorial ($G_{\mathrm{C}}^{\mathrm{E}}$) and a residual ($G_{\mathrm{R}}^{\mathrm{E}}$) contributions, as can be seen in equation (2.2). The combinatorial contribution (equation (2.3)) accounts for both size and shape effects, while the residual contribution (equation (2.4)) accounts for interactions among molecules.

$$G^{\mathrm{E,UNIQUAC}} = G_{\mathrm{C}}^{\mathrm{E}} + G_{\mathrm{R}}^{\mathrm{E}} \tag{2.2}$$

$$\frac{G_{\mathrm{C}}^{\mathrm{E}}}{R_{\mathrm{g}}T} = \sum_{i=1}^{n_{\mathrm{species}}} \left(x_i \ln\left(\frac{\phi_i}{x_i}\right)\right) + \frac{Z}{2} \sum_{i=1}^{n_{\mathrm{species}}} q_i\, x_i \ln\left(\frac{\theta_i}{\phi_i}\right) \tag{2.3}$$

$$\frac{G_{\mathrm{R}}^{\mathrm{E}}}{R_{\mathrm{g}}T} = -\sum\nolimits_{i=1}^{n_{\mathrm{species}}} q_i\, x_i \ln\left(\sum\nolimits_{j=1}^{n_{\mathrm{species}}} \theta_j\, \tau_{ji}\right) \tag{2.4}$$

where x_i is the mole fraction of component i, n_{species} is the number of species in solution, Z is the lattice coordination number, ϕ and θ are the average volume fraction and average local area fraction of component i, respectively, r_i and q_i are the van der Waals molecular volumes and surface areas, respectively, and τ_{ij} are the UNIQUAC binary interaction parameters, relative to the pair ij. UNIQUAC parameters τ_{ij} can be calculated from the interaction energies between i and j, noted as U_{ij}, following equation (2.5).

$$\tau_{ij} = e^{-\frac{Z}{2}\frac{(U_{ij}-U_{ii})}{R_{\mathrm{g}}T}} \tag{2.5}$$

From equation (2.5), it can be deduced that there are 2 interaction parameters per binary pair in solution ($\tau_{ij} \neq \tau_{ji}$), and that $\tau_{ii} = 1$. On the other hand, parameters ϕ_i and θ_i are composition-dependent variables and can be calculated from pure-component relative van der Waals molecular volumes (r_i) and surface areas (q_i).

$$\phi_i = \frac{x_i r_i}{\sum_{j=1}^{n_{\mathrm{species}}} x_j r_j} \tag{2.6}$$

$$\theta_i = \frac{x_i q_i}{\sum_{j=1}^{n_{\mathrm{species}}} x_j q_j} \tag{2.7}$$

The UNIQUAC structural parameters for each species, r_i and q_i, are traditionally calculated using Bondi's method [108]. Other methods for group contribution (GC) have been reported in literature, such as Joback's method [109] (used to calculate critical properties), the Marrero–Gani procedure [110] (applied to the estimation of thermophysical properties of pure compounds), and Atomic and Bond Contributions of van der Waals volume (or VABC, also used for the van der Waals volume) [111].

When van der Waals volumes and areas are estimated using Bondi's method [108], each functional group contribution is calculated according to:

$$r_i = \sum_k \nu_k^{(i)} R_k \tag{2.8}$$

$$q_i = \sum_k \nu_k^{(i)} Q_k \tag{2.9}$$

where $\nu_k^{(i)}$ is the number of functional groups k found in molecule i, and R and Q are the volume and surface area of each functional group, listed in literature.

Dimensionless values of these parameters, normalised with respect to the volume and surface of the CH_2 group in ethylene, are often found in literature. These are related to r_i and q_i by:

$$r_i = \frac{V_\mathrm{w}}{15.17} \tag{2.10}$$

$$q_i = \frac{A_\mathrm{w}}{2.5 \cdot 10^9} \tag{2.11}$$

where the van der Waals volume, V_w, is in $\mathrm{cm^3 \cdot mol^{-1}}$ and the van der Waals area, A_w, is in $\mathrm{cm^2 \cdot mol^{-1}}$.

By applying equation (2.1) to (2.3) and (2.4), the expression for UNIQUAC activity coefficients can be derived. The following equations are valid for multicomponent mixtures [101]:

$$\ln \gamma_i = \ln \gamma_i^\mathrm{C} + \ln \gamma_i^\mathrm{R} \tag{2.12}$$

$$\ln \gamma_i^\mathrm{C} = \ln \frac{\phi_i}{x_i} + \frac{Z}{2} q_i \ln \frac{\theta_i}{\phi_i} + l_i - \frac{\phi_i}{x_i} \sum_{j=1}^{n_\mathrm{species}} x_j l_j \tag{2.13}$$

$$\ln \gamma_i^\mathrm{R} = q_i \left(1 - \ln \left(\sum_{j=1}^{n_\mathrm{species}} \theta_j \tau_{ji} \right) - \sum_{j=1}^{n_\mathrm{species}} \frac{\theta_j \tau_{ij}}{\sum_{k=1}^{n_\mathrm{species}} \theta_k \tau_{kj}} \right) \tag{2.14}$$

An auxiliary term, l_i, is considered in the combinatorial term, and is calculated by equation (2.15), depending only on the components' van der Waals volumes and areas and on the coordination number [101]:

$$l_i = \frac{Z}{2}(r_i - q_i) - (r_i - 1) \tag{2.15}$$

2.4.2 PDH equation

In solutions with electrolytes, long-range interactions become significant due to the magnitude of electrostatic or Coulombic forces, so considering a term to account for these forces is critical. Thus, UNIQUAC has been combined with the Pitzer-Debye-Hückel (PDH) term [112] in recent works [106,107,113].

The PDH equation can be used in solutions with significant ionic strengths, up to 6 mol·kg^{-1}, as opposed to the Debye-Hückel equation [114]. This adaptation, often called PDH+UNIQUAC, allows to successfully describe the behaviour of LLE involving ionic species [75,105,115]. Particularly, PDH+UNIQUAC has been used to predict the dissociation extent of ionic liquids (ILs), both qualitatively [113] and quantitatively [106,107].

UNIQUAC was originally defined in the symmetric convention (in which the reference state is pure salt), as opposed to the unsymmetric convention (in which the reference state is infinite dilution). Therefore, when combining thermodynamic models, it is necessary to ensure that they are defined in the same convention. Hence, the PDH equation should also be defined in the symmetric convention.

Often, a Born term is also added to describe electrostatic ion-dipole interactions of the ions with the surrounding components and to account for the solvation energy of ionic species, when using the unsymmetric convention [116]. Nevertheless, it has been extensively reported that this term is not needed [104], seeing that the PDH+UNIQUAC model is in the symmetric convention, and not in the unsymmetric convention as the Born term's definition [117].

When using PDH+UNIQUAC, equation (2.16) is used:

$$G^{\mathrm{E}} = G^{\mathrm{E,UNIQUAC}} + G^{\mathrm{E,PDH}} \tag{2.16}$$

where $G^{\mathrm{E,UNIQUAC}}$ is the contribution of the UNIQUAC model and $G^{\mathrm{E,PDH}}$ the PDH equation contribution. Consequently, for activity coefficients, it can be written:

$$\ln \gamma_i = \ln\left(\gamma_i^{\mathrm{UNIQUAC}}\right) + \ln\left(\gamma_i^{\mathrm{PDH}}\right) \tag{2.17}$$

where $\gamma_i^{\mathrm{UNIQUAC}}$ is the contribution of the UNIQUAC model and γ_i^{PDH} is the activity coefficient contribution from the PDH equation.

In the symmetric convention, the PDH contribution is defined as equation (2.18) [112]:

$$\ln\left(\gamma_i^{\mathrm{PDH}}\right) = -z_i \cdot A_{\mathrm{DH},x}\left[\frac{2}{\rho}\ln\left(\frac{1+\rho_{\mathrm{CA}}\sqrt{I_x}}{1+\rho_{\mathrm{CA}}\sqrt{\frac{z_i^2}{2}}}\right) + \sqrt{I_x}\,\frac{1-2\left(\frac{I_x}{z_i^2}\right)}{1+\rho_{\mathrm{CA}}\sqrt{I_x}}\right] \tag{2.18}$$

where z_i is the electrical charge of species i, I_x is the molar ionic strength of the solution, ρ_{CA} is the closest approach parameter and $A_{\mathrm{DH},x}$ is the Debye-Hückel parameter. The molar ionic strength and the Debye-Hückel parameter can be calculated using equations (2.19) and (2.20), respectively.

$$I_x = \frac{1}{2}\sum_i^{n_{\mathrm{ions}}} z_i^2\, x_i \tag{2.19}$$

$$A_{\mathrm{DH},x} = \frac{1}{3}\frac{\sqrt{2\,N_{\mathrm{A}}\,\rho_{\mathrm{ms},x}}}{8\,\pi}\left(\frac{\mathrm{e}^2}{\varepsilon_0\,k_{\mathrm{B}}\,\varepsilon_{\mathrm{ms}}\,T}\right)^{1.5} \tag{2.20}$$

In equation (2.19), x_i is the mole fraction of species i and n_{ions} is the number of ions in solution. In equation (2.20), N_{A} represents Avogadro's constant ($6.022 \cdot 10^{23}\ \mathrm{mol^{-1}}$), e is the elementary charge ($1.602 \cdot 10^{-19}\ \mathrm{C}$), ε_0 is the vacuum permittivity ($8.854 \cdot 10^{-12}\ \mathrm{F \cdot m^{-1}}$), k_{B} is Boltzmann's constant ($1.381 \cdot 10^{-23}\ \mathrm{J \cdot K^{-1}}$), $\rho_{\mathrm{ms},x}$ is the mixed solvent's molar density and $\varepsilon_{\mathrm{ms}}$ is the mixed solvent's dielectric constant. Mixed solvent properties' calculations will be further detailed.

The closest approach parameter, ρ_{CA}, was proposed as an adjustable parameter by Pitzer [112] in 1980, fitted in the theoretical range from 8 to 15. For a wide range of salts at different temperatures, it was considered to be 14.9. However, this dimensionless parameter can be calculated according to equation (2.21) proposed by Pitzer and Simonson [118], which has been shown to yield more accurate results [105].

$$\rho_{\mathrm{CA}} = a\sqrt{\frac{2\,e^2\,N_{\mathrm{A}}\,\rho_{\mathrm{ms},m}}{M_{\mathrm{ms}}\,\varepsilon_0\,k_{\mathrm{B}}\,\varepsilon_{\mathrm{ms}}\,T}} \tag{2.21}$$

where a is the hard-core collision diameter, $\rho_{\mathrm{ms},m}$ is the mixed solvent's mass density and M_{ms} is the mixed solvent's molar mass. As shown by equation (2.21), ρ_{CA} depends on the distance between

the centres of ions with opposite electric charges, here approximated by the hard-core collision diameter.

Mixed solvent properties (molar density, mass density, molar mass and dielectric constant) are calculated using equations (2.22) to (2.25), the last being known as Oster's mixing rule [119]:

$$\frac{1}{\rho_{\mathrm{ms},x}} = \sum_i \frac{x_i'}{\rho_{i,x}} \tag{2.22}$$

$$\frac{1}{\rho_{\mathrm{ms},m}} = \sum_i \frac{w_i'}{\rho_{i,m}} \tag{2.23}$$

$$M_{\mathrm{ms}} = \sum_i x_i' M_i \tag{2.24}$$

$$\varepsilon_{\mathrm{ms}} = \varepsilon_1 \left(\frac{(\varepsilon_2 - 1)(2\,\varepsilon_2 - 1)}{2\,\varepsilon_2} - (\varepsilon_1 - 1) \right) \frac{x_2{}'}{\rho_{2,x}} \rho_{\mathrm{ms},x} \tag{2.25}$$

where the $'$ superscript denotes salt-free mass or mole fractions. Salt-free mole and mass fractions (x_i' and w_i', respectively) only consider solvent molecules, *i.e.*, neutral species. $\rho_{i,x}$, $\rho_{i,m}$ and M_i are the mole densities, mass densities and molar masses of the pure species i.

For solvents, which typically are neutral species, equation (2.18) is simplified into [112]:

$$\ln\left(\gamma_i^{\mathrm{PDH}}\right) = A_{\mathrm{DH},x} \frac{1 - I_x \sqrt{I_x}}{1 + \rho_{\mathrm{CA}} \sqrt{I_x}} \tag{2.26}$$

Due to the need to estimate thermodynamic properties (such as the enthalpy of formation, the Gibbs free energy of formation, the electronic energy, or the thermal energy), an approach based on quantum mechanics can be employed, using the Density Functional Theory.

2.5 Density Functional Theory (DFT)

Density Functional Theory (DFT) is a computational quantum mechanical modelling method used in various fields of physics, chemistry, and materials science, descending from Thomas–Fermi and Hartree–Fock–Slater methods [120]. Furthermore, it is an *ab initio* simulation method, meaning that it can predict material properties for new systems without experimental input. One of its developers, Walter Kohn, won the Nobel Prize in Chemistry in 1998 for his contributions to the development of DFT, alongside Pople, for his development of computational methods in quantum chemistry [121].

The primary use of DFT is to investigate the electronic (or nuclear) structure of many-body systems, such as atoms and molecules. DFT structure optimisation is used to determine the most stable configuration of a molecule by minimising its energy. The optimisation process involves iteratively adjusting the positions of the atoms and calculating, for each iteration, the electronic structure of the molecule, until the lowest energy state is achieved. These calculations use the electron density probability function as a variable, in contrast with wavefunction methods, which are unfeasible for large systems [120,122].

With DFT, it is possible to compute thermodynamic, electronic, mechanical, thermal, magnetic, and optic properties of components. Vibrational frequencies are also possible to compute, leading to the prediction of infrared (IR), Raman, Ultraviolet-Visible (UV-Vis) and nuclear magnetic resonance (NMR) spectra.

This technique's versatility has led to the popularity of DFT in diverse fields, such as condensed-state physics, computational physics, and computational chemistry. In fact, DFT requires a relatively low computational effort and has accurate predictive power [120]. Despite this, DFT has some limitations, such as the approximations used in hybrid functionals or the long-time needed for calculations in the liquid state [122].

Since its development in the second half of the 20th century, DFT calculations have been employed in various domains: to study surfaces and interfaces, as well as in the simulation, design, and optimisation of materials in fields as diverse as catalysis, photochemistry, or surface chemistry. Lastly, several studies have optimised the geometry of ILs [41,123,124].

3 Materials and methods

In this section, a list of chemicals and their information will be shown, experimental procedures will be detailed, and computational tools will be briefly presented.

3.1 Chemicals

Table 3.1 shows the list of chemicals used, grouped by category. Suppliers, purities, Chemical Abstracts Service (CAS) numbers and abbreviations are also reported. In addition, in Annex A1, the two-dimensional structures of these chemicals can be found (Table AA.1), as well as their molar masses (Table AA.2) and the solubilities of the pharmaceutical compounds in water (Table AA.3).

Table 3.1. List of chemicals used, with chemical formula, suppliers, purities, CAS numbers and abbreviations.

Chemical	CAS	Supplier	Purity [a] / %	Abbreviation
		SOLVENTS		
Water (H_2O)	7732-18-5	VWR Chemicals	-	-
(-)-Ethyl L-lactate ($C_5H_{10}O_3$)	687-47-8	Aldrich	98	EL
Ethanol absolute (C_2H_5OH)	64-17-5	VWR Chemicals	99.8	EtOH
		CHOLINE SALTS		
Choline chloride ($C_5H_{14}NOCl$)	67-48-1	VWR Chemicals	99	[Ch]Cl
Choline bitartrate ($C_9H_{19}NO_7$)	87-67-2	abcr GmbH	98	[Ch]Bit
Choline di-hydrogen citrate ($C_{11}H_{21}NO_8$)	77-91-8	Tokyo Chemical Industry	99	[Ch]DHCit
Choline bicarbonate ($C_6H_{15}NO_4$)	78-73-9	Sigma	80	[Ch]Bic
		OTHER SALTS		
Acetic acid (CH_3CO_2H)	64-19-7	Merck	99.8	-
Di-potassium hydrogen phosphate (K_2HPO_4)	7758-11-4	Merck	99	-
Potassium phosphate (K_3PO_4)	7778-53-2	Sigma-Aldrich	98	-
Potassium hydroxide (KOH)	1310-58-3	Merck	85	-
Sodium hydroxide (NaOH)	1310-73-2	Merck	99	-

[a] Provided by the supplier, in mass percentage.

Table 3.1. List of chemicals used, with chemical formula, suppliers, purities, CAS numbers and abbreviations (cont.).

Chemical	CAS	Supplier	Purity [a] / %	Abbreviation
CHOLINE AMINO-ACID IONIC LIQUIDS				
Cholinium alaninate ($C_8H_{20}N_2O_3$)	1361335-79-6	Synthesised [b]	> 99 [c]	[Ch][Ala]
Cholinium glycinate ($C_7H_{18}N_2O_3$)	1248335-95-6	Synthesised [b]	> 99 [c]	[Ch][Gly]
Cholinium leucinate ($C_{11}H_{26}N_2O_3$)	-	Synthesised [b]	> 99 [c]	[Ch][Leu]
Cholinium serinate ($C_8H_{20}N_2O_4$)	1248335-98-9	Synthesised [b]	> 99 [c]	[Ch][Ser]
AMINO ACIDS				
L-Alanine ($C_3H_7NO_2$)	302-72-7	Fluka	99	Ala
Glycine ($C_2H_5NO_2$)	56-40-6	Merck	99.7	Gly
L-Leucine ($C_6H_{13}NO_2$)	61-90-5	Fluka	99	Leu
L-Serine ($C_3H_7NO_3$)	56-45-1	Sigma	99	Ser
POLYMERS				
Polyethylene glycol 600 [d] ($C_{2n}H_{4n+2}O_{n+1}$)	25322-68-3	Aldrich	-	PEG600
Polyethylene glycol 1500 ($C_{2n}H_{4n+2}O_{n+1}$)	25322-68-3	Merck	-	PEG1500
Polyethylene glycol 4000 ($C_{2n}H_{4n+2}O_{n+1}$)	25322-68-3	Merck	-	PEG4000
Polyvinylpyrrolidone 29 000 ($(C_6H_9NO)_n$)	9003-39-8	Aldrich	-	PVP29000
PHARMACEUTICALS				
Acetaminophen ($C_8H_9NO_2$)	103-90-2	Cayman Chemical Europe	98	Ac
Amoxicillin trihydrate ($C_{16}H_{19}N_3O_5S{\cdot}3(H_2O)$)	61336-70-7	Tokyo Chemical Industry	98	Amox
Salicylic acid ($C_7H_6O_3$)	69-72-7	Sigma-Aldrich	99	SA

[a] Provided by the supplier, in mass percentage.
[b] Synthesised in this work or by the research group.
[c] Purity was assessed by lyophilisation.
[d] The number after the polymer name indicates its average molar mass.

3.2 Computational tools

In this work, several computational tools were employed, as explained in this section.

The spreadsheet program **Excel** (developed by Microsoft and in its version for Office 365 under the University of Porto's license) was used to organise data, to curate the experimental results from partitions and from the determination of the solubility curves of new ternary systems. It was also used to perform

fittings of the data to known correlations, using Solver with the Generalised Reduced Gradient (GRG) nonlinear solving method with central derivatives and precision of 0.001.

MATLAB is a programming language used for numerical computation. In this work, MATLAB scripts were developed from scratch by the author, so as to apply thermodynamic modelling by minimising the difference in activity coefficients of components between the two phases (isoactivity criterion), using MATLAB R2023a. When necessary, objective functions were minimised using constrained nonlinear optimisation, with $1 \cdot 10^{7}$ maximum iterations and optimality tolerance of $1 \cdot 10^{-6}$.

The geometry optimisation of molecules was carried out using **GAUSSIAN,** a computational chemistry software, created in 1970 by Pople. Version G09 was used in this work [125], with support from the Faculty of Sciences of the University of Porto. The structures obtained by the Gaussian software, as well as their infrared (IR) spectra, were visualised using the program **GaussView**.

Finally, **ChemDraw**, in its 16.0 version, was used to represent the reaction route for the synthesis of Choline Amino Acid Ionic Liquids (CAAILs). All plots presented in this document were designed using **SigmaPlot** 15.0 (a program developed for scientific graphing and data analysis, easily providing the correlations between data), with the exception of the three-dimensional plots, which were constructed using **Origin** in its 2023b version**.**

3.3 Experimental methodology

In this work, mass was measured using an Adam Equipment balance model AAA250L with a standard uncertainty in the measurement of $1 \cdot 10^{-3}\ \mathrm{g}$. pH was determined with a VWR pH 1100L pH meter with standard uncertainties of 0.001 in the measurement of pH and $0.1\ \mathrm{K}$ in the measurement of temperature. Densities were assessed using an Anton Paar DSA 4500M densimeter, with a standard uncertainty of $5 \cdot 10^{-6}\ \mathrm{g \cdot cm^{-3}}$ in density and $0.01\ \mathrm{K}$ in temperature. Electrical conductivity was measured using a Hanna EDGE EC conductivity meter, coupled with a platinum conductivity cell HI763100, with an uncertainty of $1\ \%$. Temperature was kept constant in a thermoregulated bath (Bath OvanTherm MultiMix BHM5E) with a standard uncertainty in the measurement of $0.1\ \mathrm{K}$. Stirring of the samples was performed on a VWR vortex VV3 or on an IKA RO 10P magnetic stirrer. Lastly, to avoid mass losses by evaporation, vials and flasks were sealed with parafilm.

Additionally, the Ultraviolet-Visible (UV-Vis) absorbance spectra were determined at 298.15 K, on a Greiner bio-one polystyrene flat bottom plate with 96 wells with the Thermo Scientific Varioskan Flash UV-Vis spectrophotometer, from 200 to 600 nm, by pipetting 200 µL on the plate with an Eppendorf Multipipette E3x. Absorbances measurements had a standard uncertainty of 10^{-4}. When using the 200 µL tips and pipetting 200 µL with the Eppendorf Multipipette E3x, volumes had an uncertainty of $1.0\ \%$. A Perkin Elmer Spectrum Two FT-IR, with measurement uncertainties of $0.01\ \%$ and $0.01\ \mathrm{K}$, was employed for the determination of infrared (IR) transmittance spectra.

3.3.1 Ionic liquid synthesis

Choline Amino Acid Ionic Liquids (CAAILs) are typically synthesised by the reaction of the choline cation with amino acid salts, and, in this work, a protocol from literature [126] was followed. The reaction pathway for the synthesis of Cholinium alaninate ([Ch][Ala]) is schematised in Fig. 3.1.

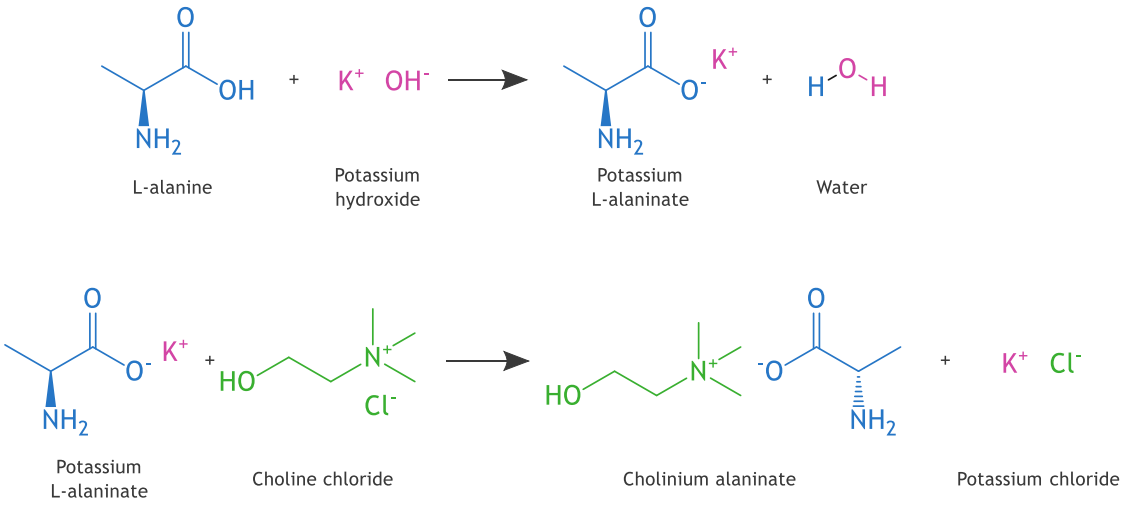

Fig. 3.1. Reaction route for the synthesis of cholinium alaninate ([Ch][Ala]).

First, the amino acid L-alanine and potassium hydroxide (KOH) were dissolved in ca. 500 mL of ethanol, yielding a solution with mass percentages of 23 % in L-alanine and 15 % in KOH. KOH was added in excess, so as to ensure all amino acid molecules reacted, forming potassium alaninate. This mixture was stirred at 303.15 K, for 3 h. Then, choline chloride was added in stochiometric proportions regarding the amino acid salt. The mixture was stirred in a thermoregulated bath, at 303.15 K, overnight (ca. 12 h), so as to ensure a higher conversion. When the choline salt was added, the suspension turned white, hence indicating that potassium chloride formed and precipitated.

The resulting ionic liquid was purified, first by vacuum filtration, in order to remove the salt formed (KCl). Then, it was distilled at 323.15 K at reduced-pressure, in an IKA RV 10 Rotary Evaporator, to evaporate the solvents present (ethanol and water).

This procedure was repeated using the amino acids glycine, leucine and serine in lieu of alanine, in order to synthesise cholinium glycinate ([Ch][Gly]), cholinium leucinate ([Ch][Leu]) and cholinium serinate ([Ch][Ser]), the synthesis pathway being analogous to the one represented in Fig. 3.1. The structures of the synthesised CAAILs were verified using Fourier Transform Infrared (FTIR) spectroscopy and compared to their theoretical spectra, determined using DFT assays, as described in section 3.3.2. Density was also measured using an Anton Paar DSA 4500M densimeter at temperatures ranging from 298.15 to 323.15 K and compared to values found in literature.

3.3.2 Theoretical infrared spectra determination

Computations were performed at DFT level of theory to get both the optimised geometry and the vibrational wave numbers of the normal modes of vibration of the CAAILs using Gaussian software, in its G09 version [125]. In this work, DFT hybrid functional B3LYP (the Becke, 3-parameter, Lee–Yang–Parr hybrid functional [127,128]) with the 6-311++G** basis set [129] was chosen, as it has shown to accurately describe ILs [123,124]. More specifically, the geometry of the isolated pairs of cation and anion were optimised using the method B3LYP 6-311++G*, then the wavenumbers of the normal modes of vibration were computed using B3LYP 6-311++G**. Visualisation of the obtained structures and the corresponding IR spectra was performed using ChemDraw 16.0.

3.3.3 LLE determination

The solubility curves of several ternary aqueous systems containing a choline salt were studied in this work.

For this, a system of the type {Polymer or EL (1) + Choline Salt (2) + Water (3)} was selected. The cloud point method, widely described in literature [74], was employed to determine the solubility curve of each system at 298.15 K and 0.1 MPa. Briefly, this method consists on the titration of EL or a saturated polymer solution (component 1) using a saturated salt stock solution (component 2). First, droplets of (2) were added to a known mass of (1) until turbidity was achieved (cloud point). Then, droplets of ultrapure water were added until the solution became clear and homogeneous. Composition of the cloudy and clear solutions were determined by mass quantification, obtaining the mass fractions (w_i) of the 3 components.

In literature, several empirical correlations are reported and widely used to perform fittings of the LLE data, such as the Merchuk equation (equation (3.1), proposed by Merchuk *et al.* [130]), the Li equation (equation (3.2), first used by Li *et al.* [131]), and the Yu equation (equation (3.3), developed by Yu *et al.* [132]), detailed below:

$$w_2 = A_1 \cdot e^{(B_1\, w_1^{0.5} - C_1\, w_1^3)} \tag{3.1}$$

$$w_1 = A_1 + B_1\, {w_2}^{0.5} + C_1\, w_2 + D_1\, w_2^2 \tag{3.2}$$

$$w_1 = e^{(A_1 + B_1\, w_2^{0.5} + C_1\, w_2 + D_1\, w_2^2)} \tag{3.3}$$

where w_i are the mass fractions of component i (though the solubility curves display the mass percentage), and A_1, B_1, C_1 and D_1 are adjustable parameters. Fittings were performed by minimising the root mean square error (E_{RMSE}, equation (3.4)):

$$E_{\mathrm{RMSE}} = \sqrt{\frac{1}{n_{\mathrm{points}}} \sum\nolimits_{i=1}^{n_{\mathrm{points}}} \left(Y_i - \hat{Y}_i\right)^2} \tag{3.4}$$

where n_{points} represents the number of points, Y is the measured dependent variable and $\hat{Y}$ is the calculated dependent variable.

Following the determination of the solubility curve, its geometry (area and shape) was assessed. If the minimal composition to form the ATPS was distant to the solubility limit of the components and the ternary system possessed sufficient area in the immiscible region (*i.e.*, the area above the solubility curve), then it was selected for further studies. For this, tie-lines were determined: the two phases' compositions were determined using an intersection of isolines of two independent properties. Isolines, as the etymology indicates, connect points of equal value for a particular variable, such as temperature, pressure, or elevation. In this work, density (ρ) and electrical conductivity (μ) isolines were used.

Binary and ternary mixtures in the monophasic region (under the solubility curve, previously determined) were prepared. After being stirred in a vortex for 30 s to ensure homogeneity, density and electrical conductivity were measured in duplicate. In order to estimate the value of μ or ρ at points where no data is available, data was fitted to third grade polynomials with respect to each composition, *i.e.* a polynomial of the form $\sum_{i=1}^{3} \sum_{j=1}^{n_{\mathrm{species}}} k_{ij} w_j^i$, by minimising E_{RMSE}, as it is common in literature and in the research group [105]. The degree of the polynomial was first verified by performing an *F*-test, then the accuracy

of the isolines was evaluated by assessing two performance indicators: E_{RMSE} (equation (3.4)) and the determination coefficient, R^2 (equation (3.5)).

$$R^2 = \frac{(n_{\mathrm{points}} \sum_{i=1}^{n_{\mathrm{points}}} X_i Y_i - \sum_{i=1}^{n_{\mathrm{points}}} X_i \cdot \sum_{i=1}^{n_{\mathrm{points}}} Y_i)^2}{(n_{\mathrm{points}} \sum_{i=1}^{n_{\mathrm{points}}} X_i^2 - \left(\sum_{i=1}^{n_{\mathrm{points}}} X_i\right)^2 \cdot (n_{\mathrm{points}} \sum_{i=1}^{n_{\mathrm{points}}} Y_i^2 - \left(\sum_{i=1}^{n_{\mathrm{points}}} Y_i\right)^2} \tag{3.5}$$

where, similarly to equation (3.4), n_{points} is the number of points, X is the independent variable and Y is the dependent variable.

The next step was to determine the tie-line compositions, for which feed compositions were selected in the biphasic region.

10 g of feed were prepared in vials, by pipetting and measuring the mass of the compounds. The vials were capped and sealed, and the feed ternary mixtures were stirred for 6 h at 298.15 K, then settled overnight (approximately 12 h) at the same temperature. This ensured that the mixtures parted into a top and a bottom phase, which were separated using an Eppendorf Multipipette E3x. Mass, UV-Vis absorbance spectra from 200 to 600 nm, pH, electrical conductivity, and density of each phase were measured using the equipment described above.

The top and bottom phases' compositions were determined by, simultaneously: minimising the difference between the experimental (exp) and calculated (calc) physical properties (density (ρ) and electrical conductivity (μ), equations (3.6) and (3.7) respectively), minimising the deviation from the mass balance in each phase (equation (3.8)), and verifying that the sum of all mass fractions relative to the same phase (w_i) equals unity (equation (3.9)). This was done iteratively using Excel's Solver functionality.

$$\rho_{\mathrm{exp}} - \rho_{\mathrm{calc}} = 0 \tag{3.6}$$

$$\mu_{\mathrm{exp}} - \mu_{\mathrm{calc}} = 0 \tag{3.7}$$

$$m_{i,\mathrm{feed}} w_{i,\mathrm{feed}} - w_{i,\mathrm{T}}\, m_{\mathrm{T}} - w_{i,\mathrm{B}}\, m_{\mathrm{B}} = 0 \tag{3.8}$$

$$\sum w_i - 1 = 0 \tag{3.9}$$

where m is the mass of the phase, and F, T and B are the feed mixture, top and bottom phase, respectively.

Lastly, the tie-line length (TLL) and slope (STL) were calculated, using equations (3.10) and (3.11), respectively.

$$\mathrm{TLL} = \sqrt{(w_1^{\mathrm{T}} - w_1^{\mathrm{B}})^2 + (w_2^{\mathrm{T}} - w_2^{\mathrm{B}})^2} \tag{3.10}$$

$$\mathrm{STL} = \frac{w_2^{\mathrm{T}} - w_2^{\mathrm{B}}}{w_1^{\mathrm{T}} - w_1^{\mathrm{B}}} \tag{3.11}$$

Several empirical correlations are often used to establish a relation between the mass fractions in the ternary system, the most widely used being the ones proposed by Othmer-Tobias [133], equation (3.12), and by Bancroft and Hubbard [134], equation (3.13).

$$\ln\left(\frac{1 - w_1^{\mathrm{T}}}{w_1^{\mathrm{T}}}\right) = k_{\mathrm{OT}} + n_{\mathrm{OT}} \ln\left(\frac{1 - w_2^{\mathrm{B}}}{w_2^{\mathrm{B}}}\right) \tag{3.12}$$

$$\ln\left(\frac{w_3^{\mathrm{B}}}{w_2^{\mathrm{B}}}\right) = k_{\mathrm{BH}} + r_{\mathrm{BH}} \ln\left(\frac{w_3^{\mathrm{T}}}{w_1^{\mathrm{T}}}\right) \tag{3.13}$$

where k_{OT}, n_{OT}, k_{BH} and r_{BH} are adjustable parameters, and $\ln$ is the natural logarithm.

3.3.4 Partition of pharmaceuticals in ATPS

Before performing a partition in an ATPS, several steps must be followed, as shown in Fig. 3.2.

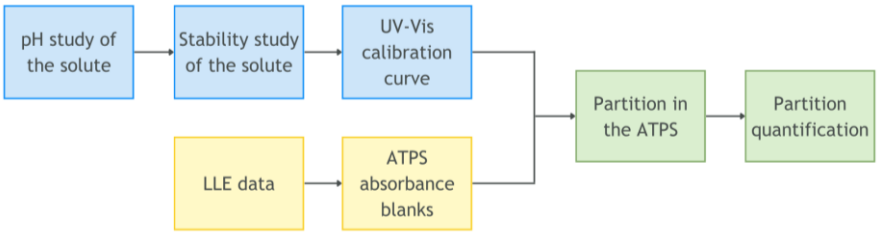

Fig. 3.2. Flowchart of the procedure for partition studies in ATPS.

▶ **pH study**

After selecting the solute, a pH study was performed. For this, the negative base-10 logarithm of the solute's acid dissociation constant ($\mathrm{p}K_{\mathrm{a}}$) values were found in literature and the solute's mean charge evolution with pH was calculated. For each $\mathrm{p}K_{\mathrm{a}}$ value that a species possessed, a proton (H^+) can be donated to its surroundings, thus leading to different charged stages of the solute. The ratio between two successive stages of the solute can be determined for a given value of the phase's pH, using equation (3.14) [66-68]:

$$\frac{\left[\mathrm{S}^{q_0-(i-1)}\right]}{\left[\mathrm{S}^{q_0-i}\right]} = 10^{\mathrm{pH}_\varphi - \mathrm{p}K_{\mathrm{a}}^i} \tag{3.14}$$

where S stands for the solute, q_0 is the initial electrical charge at $\mathrm{pH} = 0$, pH_φ denotes the pH of phase φ and $\mathrm{p}K_{\mathrm{a}}^i$ is the $\mathrm{p}K_{\mathrm{a}}$ relative to the stage i. The index i ranges from 0 to the maximum number of protons the species can donate, *i.e.*, the number of dissociation constants. $\left[\mathrm{S}^{q_0-(i-1)}\right]$ and $\left[\mathrm{S}^{q_0-i}\right]$ are the mole concentrations of the solute with electrical charges equal to $q_0 - (i-1)$ e and $q_0 - i$ elementary charges (also denoted e, $1.602 \cdot 10^{-19}$ C).

The mean electrical charge $\bar{q}$ of a solution can be calculated by relating the relative abundances of each charged stage of the solute and their respective charge, applying equations (3.15) and (3.16) [66-68].

$$\bar{q} = \sum_{i=1}^{i_{\max}} \left(x_{\mathrm{S}^{q_0-(i-1)}} \cdot \left(q_o - (i-1)\right)\right) + \left(1 - \sum_{i=1}^{i_{\max}} \left(x_{\mathrm{S}^{q_0-(i-1)}}\right)\right) \cdot \left(q_0 - i_{\max}\right) \tag{3.15}$$

$$x_{\mathrm{S}^{q_0-(i-1)}} = \frac{\left[\mathrm{S}^{q_0-(i-1)}\right]}{\left[\mathrm{S}^{q_0-i}\right]} \left(\frac{\left[\mathrm{S}^{q_0}\right]}{\left[\mathrm{S}^{q_0-1}\right]} + 1 + \sum_{j=2}^{i_{\max}} \left(\prod_{k=2}^{j} \frac{\left[\mathrm{S}^{q_0-k}\right]}{\left[\mathrm{S}^{q_0-(k-1)}\right]}\right)\right) \tag{3.16}$$

In equations (3.15) and (3.16), $x_{\mathrm{S}^{q_0-(i-1)}}$ is the fraction of molecules of species S with an electrical charge of $q_0 - (i-1)$ e and $i_{\max}$ the maximum number of protons the species can donate.

▶ **Stability study of the solute**

Following the study of the distribution of charges and according to previous works of the research group [66-69], the stability over time of the solute's UV-Vis absorbance spectrum was studied at different pH

values, either at conditions near integer values of the mean charge $\bar{q}$ (to allow determining the UV-Vis absorbance spectra of each differently-charged antioxidant species) or near the known pH values of the chosen ATPS (to analyse a distribution of antioxidant species which is similar to the future extractive conditions). For this, an aqueous stock solution was prepared at the maximum measurable concentration (*i.e.*, the maximum concentration at which the UV-Vis spectrophotometer did not saturate). In this case, concentrations of $1.5 \cdot 10^{-4}$ g·mL^{-1} for amoxicillin, $1.5 \cdot 10^{-4}$ g·mL^{-1} for acetaminophen, and $1.8 \cdot 10^{-3}$ g·mL^{-1} for salicylic acid were chosen. These concentrations are also close to the ones measured in the influent of a wastewater treatment plant in Leiria, Portugal: 0.683 μg·L^{-1} for acetaminophen and 1.099 μg·L^{-1} for salicylic acid (amoxicillin was not detected in the studied influents) [17].

The pH was adjusted using either a 0.5 M aqueous solution of acetic acid or NaOH. Then, the UV-Vis absorbance spectrum of each solution was measured at the day the solutions were prepared and 3 days after, to verify whether the solute's absorbance spectrum and intensity were maintained after 3 days of settling.

- **Determination of the blanks of the ATPS**

For each ATPS used in this work, the system's blanks must be determined before performing the solute partitioning. For this, aqueous solutions of salts and polymers were prepared, and solvents (IL, EL and water) were used directly. Then, 10 g of feed were prepared in vials, according to the known tie-lines, by pipetting and measuring the mass of the compounds. The vials were capped and sealed, and the feed ternary mixtures were stirred for 6 h at 298.15 K, then settled overnight (around 12 h) at the same temperature. This allowed for the separation of top and bottom phases, which were separated using an Eppendorf Multipipette E3x. Mass, UV-Vis spectra from 200 to 600 nm, pH and density of each phase were measured using the previously described equipment.

- **Calibration curve of the solute**

The calibration curve of the solute must be determined at the system's pH (reported in literature or measured in the blanks) and having in mind an optimal concentration of solute. This concentration is limited by the solute's solubility in water and the useful range in the spectrophotometer (it should be the highest concentration possible, at which the instrument does not saturate). A stock solution of solute was prepared, and its pH was adjusted to the ATPS's pH. This solution was then left to settle overnight, so as to ensure that the curve was done roughly 24 h after preparing the solution, hence simulating the duration of a partition.

Solutions with different known concentrations were prepared by diluting the stock solution in 5 mL vials, yielding 2 mL solutions. Vials were capped, sealed, and stirred, after which 200 μL were pipetted with an Eppendorf Multipipette E3x on a Greiner bio-one polystyrene flat bottom plate with 96 wells. An absorbance scanning was carried out with the Thermo Scientific Varioskan Flash UV-Vis spectrophotometer, from 200 to 600 nm. For each solute, the wavelength of a local maximum of UV-Vis spectra ($\lambda_{\max}$) was chosen, provided that the other species in the ATPS did not absorb at that wavelength.

Finally, the water and plate absorbance were subtracted to the absorbance of each solution, the resulting absorbance at $\lambda_{\max}$ was plotted against the solute's concentration and the data were fitted to a first-degree polynomial.

- **Partition of the solute**

Analogously to the preparation of the ATPS blanks, aqueous solutions of salts and polymers needed were prepared, and solvents (IL, EL and water) were used directly. A concentrated stock solution of solute was prepared, and its pH was adjusted to the ATPS's pH. Then, 10 g of feed were prepared in vials, according to the known tie-lines' compositions, but replacing 1 mL of water with the solute's stock solution. The remaining procedure was carried out identically to the one described above.

- **Analysis of the results**

Afterwards, in order to evaluate the extractions carried out, losses in the partition and performance indicators were calculated.

Mass losses (L_{m}) in the phase separation were calculated as:

$$L_{\mathrm{m}} = \frac{m_{\mathrm{T}} + m_{\mathrm{B}} - m_{\mathrm{feed}}}{m_{\mathrm{feed}}} \cdot 100\ \% \tag{3.17}$$

where m_{feed}, m_{T} and m_{B} are the masses of feed, top phase, and bottom phase, respectively.

After measuring the absorbance of each phase and subtracting the corresponding blank, the solute's calibration curve was used to determine its concentration. These concentrations were used to calculate the partition coefficients (K), which are defined as the ratio between the solute concentration in top and bottom phases (C_j^{T} and C_j^{B}, respectively), and were calculated according to equation (3.18).

$$K_j = \frac{C_j^{\mathrm{T}}}{C_j^{\mathrm{B}}} \tag{3.18}$$

The volume of each phase φ was calculated for each tie-line j using the measured masses and densities, following equation (3.19). The calculated volumes were then used to determine the solute losses (L_{s}) and the extraction efficiencies (E) of the partition, for each tie-line j, using equation (3.20) and (3.21).

$$V_j^{\varphi} = \frac{m_j^{\varphi}}{\rho_j^{\varphi}} \tag{3.19}$$

$$L_{\mathrm{s},j} = \frac{C_j^{\mathrm{T}} V_j^{\mathrm{T}} + C_j^{\mathrm{B}} V_j^{\mathrm{B}} - m_{\mathrm{s,feed},j}}{m_{\mathrm{s,feed},j}} \cdot 100\ \% \tag{3.20}$$

$$E_j = \frac{C_j^{\mathrm{T}} V_j^{\mathrm{T}} + C_j^{\mathrm{B}} V_j^{\mathrm{B}}}{m_{\mathrm{s,feed},j}} \cdot 100\ \% \tag{3.21}$$

where V_j^{φ} is the volume of phase φ in tie-line j, m_j^{φ} and ρ_j^{φ} are the phase's mass and density, and $m_{\mathrm{s,feed},j}$ is the mass of solute, present in 1 mL of added stock solution, as explained before. The maximum value of the extraction efficiency is the sum of E and solute losses for that tie-line, as equation (3.22) shows.

$$E_{\mathrm{max},j} = E_j + L_{\mathrm{s},j} \tag{3.22}$$

3.4 Thermodynamic modelling

As previously mentioned, a MATLAB script was developed for the thermodynamic modelling. In this work, the PDH+UNIQUAC (described in section 2.4) was employed, seeing that the research group had previous

experience with this model [76,104-107]. Nonetheless, improvements were tested: in section 3.4.1, the novelty in the chosen approach will be detailed, whereas in section 3.4.2 the applied algorithm will be presented.

3.4.1 A novel approach for the lattice coordination number

The lattice coordination number influences the UNIQUAC model at two different levels. Z is used in equation (2.13), where it has a linear influence in the activity coefficient's natural logarithm. Moreover, the term $Z/2$ also appears in the exponential factor (equation (2.5)). However, it is often omitted in literature, as parameters τ_{ij} or u_{ij} are fitted in modelling without taking into consideration this parameter since U_{ij} are often replaced by the expression presented in equation (3.23) [101].

$$u_{ij} = \frac{Z}{2}(U_{ij} - U_{jj}) \tag{3.23}$$

Due to its physical significance in physical chemistry, Z can vary between 6 and 12. However, in UNIQUAC, it is usually set to 10. This value was chosen by Abrams and Prausnitz in the model's original paper [101] as a coordination number for a state between the solid and gas states. This means that the same value is adopted for compounds of different nature, with varied sizes and polarities.

Kontogeorgis and Folas [103] highlighted that local composition models, including UNIQUAC, have problems due to the use of a fixed coordination number. Thus, taking all this into consideration, a novel approach was developed in this work.

Following the reasoning applied in the NRTL model [103,116], the non-randomness factor (α) was inserted in the UNIQUAC model. This parameter is a dimensionless number that measures the randomness of a mixture, and varies between 0 and 1 (only taking the value of 0 for completely random mixtures) [103].

According to the NRTL model, the coordination number is closely related with α, with many reporting a proportionality between $Z/2$ and $1/\alpha$. Hence, the non-randomness factor was inserted in the PDH+UNIQUAC model, according to the following arbitrated expression:

$$Z = 2/\alpha \tag{3.24}$$

The non-randomness factor of each component was predicted using a geometric approach, based on the polarity of chemical bonds. First, the geometry of the molecule was optimised using Density Functional Theory (DFT). The cartesian coordinates of each atom, as well as the respective electrical charge, were obtained from the optimised geometry, which then allowed to determine the bonds' lengths.

Using the data returned by the Gaussian software (cartesian coordinates and charges of each atom for the optimised geometry), MATLAB codes were developed by the author so as to apply the following reasoning.

The overall dipole moment of the molecule was evaluated as a way to measure its polarity, or asymmetry ($\vec{A}$, expressed in Debye), and was calculated according to:

$$\vec{A} = \sum_{i}^{n_{\text{bonds}}} \left((\delta q_i - \delta q_j) \cdot \vec{d}_{ij} \right) \tag{3.25}$$

where δq_i and δq_j are the partial charges of the bonded atoms (i, j), obtained from DFT calculations, and $\vec{d}_{ij}$ is the distance vector between the two atoms along the 3 axes (x, y, z). Therefore, the asymmetry $(\vec{A})$ can be written as a function of the three unitary vectors of each cartesian axis, as shown in equation (3.26):

$$\vec{A} = a\,\vec{\imath} + b\,\vec{\jmath} + c\,\vec{k} \tag{3.26}$$

The non-randomness factor of the molecule was estimated using equation (3.27):

$$\alpha = \sqrt{\left(\left(\frac{a}{\vec{A}_{\max,x}}\right)^2 + \left(\frac{b}{\vec{A}_{\max,y}}\right)^2 + \left(\frac{c}{\vec{A}_{\max,z}}\right)^2\right) \cdot \frac{1}{3}} \tag{3.27}$$

where $\vec{A}_{\max,x}$, $\vec{A}_{\max,y}$ and $\vec{A}_{\max,z}$ denote the maximum value of the asymmetry along the x, y and z axes, respectively. The formula for the term $\vec{A}_{\max,x}$ is shown on equation (3.28), the other two being analogous. Coefficients a, b, c come from equation (3.26).

$$\vec{A}_{\max,x} = \sum_i^{n_{\text{bonds}}} (\delta q_i - \delta q_j) \left|\vec{d}_{ij}\right|_x \tag{3.28}$$

where $\left|\vec{d}_{ij}\right|_x$ is the absolute value of the distance along the x axis.

The mixture's non-randomness factor (α_{mixture}) is calculated with the mixing rule of equation (3.29), which allows to calculate a Z for the mixtures with equation (3.24).

$$\alpha_{\text{mixture}} = \sum_{i=1}^{n_{\text{species}}} \alpha_i x_i \tag{3.29}$$

where α_i is the non-randomness factor and x_i are the mole fractions.

Each binary pair's non-randomness factor (α_{ij}) is calculated according to equation (3.30). As can be seen, it is not dependent on the mixture's composition, as it is used to estimate the interaction between each pair of components. In fact, this value will be used to calculate the Z for binary interactions in equation (3.23).

$$\alpha_{ij} = (\alpha_i + \alpha_j)/2 \tag{3.30}$$

In closing, this method allows to calculate the lattice coordination number (Z) in UNIQUAC, taking into account the species in solution, as opposed to attributing the value of 10 regardless of the composition.

3.4.2 Application of PDH+UNIQUAC

The novel method, described in section 3.4.1, was first validated, using for this LLE data of ternary systems composed only of neutral species. Hence UNIQUAC was used without considering the PDH term, since there were no electrolytes in solution. The objective of this validation was to assess if the modelling using the Z calculated as a function of α (equation (3.24)) was better than using $Z = 10$.

Validation was carried out by modelling the same LLE data with UNIQUAC with the calculated coordination number, and UNIQUAC with $Z = 10$. The values of standard deviation of modelled data from the LLE data reported in literature were calculated according to:

$$\sigma = \sqrt{\frac{\sum_{i=1}^{n_{\text{points}}} \sum_{j=1}^{n_{\text{species}}} \sum_{k=1}^{2} \left(x_{i,j_{\text{calc}}}^k - x_{i,j_{\text{exp}}}^k\right)^2}{2\, n_{\text{points}}\, n_{\text{species}}}} \tag{3.31}$$

where $x^{k}_{i,j\,\mathrm{calc}}$ and $x^{k}_{i,j\,\mathrm{exp}}$ are, the mole fraction of component i in phase k on the point j of the data set calculated and reported in literature, respectively, n_{points} is the number of points and n_{species} is the number of species in solution.

If the LLE modelling using the calculated coordination number displayed a lower standard deviation than UNIQUAC using the "traditional" value of $Z = 10$, then this novel method was considered validated. The adopted procedure is schematised in Fig. 3.3.

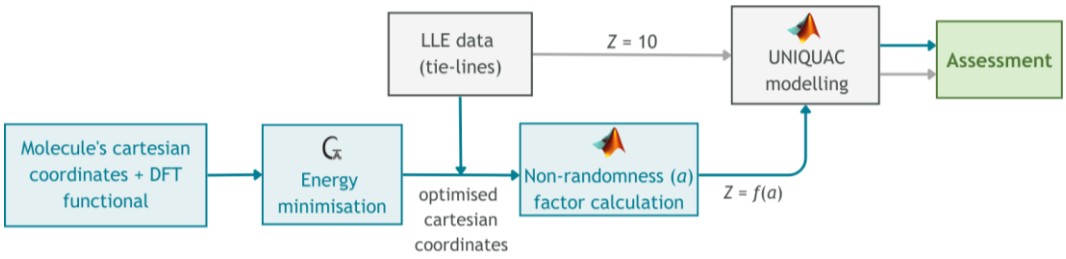

Fig. 3.3. Validation algorithm of the novel non-randomness calculation method.

Consequently, the method was applied to the ternary systems with electrolytes studied in this work. Since UNIQUAC was not originally developed for electrolytes, salts were considered to be in their molecular form (as neutral species), and thus their geometry is optimised in this form. Hence, their non-randomness factor, α, and coordination number, Z, were only calculated for neutral species, as the dissociation of salts was only considered in the PDH term. Fig. 3.4 presents the applied algorithm.

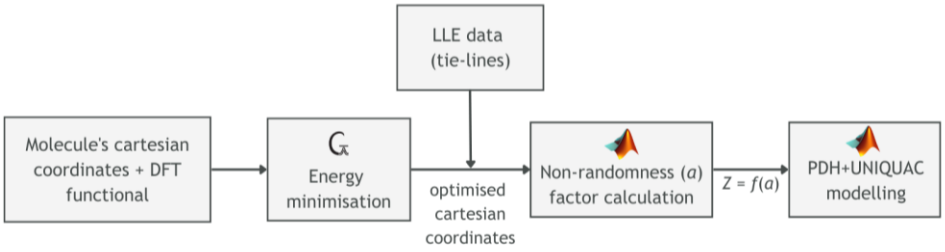

Fig. 3.4. Algorithm for the application of the new non-randomness calculation method in thermodynamic modelling.

In order to calculate α for the validation and the application of this methodology, computations were performed at DFT level of theory to get the optimised geometry using Gaussian software. In this work, a combination of the DFT hybrid functional B3LYP ([127,128]) with the basis set 6-311++G ([129]) were considered and solvation according to the Polarizable Continuum Model (PCM). For this, in the validation step, neutral solvents were considered to be in a cavity within the solvent reaction field, composed of solvent molecules of their own. In order to create the cavity of solvent molecules, it was necessary to compile dielectric constants, refractive indices, densities, and molar masses of each species, as described in Annex B.2. In addition, a population analysis was performed after the geometry optimisation, using Natural Bond Orbital (NBO), so as to determine atomic charge distribution. In the case of ternary systems with salts, PCM was only applied to solvents.

Then, using the optimised geometry, the procedure described in section 3.4.1 was applied and α were calculated for all species.

4 Liquid-liquid equilibria

In this chapter, the attained results regarding Liquid-Liquid Equilibria (LLE) of novel choline-based systems will be shown and fitted to correlations, as described in section 3.3.3. Then an innovative thermodynamic modelling approach will be validated and applied to these systems.

4.1 Liquid-Liquid Equilibria (LLE) of ternary systems

In this work, the immiscibility of a total of 11 systems, shown in Table 4.1, was tested. The tested ranges of compositions and the experimental mass fractions of the points in the solubility curves can be found in Appendix A1 (Tables A1.1 and A1.2 respectively).

Table 4.1. Ternary systems {ethyl lactate (EL) or polyethylene glycol (PEG) or polyvinylpyrrolidone (PVP) (1) + choline salt (2) + water (3)} studied in this work, at 298.15 K and 0.1 MPa.

Components	Ethyl lactate (EL)	Polyethylene glycol 1500 (PEG1500)	Polyethylene glycol 4000 (PEG4000)	Polyvinyl pyrrolidone 29 000 (PVP29000)
Choline chloride ([Ch]Cl)	×		×	×
Choline bitartrate ([Ch]Bit)	✓	✓	✓	×
Choline di-hydrogen citrate ([Ch]DHCit)	✓	✓		×
Choline bicarbonate ([Ch]Bic)	✓			

✓ denotes immiscibility of components (existence of LLE), whereas × indicates that the phases are totally miscible in the assessed range of concentrations.

Mourão *et al.* [135] report LLE data for the system {PEG4000 (1) + [Ch]DHCit (2) + water (3)}. Moreover, it has been stated that the system {PEG1500 (1) + [Ch]Cl (2) + water (3)} undergoes phase separation, yet the bottom phase was instantly jellified, and within 24 hours both phases solidified [136]. As best of the author's knowledge, there were no reports of other EL-based systems containing choline salts, so these systems were being studied first-hand in this work.

In Fig. 4.1, the solubility curves for the six choline-based systems determined in this work are plotted.

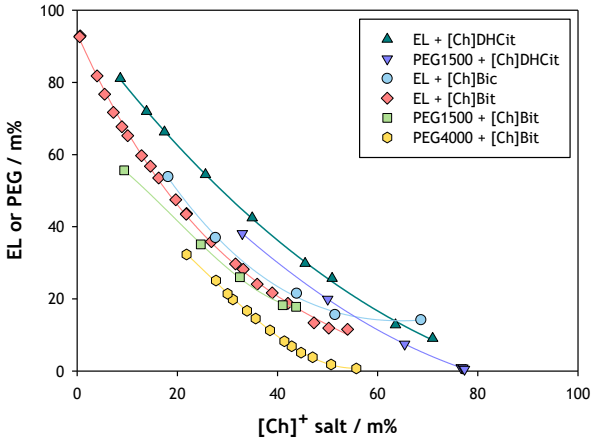

Fig. 4.1. Solubility curves determined in this work at 298.15 K and 0.1 MPa.

Furthermore, data of the solubility curves was then fitted to the Merchuk [130], Li [131], and Yu [132] correlations (equations (3.1) to (3.3)), by minimisation of the Root Mean Squared Error (E_{RMSE}, equation (3.4)). For each system, the optimised parameters are shown in Table A3.1 of Appendix A3. For the systems {EL (1) + [Ch]Bit or [Ch]Bic (2) + water (3)}, the Li fittings showed a smaller error and R^2 closer to unity, while for the system {EL (1) + [Ch]DHCit (2) + water (3)}, the model proposed by Merchuk resulted in the best fitting to the experimental data. For the system based on PEG4000 and [Ch]Bit and for the two systems containing PEG1500, the Li correlation had the best performance.

Several systems based on PEG with different average molar masses and choline salts/ILs were found on the literature. Comparison between the new solubility curve for the system {PEG4000 (1) + [Ch]Bit (2) + water (3)} and the ones previously reported can be seen in Fig. 4.2 and Fig. 4.3. While Fig. 4.2 compares the influence of PEG with different molar masses on the solubility curves of systems containing choline bicarbonate, Fig. 4.3 shows the effect of different anions in choline-based salts or ILs in the solubility curves of ternary systems with PEG4000.

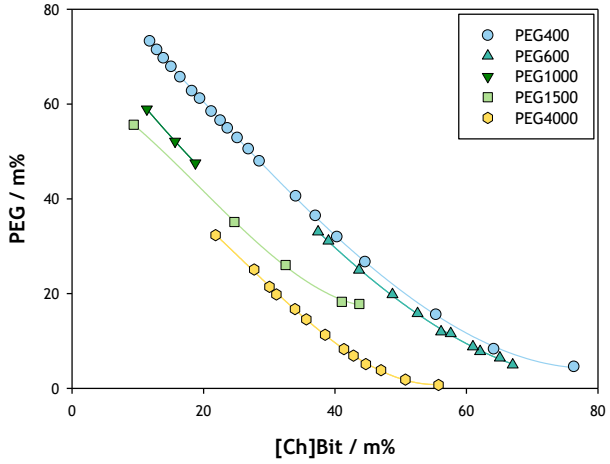

Fig. 4.2. Comparison between solubility curves of ternary systems composed of PEG with different molar masses and choline bitartrate, at 298.15 K and 0.1 MPa: {PEG400 [137] or PEG600 [137] or PEG1000 [137] or PEG1500 (this work) or PEG4000 (this work) (1) + [Ch]Bit (2) + water (3)}.

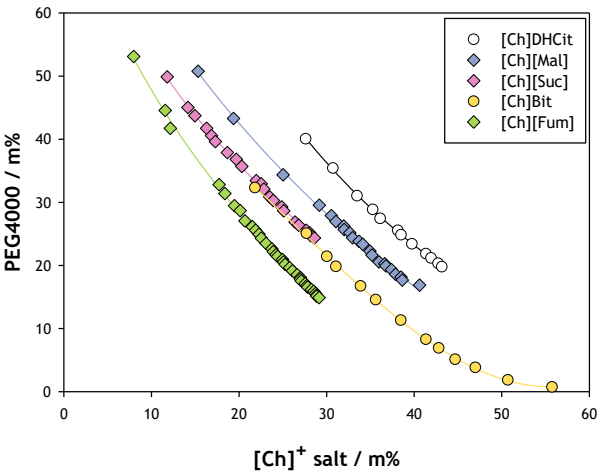

Fig. 4.3. Comparison between solubility curves of ternary systems composed of {PEG4000 (1) + choline salts (●) or ILs (♦) (2) + water (3)} at 298.15 K and 0.1 MPa: cholinium malonate ([Ch][Mal]) [135], cholinium succinate ([Ch][Suc]) [135], cholinium fumarate ([Ch][Fum]) [135], [Ch]DHCit [135] and [Ch]Bit (this work).

Analysing Fig. 4.2, it can be suggested that the higher the molar mass of PEG, the closer the solubility curve is to the origin of the phase diagram, for systems containing choline bitartrate. This means that lower concentrations of each component are required in order to attain the immiscible region and form the ATPS. This is due to the fact that PEG with lower molar masses have shorter alkyl chain lengths and higher solubilities in water, in the presence of [Ch]Bit, since the monomer (ethane-1,2-diol) is non-polar. Similarly, when comparing the two systems with conventional salts in Fig. 4.3 ([Ch]Bit and [Ch]DHCit), it can be seen that lower concentrations of PEG4000 and [Ch]Bit are required to induce phase separation than in the system containing [Ch]DHCit, as the solubility curve of the system with the bitartrate anion is closer to the origin than the solubility curve of the citrate system. A definite trend cannot be postulated when comparing the novel system, {PEG4000 (1) + [Ch]Bit (2) + water (3)}, to CAAIL-based ternary systems (Fig. 4.3), as their solubility curves are in similar positions. For the anions, van der Waals volumes and surface areas were calculated (Table B1.2 in Appendix B) with Bondi's method, but they allowed no conclusion.

The system {EL (1) + [Ch]Bit (2) + water (3)} was selected for further studies, as its solubility curve presented suitable area and shape. Isolines of density and electrical conductivity of the homogeneous zone were determined, leading to the following correlations for these thermophysical properties (Table 4.2).

Table 4.2. Polynomial expressions (isolines) for density and electric conductivity as a function of the composition for the ternary system {EL (1) + [Ch]Bit (2) + water (3)} at 298.15 K and 0.1 MPa, and respective relative errors and determination coefficients (R^2).

	Density (ρ, in $\mathbf{g \cdot cm^{-3}}$) isoline					Electrical conductivity (μ, in $\mathbf{mS \cdot cm^{-1}}$) isoline				
	$A_1\, w$	$B_1\, w^2$	$C_1 w^3$	relative error*	R^2	$A_1\, w$	$B_1\, w^2$	$C_1 w^3$	relative error*	R^2
EL (1)	1.071	-0.1567	0.1222			-99.22	163.83	-64.61		
Salt (2)	1.247	0.0120	0.0629	$6.69 \cdot 10^{-4}$	0.9995	90.92	-210.64	111.19	0.229	0.9859
Water (3)	1.134	-0.2378	0.0995			34.52	30.37	-64.88		

*The average relative error of property k was calculated by: $\frac{1}{n_{\text{points}}} \cdot \sum \frac{|k_{\text{exp}} - k_{\text{calc}}|}{k_{\text{exp}}}$

Isoline data and plots for density and electrical conductivity can be found in Appendix A4. *F*-tests were performed to these isolines: the critical value of *F* was superior to the *F* value of the data sets, so the proposed regressions were validated.

With these correlations, it was possible to apply equations (3.6) to (3.9) and determine three tie-lines (TL) and their phase equilibrium compositions, yielding the experimental mass fractions, tie-line lengths (TLL) and slope (STL) seen in Table 4.3. The complete ternary diagram can be seen in Fig. 4.4. TL numbering was done so as to ensure that the longest tie-line (the one with the highest value of TLL) always corresponded to the one with the lowest index, keeping the trend observed in the literature data presented in Annex C, so as to simplify result analysis.

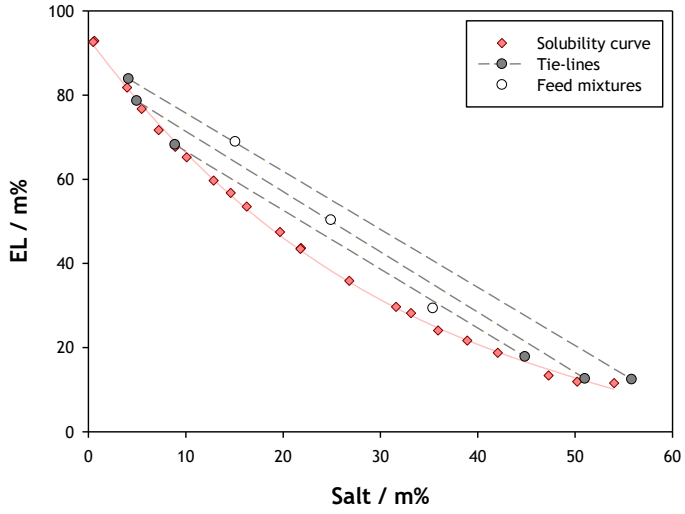

Fig. 4.4. Solubility curve and tie-lines of the novel system {EL (1) + [Ch]Bit (2) + water (3)}, at 298.15 K and 0.1 MPa.

Table 4.3. Phase equilibrium compositions (mass fractions), tie-line lengths (TLL) and slopes (STL) for the system {EL (1) + [Ch]Bit (2) + water (3)} at 298.15 K and 0.1 MPa.

Tie-line (TL)	$w_{1,\text{F}}$ [a]	$w_{2,\text{F}}$	$w_{1,\text{T}}$	$w_{2,\text{T}}$	$w_{1,\text{B}}$	$w_{2,\text{B}}$	TL Slope (STL)	TL Length (TLL) / m%
TL1	0.2940	0.3536	0.6829	0.0886	0.1788	0.4482	-1.40	101.53
TL2	0.5039	0.2488	0.7869	0.0494	0.1267	0.5098	-1.43	107.12
TL3	0.6899	0.1505	0.8391	0.0409	0.1250	0.5578	-1.38	113.49

[a] Indices F, T and B stand for the feed solution, top and bottom phases, respectively.

The three tie-lines presented a similar slope (STL) and were nearly parallel. Tie-line lengths (TLL) increased with the increase in EL and decrease in salt in the initial feed mixtures. By extrapolating the tie-line compositions ($w_{1,\mathrm{T}}$ and $w_{2,\mathrm{B}}$) and using the best fitting for each system, the critical point was calculated. A plot with the method applied as well as the critical point can be found in Appendix A4 (Fig. A4.3). The composition of the critical point of this ATPS is $w_1 = 0.2443$ and $w_2 = 0.3944$.

Additionally, as it is common in literature, tie-line phase equilibrium compositions were fitted to the Othmer-Tobias [133] and the Bancroft and Hubbard [134] correlations (equations (3.12) and (3.13), respectively). The optimised parameters are presented in Table 4.4.

Table 4.4. Parameters obtained using Othmer–Tobias (OT) and Bancroft-Hubbard (BH) equations and respective coefficients of determination (R^2) for the system {EL (1) + [Ch]Bit (2) + water (3)} at 298.15 K and 0.1 MPa.

	Othmer-Tobias			**Bancroft and Hubbard**		
	k_{OT}	n_{OT}	R^2	k_{BH}	n_{BH}	R^2
Parameters	-1.1990	2.0183	0.9969	0.3173	0.4421	0.9689

A satisfactory linearisation was obtained in both cases, although the Othmer-Tobias fitting showed a R^2 closer to unity.

In summary, the novel ternary system {EL (1) + [Ch]Bit (2) + water (3)} determined in this work had three tie-lines, all with a considerable length (superior to 1). This system could be applied in the scope of this work, to extract active pharmaceutical ingredients (APIs). It could also be applied to other extractions, as the top phase is rich in EL and water, and contains less than 10 % of salt. Since the used solvents, EL and water, are easily evaporated at reduced pressure (in a rotary evaporator), after partitioning, the extracted solute could be obtained in its solid state. In the case of vitamins or antioxidants, they would be obtained in an extract also containing a small percentage of choline bitartrate – an organic salt, commonly used as a food additive and possessing lipotropic (increasing the transport of lipids in the organism) and nootropic (facilitating memory and learning, used to prevent dementia) properties [54]. Hence, the obtained extracts could safely be applied in food supplementation, for example.

4.2 Thermodynamic modelling

4.2.1 Validation

A total of 6 ternary systems, with only neutral constituents, were chosen. In order to apply the modelling described before, it was necessary to compile the LLE data (Table BB1.1 of Annex B1), as well as some physical properties of the pure species (dielectric constant, refractive index, density and molar mass, found in Table BB3.1 of Annex B3). For these species, van der Waals volumes and areas were calculated using Bondi's method, then the geometries of the components were optimised, and non-randomness factors were computed for all species. These values can be consulted in Appendix B, in Table B1.1 and Table B2.1, respectively.

From equation (3.24), it can easily be deduced that, in this approach, to the value of $Z = 10$ corresponds $\alpha = 0.2$. For the ternary systems of the validation, the average non-randomness factor was calculated for each phase, following equation (3.29). An overall value was also calculated, as the average of the non-randomness factors of both phases. There values are presented in Table B3.1 of Appendix B3. It can be seen that there were two classes of systems: four systems with $\alpha > 0.2$ and two systems with $\alpha \approx 0.2$.

It was expected that, for systems in which $\alpha \approx 0.2$, the performance of classical UNIQUAC and this methodology were similar. The systems with $\alpha \neq 0.2$ were expected to produce different results.

Modelling of the ternary systems was carried out as described in section 3.4.2. Tables B3.2 through B3.8 of Appendix B3 detail the obtained UNIQUAC binary interaction parameters (u_{ij}) as well as the calculated standard deviation between the modelled compositions and the data from literature.

For the 6 systems, the isoactivity criterion was verified. The standard deviations calculated with UNIQUAC and with the novel methodology were identical, therefore proving that this new approach led to results of similar quality that the traditional UNIQUAC model.

Although the modelling results were already satisfactory without the calculated α (as UNIQUAC is a model that has been vastly used with success), this parameter now allows the models to maintain a geometrical significance behind the values of Z, in particular, regarding the values of the interaction energies. The method for the calculation of α and subsequent application in thermodynamic modelling was thus validated.

4.2.2 Application to the novel ATPS

For the system {EL (1) + [Ch]Bit (2) + water (3)}, determined in this work, PDH+UNIQUAC (a combination of the UNIQUAC model and the Pitzer-Debye-Hückel equation) was used, since the system contained electrolytes. Since the novel approach did not produce better results than the traditional UNIQUAC, both models were used separately: the LLE data was modelled with PDH+UNIQUAC using $Z = 10$, then, following a geometry optimisation of all species in solution, the LLE data was modelled using Z calculated as a function of α.

The overall α was also calculated and showed a slight deviation from the value of 0.2 ($\alpha = 0.1480$). Results can be found in Tables B4.1 and B4.2 of Appendix B4. Both modelling approaches produced identical results, with standard deviations to the known tie-line compositions of $3.2049 \cdot 10^{-17}$, a value very close to zero. Fig. 4.5 represents a plot of the two models' results. The results were once again coherent between both models used and showed that the calculation of α was compatible with modelling using PDH+UNIQUAC.

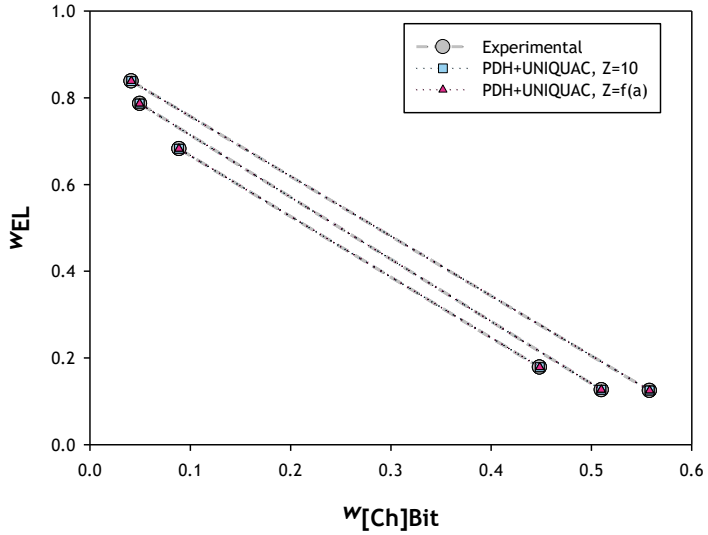

Fig. 4.5. Tie-lines for the ternary system {ethyl lactate (1) + [Ch]Bit (2) + water (3)} at 298.15 K and 0.1 MPa: feed compositions (●), traditional PDH+UNIQUAC modelling (■) and novel PDH+UNIQUAC modelling (▲).

4.2.3 Additional applications

Besides the previously described modelling objectives, the calculated non-randomness factors were applied to the analysis of Fig. 4.3.

In fact, the solubility of each salt or IL in water, as well as their relative polarities, are linked to the relative positions of solubility curves. Since reliable solubilities in water of the salts present in Fig. 4.3 could not be found, each anion's polarity was compared, as anions are the only different species between the compared systems. For this, the reasoning explained in section 3.4.1 was applied to the anions: their geometry was optimised using the hybrid functional B3LYP with the basis set 6–311++G, computing NBO population analysis. Using the optimised coordinates, the non-randomness factor was computed. These values can be found in Table B2.2 of Appendix B.

It can be observed that the solubility curve is closest to the origin of the plot for systems with a high anion non-randomness factor. Therefore, even though this approach does not improve drastically the performance of UNIQUAC or PDH+UNIQUAC modelling, it could become useful in predicting other thermodynamic properties, as it allows to predict relative polarities.

In fact, the non-randomness factor is an important parameter in thermodynamic models, which recent studies have looked into so as to improve its estimation. For instance, there have been efforts to simplify and improve the parameterization of multicomponent phase equilibria modelling (with NRTL for example [138]), which involve trying to estimate the non-randomness factor. Klerk and Schwarz [138] have looked into the influence of parametrising the non-randomness factor (by assigning values between 0.20 and 0.47) and predicting azeotropes for Vapour-Liquid Equilibrium data. The methodology for the calculation of the non-randomness factor described in this work could also be applied to determine azeotropes or improve thermodynamic models, based on this factor, such as the Non-Random Two-Liquid model (NRTL).

In conclusion, this pioneering geometric approach could become a powerful tool to enhance thermodynamic models, particularly in the prediction of multicomponent phase equilibria, and is undoubtedly a major contribution to the field.

5 Partitions of pharmaceuticals in ATPS

In this chapter, results of the performed partitions in choline-based Aqueous Two-Phase Systems (ATPS) will be shown and compared. In this work, partitions of three pharmaceuticals (amoxicillin, acetaminophen, and salicylic acid) were performed in 7 different ATPS containing either Choline Amino Acid Ionic Liquids (CAAILs) or conventional choline salts, by following the procedure described in section 3.3.4.

5.1 Ionic liquid synthesis

Some of the used ternary systems contained Choline Amino Acid Ionic Liquids (CAAILs), which needed to be synthesised prior to application. Pictures of the apparatus can be found in Appendix C (Fig. C1.1 to C1.4). The four ionic liquids cholinium L-alaninate ([Ch][Ala]), cholinium glycinate ([Ch][Gly]), cholinium leucinate ([Ch][Leu]) and cholinium L-serinate ([Ch][Ser]) were successfully synthesised. The obtained products were viscous, pale-yellow liquids, which was consistent with the common appearance of ionic liquids. Additionally, the synthesis was verified by a global agreement between the measured density and the values found in literature, and between the measured Fourier Transform Infrared Spectra (FTIR) and the one predicted by DFT, using hybrid functional B3LYP and the 6-311+G(*,*) basis set.

The plots of density measurements, FTIR and the infrared predicted spectra for [Ch][Ala] are shown below (Fig. 5.1 and Fig. 5.2), while the ones for [Ch][Gly], [Ch][Leu] and [Ch][Ser] are in Appendix C.2. The experimental densities (ρ) were fitted to first-degree polynomials using the least-square method. Tables C2.1 through C2.4 of Appendix C present the predicted frequencies of each FTIR spectra.

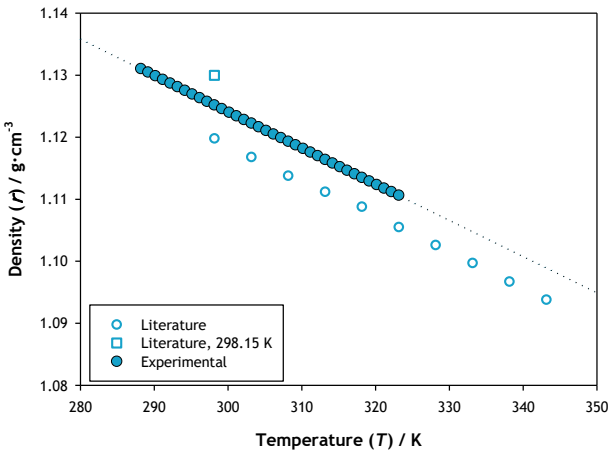

Fig. 5.1. [Ch][Ala] density measurements as a function of temperature and respective linear regression, and comparison with literature data (scanning [56] and at 298.15 K [139]). The first-degree fitting follows the equation: $\rho = 1.299 - 5.843 \cdot 10^{-4} \cdot T$ with $R^2 = 1.0000$.

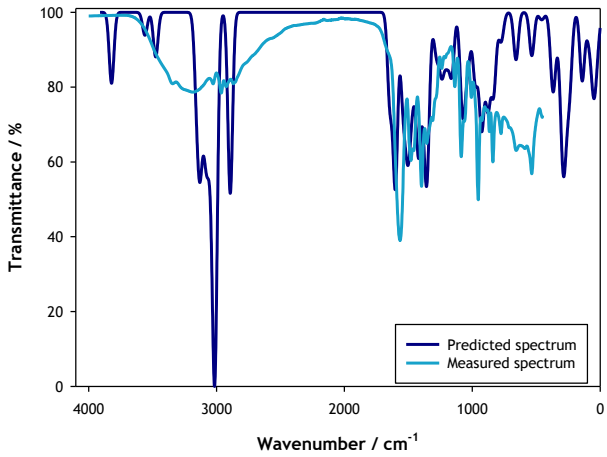

Fig. 5.2. Experimental Fourier Transform Infrared Spectra (FTIR) for cholinium L-alaninate ([Ch][Ala]) and predicted infrared absorption spectra. The intensity of the predicted spectrum's peaks was normalised to the one with the strongest intensity.

As can be seen in Fig. 5.1, the measured density values of cholinium L-alaninate ([Ch][Ala]) were slightly superior to the density scanning data found in literature. This can be explained by a lower water content and lower percentage of impurities in the CAAIL synthesised in this work. Similar conclusions can be drawn regarding ionic liquids [Ch][Gly] and [Ch][Leu], but not from [Ch][Ser]: this CAAIL could have a higher

humidity content. Samples of the four CAAILs were lyophilised, so as to determine their purity, and it was found that all CAAILs had less than 1 % impurities in mass.

The densities of the four CAAILs follow the trend [Ch][Ser] > [Ch][Gly] > [Ch][Ala] > [Ch][Leu], which can be explained by steric effects. In fact, due to the isopropyl functional group, the leucinate anion has the largest steric hindrance, hence the lowest density. On the other hand, the serinate anion had an additional hydroxyl group, compared to the other anions, which allows hydrogen bonding, causing the particles to be more closely packed and the IL to have a higher density.

Regarding Fig. 5.2, the intensity of the peaks of predicted and experimental FTIR spectra could not be compared, as the one from the predicted spectrum is normalised to the peak with maximum intensity. The most intense peak predicted was one at 2893 cm^{-1}, corresponding to the stretching of bonds of the carboxyl group. There were also peaks at 3021, 3013 and 3126 cm^{-1}, which, in the experimental spectrum, were all under the same broad and round band, due to the vibration of the O-H bond of the hydroxyl groups. Theoretically, a strong band at ~3000-3200 cm^{-1} indicated stretching of the N-H bonds of the amino acid. The following most intense peaks were at 1601 cm^{-1} and 1643 $\mathrm{cm}^{-1}$and were due to the bending of the N-H bond in alaninate. The stretching of the C-N bond in both ions was seen by the peak at 1361 cm^{-1}, and the stretching of the C-O bond of cholinium corresponded to the wavenumber of 1069 cm^{-1}. Finally, considerable CH_2 and CH_3 deformation modes (in the 1350 cm^{-1} region) were predicted at 1346 and 1358 cm^{-1}. In conclusion, there was a global agreement in the locations of the peaks.

5.2 Effect of pH in the mean electrical charge

The $\mathrm{p}K_\mathrm{a}$ values of acetaminophen, amoxicillin and salicylic acid are reported in literature [140] and were used to calculate the mean electrical charge $(\bar{q})$ as a function of pH, using equations (3.14) to (3.16) as Fig. 5.3 shows. Seeing that the first $\mathrm{p}K_\mathrm{a}$ of salicylic acid and amoxicillin were close in value (2.78 and 2.60, respectively), the charge distributions of these two species were similar for pH values inferior to 5.

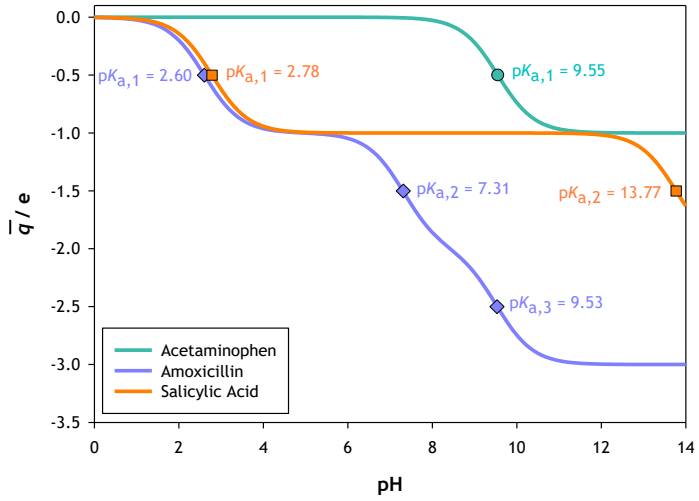

Fig. 5.3. Calculated mean electrical charge $(\bar{q})$ for acetaminophen, amoxicillin, and salicylic acid, expressed in terms of the elementary charge (e, *i.e.*, $1.602{\cdot}10^{-19}$ C).

Tables E.1 to E.2 of Appendix E contain the calculated values of the mean charges as well as the relative abundances of the different stages of the pharmaceuticals.

5.3 Effect of pH in the absorbance spectra

After having determined the mean electrical charges ($\bar{q}$) as a function of pH for the three pharmaceutical compounds, the effect of pH on their UV-Vis absorbance spectra was assessed. For this, solutions with a definite concentration of each solute were prepared, their pH adjusted at different values and absorbance spectra measured. Absorbances were normalised using a ratio of concentrations. Table 5.1 summarises the stability of the UV-Vis absorbance spectra of acetaminophen, amoxicillin and salicylic acid. In Appendix F, the UV-Vis spectra of the solutions at the day of preparation and 3 days after are plotted.

Table 5.1. Stability of the UV-Vis absorbance spectra of acetaminophen (Ac), amoxicillin (Amox) and salicylic acid (SA) after settling for 3 days at 298.15 K and 0.1 MPa.

	pH = 3	pH = 5	pH = 6	pH = 7	pH = 9	pH = 10	pH = 12
Ac	mostly stable	-	stable	stable	stable	-	stable
Amox	stable	stable	-	stable	-	-	stable
SA	mostly stable	-	-	-	-	stable	stable

The chosen ternary systems exhibited pH values in two ranges: systems based on Choline Amino Acid Ionic Liquids (CAAILs) and the system {PEG600 (1) + [Ch]Bic (2) + water (3)} had pH values of ca. 12, while the novel system, containing ethyl lactate (EL) and [Ch]Bit, had a pH of 3-4. It is worth noting that, at pH values of 3 and 12, the UV-Vis absorbance spectra of the three solutes were stable. Due to an increase in absorbance of amoxicillin at pH 12, its spectrum's stability was assessed at a lower concentration.

5.4 Ultraviolet-Visible (UV-Vis) absorbance calibration curves

Before determining the calibration curves, the Ultraviolet-Visible (UV-Vis) spectra of the three pharmaceuticals were assessed at the system's pHs (~4 and 12) so as to determine the wavelength of the local maximum of each UV-Vis spectrum, $\lambda_{\max}$. According to Fig. 5.3, at pH 4, only the neutral form of acetaminophen exists, and only the stages with charge -1 e of amoxicillin and salicylic acid exist in solution. Likewise, at pH 12, only the form of amoxicillin with charge -3 e exists, as well as the stages with charge -1 e of salicylic acid and acetaminophen. The UV-Vis spectra are represented in Fig. 5.4 and Fig. 5.5, as well as the values of the chosen $\lambda_{\max}$ at those pHs.

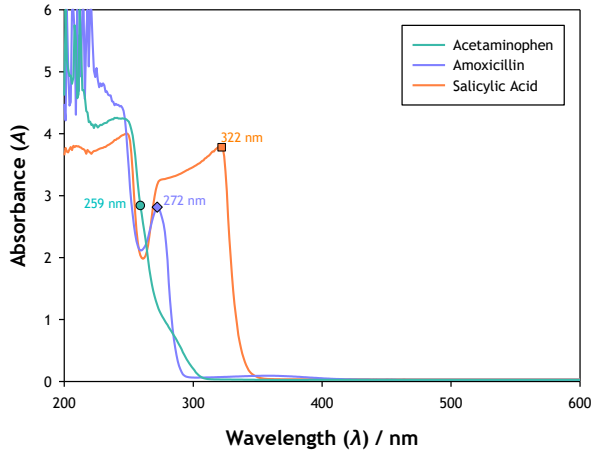

Fig. 5.4. UV-vis absorbance spectra at pH = 3, from 200 to 600 nm, for acetaminophen, amoxicillin and salicylic acid, at $(0.144, 1.66 \text{ and } 1.83) \cdot 10^{-3}$ g · mL^{-1}, respectively.

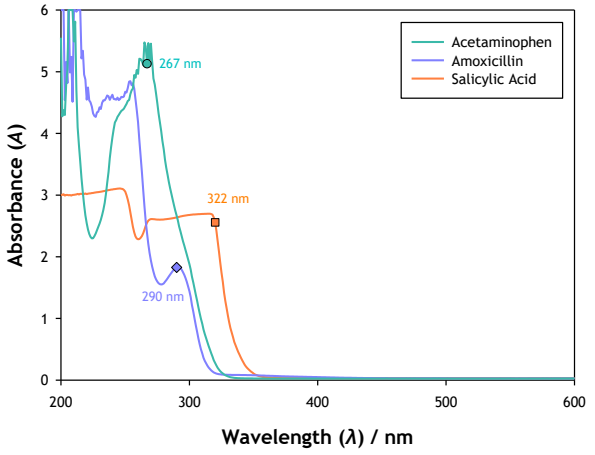

Fig. 5.5. UV-vis absorbance spectra at pH = 12, from 200 to 600 nm, for acetaminophen, amoxicillin and salicylic acid, at $(0.144, 1.66 \text{ and } 0.493) \cdot 10^{-3}$ g · mL^{-1}, respectively.

Observing the UV-Vis absorbance spectra in Appendix D, it is possible to verify that none of the components present in the used ATPS have significant absorbance at the chosen wavelengths. It is also worth noting that for salicylic acid, at pH 12, λ_{max} is slightly inferior to 322 nm and has a value of 317 nm. Despite this, this calibration curve was performed at 322 nm, because the absorbance at this point has a lower variation between pH 12 and lower, as can be observed in Appendix F. For acetaminophen, the wavelengths of 259 nm for pH 3 and 267 nm for pH 12 were chosen, while for amoxicillin the wavelengths of 272 and 290 nm were selected, respectively, for pH 3 and pH 12.

The UV–Vis absorbance spectra of the studied pharmaceuticals varied with pH, as two successive stages may absorb at different wavelengths. Hence it is crucial to have different calibration curves, when different charged stages present different UV-Vis absorbance spectra, so as to ensure a proper solute quantification in partitions.

The calibration curves plotted in Fig. 5.6 and Fig. 5.7, their respective fittings and determination coefficients (R^2) were obtained.

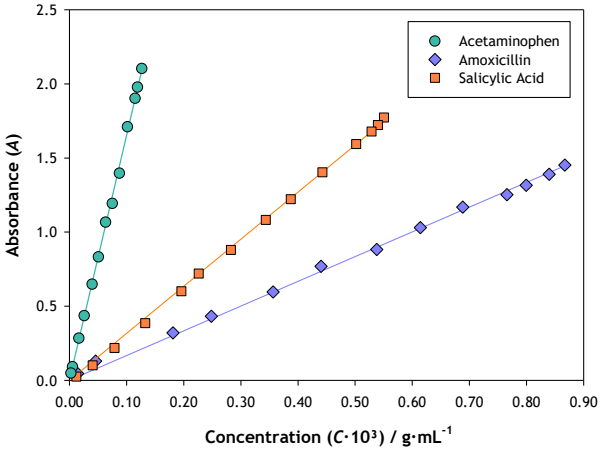

Fig. 5.6. UV-Vis absorbance calibration curves at pH 3 for acetaminophen (259 nm), amoxicillin (272 nm) and salicylic acid (322 nm). The first-degree fittings follow equations: $A = 16\,525.5 \cdot C_{Ac} + 0.00198$ with $R^2 = 0.9991$, $A = 1617.00 \cdot C_{Amox} - 0.0347$ with $R^2 = 0.9989$ and $A = 3244.8 \cdot C_{SA} + 0.0289$ with $R^2 = 0.9988$.

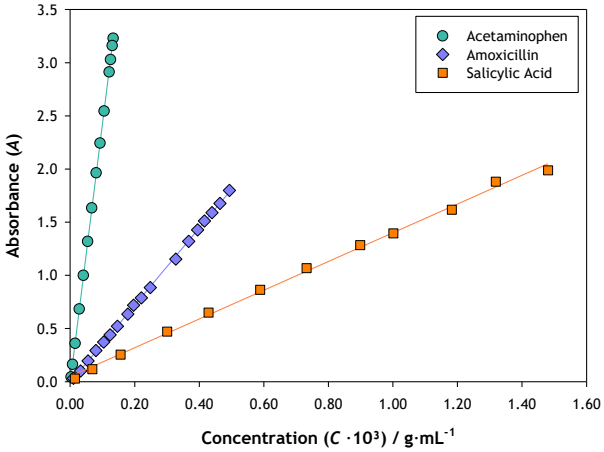

Fig. 5.7. UV-Vis absorbance calibration curves at pH 12 for acetaminophen (265 nm), amoxicillin (272 nm) and salicylic acid (322 nm). The first-degree fittings follow equations: $A = 24\,315.5 \cdot C_{Ac} - 0.00663$ with $R^2 = 0.9999$, $A = 3634.68 \cdot C_{Amox} - 0.00712$ with $R^2 = 0.9997$ and $A = 1378.12 \cdot C_{SA} + 0.0487$ with $R^2 = 0.9977$.

All the obtained calibration curves (Fig. 5.6 and Fig. 5.7) showed a determination coefficient superior to 0.995 and were validated. Subsequently, the limits of detection and quantification were calculated for each curve, and the values obtained can be found in Tables G1.2, G2.2 and G3.2 of Appendix G.

5.5 Partition coefficients and extraction efficiencies

A total of 15 partitions in 7 different systems were performed, as listed in Table 5.2, by following the procedure described in section 3.3.4. Additionally, the blanks of each system were also determined. Tie-line compositions of the used ternary systems found in literature are compiled in Annex B. It is worth noting that, in the studied systems, the top phase was always the salt-poor phase (therefore the phase with higher concentration of component (1): IL, PEG or EL). Hence, the definitions of K and E were kept as described in equations (3.18) and (3.21) respectively, as the goal was to remove the solutes from the aqueous phase, *i.e.*, the bottom phases.

Table 5.2. Liquid-liquid extractions (partitions) performed in this work.

Systems	Acetaminophen	Amoxicillin	Salicylic acid
{[Ch][Ala] (1) + K_2HPO_4 (2) + water (3)}	✓	✓	
{[Ch][Gly] (1) + K_2HPO_4 (2) + water (3)}	✓	✓	✓
{[Ch][Ser] (1) + K_2HPO_4 (2) + water (3)}	✓		✓
{[Ch][Ala] (1) + K_3PO_4 (2) + water (3)}	✓		
{[Ch][Leu] (1) + K_3PO_4 (2) + water (3)}	✓	✓	
{PEG600 (1) + [Ch]Bic (2) + water (3)}	✓	✓	
{EL (1) + [Ch]Bit (2) + water (3)}	✓	✓	✓

When performing partition of salicylic acid (SA) in systems with CAAILS, a slight change in colour was observed in the top (IL-rich) phase. This could be caused by a change in chemical composition due to a reaction between salicylic acid and the ATPS components: for instance, there are reports of cholinium salicylate, an ionic liquid, being a stable form of pharmaceutical [141] or a hydrotrope, thereby increasing the solubility of other pharmaceuticals (such as ibuprofen or naproxen) in ATPS [142]. Cholinium salicylate is a possible product of an anion exchange reaction between the choline cation in ILs (common to all studied systems in the scope of this work) and salicylic acid, which could explain the impossibility of the quantification of salicylic acid. Hence, this solute was not further studied.

The extractions of the other pharmaceuticals, acetaminophen and amoxicillin, were performed in these systems at 298.15 K and 0.1 MPa, yielding the partition coefficients plotted in Fig. 5.8 and Fig. 5.10, and the extraction efficiencies represented in Fig. 5.9 and Fig. 5.11. The remainder of the results, such as the measured phase masses, density, pH, phase concentrations and solute losses, as well as the values of partition coefficients and extraction efficiencies with their respective uncertainties, are found in Appendix H.

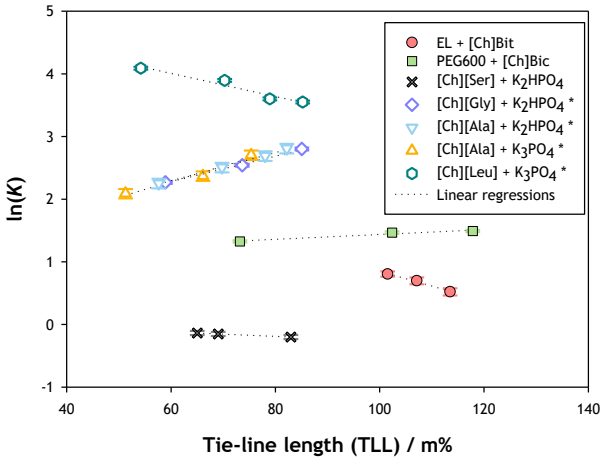

Fig. 5.8. Relation of the tie-line length (TLL) with the natural logarithm of the partition coefficients (K) for acetaminophen, in the studied ATPS, at 298.15 K and 0.1 MPa.

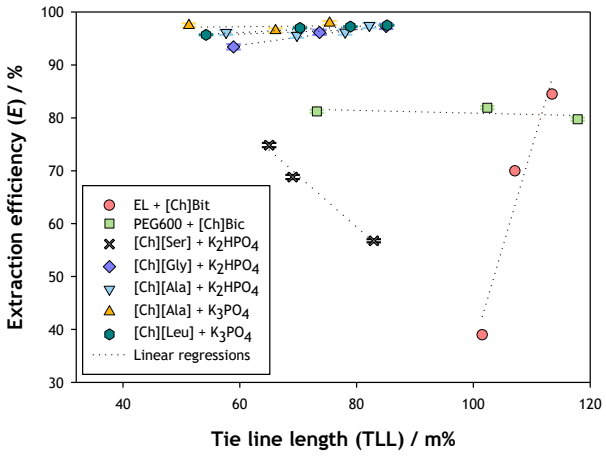

Fig. 5.9. Relation of the tie-line length (TLL) with the extraction efficiencies (E) for acetaminophen, in the studied ATPS, at 298.15 K and 0.1 MPa.

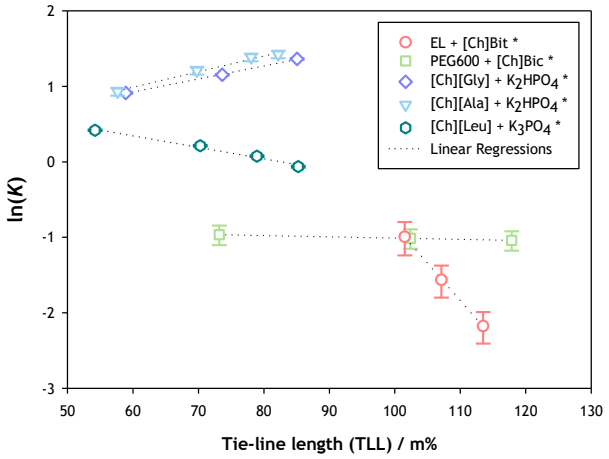

Fig. 5.10. Relation of the tie-line length (TLL) with the natural logarithm of the partition coefficients (K) for amoxicillin, in the studied ATPS, at 298.15 K and 0.1 MPa.

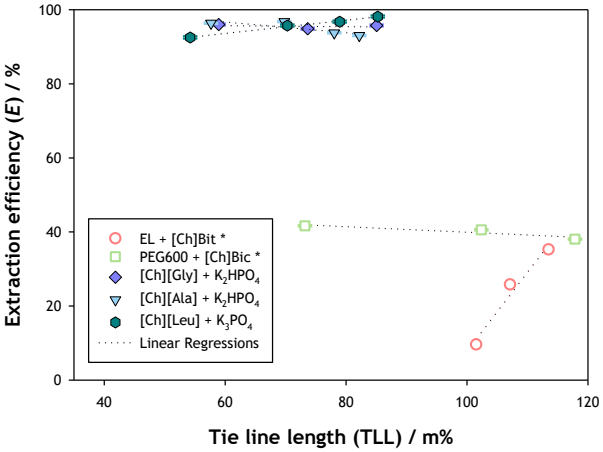

Fig. 5.11. Relation of the tie-line length (TLL) with the extraction efficiencies (E) for amoxicillin, in the studied ATPS, at 298.15 K and 0.1 MPa.

All partitions were performed with mass losses in the phase separation inferior to 5 %.

In the partitions marked with *, the solute could not be detected and/or quantified in one of the phases using the obtained calibration curves. The values of K and E, as well as the respective uncertainties, shown in Appendix G and plotted above, were calculated using the respective quantification limit instead of the indeterminate concentration: therefore, these values are only less "extreme" estimates of the real partition coefficients (K) and extraction efficiencies (E). In these cases, solute losses (L_S) were not calculated, which results in the lack of intervals for E.

In systems containing CAAILs, the pharmaceutical was not detected in the bottom phases, therefore, the values of K plotted are smaller than the real ones, and the extraction efficiency is not affected. In these partitions, the extraction was successful, but the results obtained showed that UV-Vis spectroscopy is not the most indicated means of quantification. Nonetheless, it was the method used, since the contemplated alternative method, High Performance Liquid Chromatography (HPLC), could not be applied due to the equipment being not operating.

On the other hand, in the remaining two systems (the ones containing PEG and ethyl lactate), amoxicillin was not quantified in the top phase: the values of K were higher than the real values, and the extraction efficiency was also higher than the plotted value. In the successful partitions, quantified solute losses were inferior to 5 %.

Acetaminophen was successfully extracted from aqueous media using four ATPS: {[Ch][Ala] or [Ch][Gly] (1) + K_2HPO_4 (2) + water (3)} and {[Ch][Ala] or [Ch][Leu] (1) + K_3PO_4 (2) + water (3)}. With these systems, partition coefficients were greater than unity, therefore indicating that the top phase (the IL-rich phase) had a higher concentration of acetaminophen than the bottom phase. Fig. 5.9 confirms successful extractions, as the extraction efficiencies are superior to 90 %.

Likewise, as can be seen in Fig. 5.10 and in Appendix G, in systems containing CAAILs, amoxicillin can be extracted: with the three systems studied, there is at least one tie-line for which the top phase presents a higher concentration of amoxicillin than the bottom phase (hence resulting in $K > 1$ or $\ln(K) > 0$). Additionally, the extraction efficiency of these systems is higher than 92 %, meaning that more than 92 % of the solute that is introduced in the initial mixture migrates to the top phase.

For these pharmaceuticals, in the case of the systems composed of [Ch][Ala], [Ch][Gly] and [Ch][Ser], the longest tie-line (the one with the most distinct phase compositions) provides the best results. The [Ch][Leu] ATPS provides better extraction conditions with the shortest tie-line, for both amoxicillin and acetaminophen. The ATPS {PEG600 (1) + [Ch]Bic (2) + water (3)} and {EL (1) + [Ch]Bit (2) + water (3)} proved not to be suitable extraction media for amoxicillin.

Fig. 5.8 shows that acetaminophen has no particular affinity for the [Ch][Ser]-rich or K_2HPO_4-rich phases, as values of the partition coefficient were close to 1 (visible in the plot as $\ln(K) \approx 0$). Therefore, there is no difference in concentration of acetaminophen in the top and bottom phases. Additionally, when comparing both systems containing [Ch][Ala], the effect of the salt (K_2HPO_4 or K_3PO_4) can be assessed. It can be seen that acetaminophen has the same affinity for either salt, as partition coefficients and extraction efficiencies are similar.

Partitions in the novel ATPS {EL (1) + [Ch]Bit (2) + water (3)} will now be analysed in greater detail. Fig. 5.12 and Fig. 5.13 compare the natural logarithms of the experimental partition coefficients and the extraction efficiencies with the tie-line length, respectively, for partitions of the three studied pharmaceuticals in this ternary system. Similar plots can be found in Appendix H, comparing the performance of the remaining systems for the partitioned pharmaceuticals.

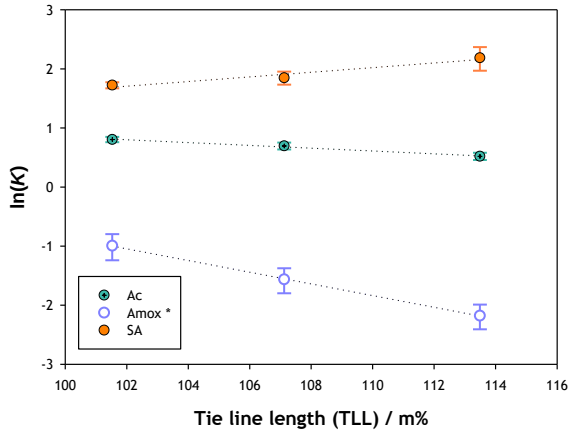

Fig. 5.12. Relation of the tie-line length (TLL) with the natural logarithm of the experimental partition coefficients (K) for acetaminophen (Ac), amoxicillin (Amox) and salicylic acid (SA) and respective linear regressions (···), in the system {EL (1) + [Ch]Bit (2) + water (3)} at 298.15 K and 0.1 MPa.

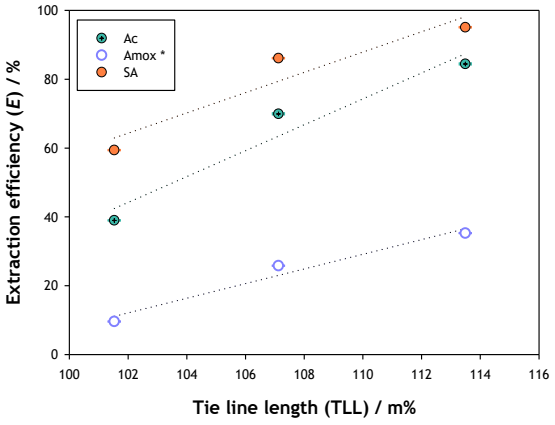

Fig. 5.13. Relation of the tie-line length (TLL) with the extraction efficiencies (E) for acetaminophen (Ac), amoxicillin (Amox) and salicylic acid (SA) and respective linear regressions (···), in the system {EL (1) + [Ch]Bit (2) + water (3)} at 298.15 K and 0.1 MPa.

As illustrated by Fig. 5.12 and Fig. 5.13, this system is more selective towards the extraction of salicylic acid and acetaminophen rather than amoxicillin. In fact, values of the partition coefficient inferior to unity were obtained for amoxicillin, showing that the top phase had a lower concentration of amoxicillin than the top phase. For acetaminophen and salicylic acid, larger values of K were obtained. Furthermore, the extraction efficiency was higher for the longest tie-line (TL1).

Regarding the case of amoxicillin, it can be noticed that the values of $\ln(K)$ decreases with increasing TLL, whereas E increased. This could be explained by a lower concentration of amoxicillin in the top phase (hence the lower values of K), but, globally, a higher mass of amoxicillin present in the top phase. This is due to an increase in the mass and volume of the top phase with TLL.

Further analysis of the systems' performance was carried out using the values of the pH measured in each phase. It was possible to assess the effect of tie-line composition in the distribution of the differently charged stages: box plots (such as Fig. 5.14) allow to visualise the relative abundances of the various forms of the pharmaceuticals in solution. Plots for the remaining systems can be found in Appendix H.

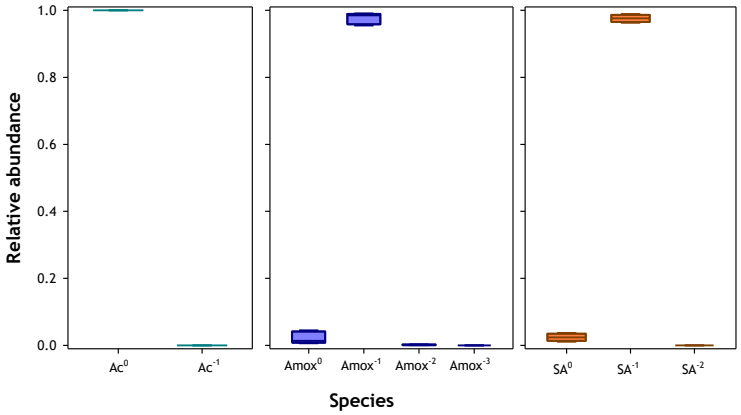

Fig. 5.14. Influence of the tie-line compositions in the relative abundance (fraction) of the stages of the studied pharmaceuticals, in the ATPS {EL (1) + [Ch]Bit (2) + water (3)} at 298.15 K and 0.1 MPa. Ac^0 and Ac^{-1} stand for the stages of acetaminophen with electrical charges equal to 0 and −1 e, respectively. $Amox^0$, $Amox^{-1}$, $Amox^{-2}$ and $Amox^{-3}$ stand for the stages of amoxicillin with electrical charges equal to 0, - 1, -2 and −3 e, respectively. SA^0, SA^{-1} and SA^{-2} stand for the stages of salicylic acid with electrical charges equal to 0, - 1 and -2 e. e stands for the elementary charge ($1.602 \cdot 10^{-19}$ C).

Fig. 5.14 shows that the tie-lines of the novel system {EL (1) + [Ch]Bit (2) + water (3)} allowed to only have the neutral form of acetaminophen. Amoxicillin and salicylic acid are predominantly found at their form with charge -1 e.

The remainder of the studied systems had pH close to 12, at which only the form of the pharmaceuticals with charge -1 e (acetaminophen) and -3 e (amoxicillin) was present. The only exception to this is the ATPS {PEG600 (1) + [Ch]Bic (2) + water (3)}: in this system, despite the pH being very similar between the top and bottom phases of all tie-lines, the relative abundance of the pharmaceutical stages varied, leading to the existence of differently charged species in solution. This wide range in compositions could explain the poor results observed for this ATPS in Fig. 5.12 and Fig. 5.13.

6 Conclusions

Following the need to remove contaminants from water, the partitioning of pharmaceutical compounds in Aqueous Two-Phase Systems (ATPS) containing salts or ionic liquids based on choline was studied in this work. ATPS are biocompatible extractive media with applicability to an industrial scale, composed of two salts, a salt and a solvent, or a salt and a polymer with considerable solubility in water. In this work, green solvents such as ethyl lactate or Choline Amino Acid Ionic Liquids (CAAILs), possessing low environmental impact, were selected.

For this purpose, it was intended to determine the liquid-liquid equilibria (LLE) of novel choline-based ATPS and to describe them using thermodynamic models for electrolytes, namely PDH+UNIQUAC. PDH+UNIQUAC combines the UNIQUAC model (which accounts for short-range interactions) with the Pitzer-Debye-Hückel equation (which combines long-range interactions, present due to electrolytes). Additionally, this work sought testing novel methodologies to enhance the predictability of the thermodynamic modelling parameters, whilst keeping their physical meaning.

A total of 11 aqueous ternary systems containing choline salts (choline chloride, choline bicarbonate, choline bitartrate and choline di-hydrogen citrate) and either ethyl lactate, polyethylene glycol (PEG) or polyvinylpyrrolidone were tested for LLE at 298.15 K and 0.1 MPa, and solubility curves were obtained for 6 of them. These solubility curves were fitted to common correlations used in literature (Merchuk, Li and Yu equations). Choline bitartrate and PEG-based ATPS were compared to other systems found in literature, showing that the immiscible zone was larger for systems with polymers with longer alkyl chain lengths.

Furthermore, the system {ethyl lactate (1) + choline bitartrate (2) + water (3)} was selected for additional studies, due to the promising shape and area of the solubility curve. Electrical conductivity and density isolines were determined by fitting experimental data to third-degree polynomials, resulting in the determination of 3 nearly parallel tie-lines, with lengths superior to unity. The ethyl lactate-rich phase was the top phase, and the bottom phase was rich in salt. Besides, the tie-lines were accurately fitted using the Othmer-Tobias and Bancroft-Hubbard equations.

Then, this obtained LLE data was modelled using PDH+UNIQUAC. An innovative methodology to calculate the non-randomness factor (α), a parameter which is considered to be closely related to the lattice coordination number (Z). In UNIQUAC, Z is traditionally set to 10, regardless of the species in solution or their concentrations. This novel approach allowed to compute a specific non-randomness factor, dependent on the species present and on their relative abundances. For this, after optimising the cartesian coordinates of the molecules using Density Functional Theory (DFT), the non-randomness factors were calculated based on a geometric approach, in which it is closely related to the dipole moment and the polarity of the species.

The proposed method for the calculation of the non-randomness factor was first validated using only UNIQUAC, by comparing the model's performance with the one of the classical UNIQUAC (with $Z = 10$). Both approaches described well the studied systems and showed identical standard deviations from the experimental data collected from literature, therefore validating the approach. Although the

results were identical, it is believed that crucial steps in the enhancement of the predictability of thermodynamic modelling were taken, as this methodology allowed to calculate a parameter specific to the species, instead of arbitrating the same value regardless of the component.

The novel ATPS's LLE data was also modelled using PDH+UNIQUAC in its classical version ($Z = 10$) and adapted version (with Z as a function of α), in which, once again, both models performed identically. Although the modelling results were already satisfactory without the calculated α, this parameter now allows the models to have a geometrical meaning behind the values of Z.

Nonetheless, seeing that the calculated non-randomness factor is closely related to the species' polarity, it was used to predict and compare the relative position of solubility curves, leading to other applications of this method. Therefore, this innovative methodology for the calculation of α is seen as a major contribution to the field.

Finally, ternary systems containing choline salts or ionic liquids (ILs) were evaluated regarding their potential for removing pharmaceuticals from aqueous samples.

For this purpose, it was first necessary to synthesise Choline Amino Acid Ionic Liquids (CAAILs), which were needed in 5 out of the 7 studied systems. Cholinium L-alaninate ([Ch][Ala]), cholinium glycinate ([Ch][Gly]), cholinium leucinate ([Ch][Leu]) and cholinium L-serinate ([Ch][Ser]) were synthesised. The success of the syntheses was confirmed by infrared spectroscopy and density measurements. In fact, the measured infrared spectra were compared to those predicted by DFT, and there was a general agreement between the data.

A total of 3 pharmaceuticals (acetaminophen, amoxicillin and salicylic acid) were selected and studied, comprising 14 partitions in 7 different ATPS. Salicylic acid could not be extracted and quantified using ATPS containing ILs, due to a chemical reaction. Nonetheless, for amoxicillin and acetaminophen, three CAAIL-based ATPS were identified as the most promising to remove these components from polluted water streams.

The novel ATPS determined in this work was also applied to extract these active pharmaceutical ingredients (APIs), with promising results for the extraction of salicylic acid. Salicylic acid was successfully extracted to the top phase, with the highest partition coefficients (K) being obtained for the longest tie-line, which had a length of 115.1 % ($K = 9 \pm 2$ and $E \geq 95\,\%$). On the other hand, acetaminophen was best extracted with the shortest tie-line, which had a length of 101.5 % ($K = 2.2 \pm 0.1$) and amoxicillin showed no affinity for the ethyl lactate-rich phase ($K \leq 0.11$ and $E < 35\,\%$).

Due to the versatility of ATPS, the system determined in this work has other applications. Seeing that it is composed of two solvents, that can easily be evaporated at reduced pressure, and of an organic salt, commonly used as a food supplement, this ATPS could be applied in the future to extract bioactive species from bioresidues, thus leading to a more circular economy.

7 Project assessment

7.1 Degree of completion

In this work, four main objectives, which will be reviewed in this section, were defined and successfully completed.

First, liquid-liquid equilibria (LLE) of choline-based Aqueous Two-Phase Systems (ATPS) were to be determined. A total of 11 systems were studied, and 6 solubility curves were obtained and fitted to correlations. One of these systems was selected for further studies: 3 tie-lines were determined, and this novel system was applied in 3 partitions.

The following objective, modelling LLE data using PDH+UNIQUAC, was effectively completed. This common thermodynamic model for electrolytes was used in its traditional form and improved with a novel approach developed in this work, attempting to enhance the predictability and performance of this model. Even though the novel approach for the prediction of the non-randomness factor did not enhance the used thermodynamic models, it led to results of identical quality. Additionally, this parameter could be calculated and used to determine other thermodynamic properties, such as relative polarities and solubilities, which was done in this work.

Choline Amino Acid Ionic Liquids (CAAILs) were successfully synthesised and used in this work. Although this was not an objective set out in the Introduction, it was crucial to the success of this work, seeing that 5 out of the 7 systems studied were based on CAAILs. Density measurements and infrared spectroscopy assessed the success of the syntheses.

The last aim of this work was to study the partitioning of pharmaceutical compounds in ATPS containing salts or solvents based on choline, in order to evaluate the potential of these systems in the removal of contaminants from water bodies. A total of 3 pharmaceuticals were selected and studied, comprising 14 partitions in 7 different systems. Three CAAIL-based ATPS were identified as the most promising to remove these components from water samples, thus completing the scope of this work.

7.2 Future work

In this work, liquid-liquid equilibria (LLE) of choline-based Aqueous Two-Phase Systems (ATPS) were effectively determined, and, in one case, tie-lines were determined using electrical conductivity and density isolines. This sets the ground for the study of new sustainable systems using this methodology, which will in turn make possible the study of new partitions, more specifically, partitions of biomolecules.

In fact, the novel choline-based system presented in this work could be used to extract more pharmaceuticals and pollutants. Partition studies could also be extended to other types of solutes, such as antioxidants or vitamins, which are a current focus of the research group.

The poor quantification of the solutes using UV-Vis spectroscopy indicates the need for alternative quantification methods, such as High Performance Liquid Chromatography (HPLC) which could not be

applied during the time of this work. Therefore, the partitions performed in this work could be carried out with this alternative quantification method.

Suggestions for future work also include applying the predictive non-randomness factor methodology to other thermodynamic models, such as Non-Random Two-Liquid (NRTL) or the Wilson model. Furthermore, the modified PDH+UNIQUAC could be applied to other systems, notably those containing polymers or ionic liquids (ILs). In this latter case, it would be necessary to optimise IL geometry, and take into account their dissociation extent, as previously determined by the research group.

Additionally, the non-randomness factor could also be calculated for other species and predict relative solubilities, with eventual applications on LLE prediction.

On a final note, it is believed that this work opened the door to further studies on Density Functional Theory and its applications to the work carried out at the Thermodynamics Group of LSRE-LCM.

7.3 Final assessment

The development of this master's dissertation allowed psychological, emotional, and academic growths. Thanks to the supervisor's precious help and invaluable guidance from more senior members of the research group, the work was successfully performed while learning deeply about the subject.

Areas such as thermodynamic modelling and computational chemistry became less vague during the course of this work, which, alongside a fondness for the subject, allowed the author to create a good work.

8 References

1. European Federation of Pharmaceutical Industries and Associations, E. *The Pharmaceutical Industry in Figures - Key Data*; **2022**. www.efpia.eu/.
2. VALORMED *Relatório de Actividades 2022*; **2023**. https://valormed.pt/2023/04/04/relatorios-de-actividades/.
3. Kümmerer, K., Pharmaceuticals in the Environment. *Annu. Rev. Environ. Resour.* **2010**, *35*, 57-75. https://doi.org/10.1146/annurev-environ-052809-161223.
4. World Health Organization, W. Antimicrobial resistance. www.who.int/news-room/fact-sheets/detail/antimicrobial-resistance (accessed 12/06/2023).
5. United Nations, U. The 17 Sustainable Development Goals. https://sdgs.un.org/goals (accessed 13/06/2023).
6. Köktaş, İ.Y.; Gökkuş, Ö., Removal of salicylic acid by electrochemical processes using stainless steel and platinum anodes. *Chemosphere* **2022**, *293*, 133566. https://doi.org/10.1016/j.chemosphere.2022.133566.
7. Kommineni, S.; Zoeckler, J.; Stocking, A.; Liang, P.; Flores, A.; Rodriguez, R.; Brown, T.; Brown, A., Advanced oxidation processes. In *Treatment Technologies for Removal of Methyl Tertiary Butyl Ether (MTBE) from Drinking Water: Air Stripping, Advanced Oxidation Processes, Granular Activated Carbon and Synthetic Resins Adsorbents*, National Water Research Institute: California, USA, **2000**; pp 109-208.
8. Zakrzewska, M.E.; Nunes, A.V.M.; Barot, A.R.; Fernández-Castané, A.; Visak, Z.P.; Kiatkittipong, W.; Najdanovic-Visak, V., Extraction of antibiotics using aqueous two-phase systems based on ethyl lactate and thiosulphate salts. *Fluid Phase Equilib.* **2021**, *539*, 113022. https://doi.org/10.1016/j.fluid.2021.113022.
9. Almeida, H.F.D.; Marrucho, I.M.; Freire, M.G., Removal of Nonsteroidal Anti-Inflammatory Drugs from Aqueous Environments with Reusable Ionic-Liquid-Based Systems. *ACS. Sustain. Chem. Eng.* **2017**, *5*, 2428-2436. https://doi.org/10.1021/acssuschemeng.6b02771.
10. Silva, F.A.; Sintra, T.; Ventura, S.P.M.; Coutinho, J.A.P., Recovery of paracetamol from pharmaceutical wastes. *Sep. Purif. Technol.* **2014**, *122*, 315-322. https://doi.org/10.1016/j.seppur.2013.11.018.
11. Richardson, S.D.; Kimura, S.Y., Emerging environmental contaminants: Challenges facing our next generation and potential engineering solutions. *Environ. Technol. Innov.* **2017**, *8*, 40-56. https://doi.org/10.1016/j.eti.2017.04.002.
12. Kümmerer, K., Significance of antibiotics in the environment. *J. Antimicrob. Chemother.* **2003**, *52*, 5-7. https://doi.org/10.1093/jac/dkg293.
13. Hilton, M.; Thomas, K.; Ashton, D., *Targeted monitoring programme for pharmaceuticals in the aquatic environment*. Environment agency Bristol: **2003**. ISBN: 184432026X.
14. David, A.; Pancharatna, K., Effects of acetaminophen (paracetamol) in the embryonic development of zebrafish, Danio rerio. *J. Appl. Toxicol.* **2009**, *29*, 597-602. https://doi.org/10.1002/jat.1446.
15. Al-Saidi, S.; Mjalli, F.S.; Al-Azzawi, M.; Abutarboosh, B.; AlSaadi, M.A.; Al-Wahaibi, T., Amoxicillin removal from medical wastewater using an eco-friendly aqueous two-phase extraction system. *Sep. Sci. Technol.* **2023**, *58*, 61-74. https://doi.org/10.1080/01496395.2022.2102998.
16. Boullard, O.; Leblanc, H.; Besson, B., Salicylic Acid. In *Ullmann's Encyclopedia of Industrial Chemistry*. https://doi.org/10.1002/14356007.a23_477.
17. Paíga, P.; Correia, M.; Fernandes, M.J.; Silva, A.; Carvalho, M.; Vieira, J.; Jorge, S.; Silva, J.G.; Freire, C.; Delerue-Matos, C., Assessment of 83 pharmaceuticals in WWTP influent and effluent samples by UHPLC-MS/MS: Hourly variation. *Sci. Total Environ.* **2019**, *648*, 582-600. https://doi.org/10.1016/j.scitotenv.2018.08.129.
18. Galiński, M.; Lewandowski, A.; Stępniak, I., Ionic liquids as electrolytes. *Electrochim. Acta* **2006**, *51*, 5567-5580. https://doi.org/10.1016/j.electacta.2006.03.016.
19. Walden, P., Über die Molekulargrösse und elektrische Leitfähigkeit einiger geschmolzenen Salze. *Bull. Acad. Imp. Sci. Saint-Pétersbourg* **1914**, *8*, 405-422.
20. Graenacher, C. Cellulose solution. US Patent US1943176A, **1934**.
21. Wilkes, J.S.; Zaworotko, M.J., Air and water stable 1-ethyl-3-methylimidazolium based ionic liquids. *J. Chem. Soc., Chem. Commun.* **1992**, 965-967. https://doi.org/10.1039/C39920000965.
22. Silva, W.; Zanatta, M.; Ferreira, A.S.; Corvo, M.C.; Cabrita, E.J., Revisiting Ionic Liquid Structure-Property Relationship: A Critical Analysis. *Int. J. Mol. Sci.* **2020**, *21*, 7745. https://doi.org/10.3390/ijms21207745.
23. Freire, M.G.; Carvalho, P.J.; Silva, A.M.S.; Santos, L.M.N.B.F.; Rebelo, L.P.N.; Marrucho, I.M.; Coutinho, J.A.P., Ion Specific Effects on the Mutual Solubilities of Water and Hydrophobic Ionic Liquids. *J. Phys. Chem. B* **2009**, *113*, 202-211. https://doi.org/10.1021/jp8080035.
24. Thuy Pham, T.P.; Cho, C.-W.; Yun, Y.-S., Environmental fate and toxicity of ionic liquids: A review. *Water Res.* **2010**, *44*, 352-372. https://doi.org/10.1016/j.watres.2009.09.030.
25. Brennecke, J.F.; Maginn, E.J., Ionic liquids: Innovative fluids for chemical processing. *AlChE J.* **2001**, *47*, 2384-2389. https://doi.org/10.1002/aic.690471102.
26. M. S. S. Esperança, J.; Canongia Lopes, J.N.; Tariq, M.; Santos, L.M.N.B.F.; Magee, J.W.; Rebelo, L.P.N., Volatility of Aprotic Ionic Liquids — A Review. *J. Chem. Eng. Data* **2010**, *55*, 3-12. https://doi.org/10.1021/je900458w.
27. Marsh, K.N.; Boxall, J.A.; Lichtenthaler, R., Room temperature ionic liquids and their mixtures—a review. *Fluid Phase Equilib.* **2004**, *219*, 93-98. https://doi.org/10.1016/j.fluid.2004.02.003.
28. Garcia, B.; Lavallée, S.; Perron, G.; Michot, C.; Armand, M., Room temperature molten salts as lithium battery electrolyte. *Electrochim. Acta* **2004**, *49*, 4583-4588. https://doi.org/10.1016/j.electacta.2004.04.041.
29. Gómez, E.; Macedo, E.A., Partitioning of DNP-amino acids in ionic liquid/citrate salt based Aqueous Two-Phase System. *Fluid Phase Equilib.* **2019**, *484*, 82-87. https://doi.org/10.1016/j.fluid.2018.11.021.
30. Gómez, E.; Requejo, P.F.; Tojo, E.; Macedo, E.A., Recovery of flavonoids using novel biodegradable choline amino acids ionic liquids based ATPS. *Fluid Phase Equilib.* **2019**, *493*, 1-9. https://doi.org/10.1016/j.fluid.2019.03.024.
31. Newington, I.; Perez-Arlandis, J.M.; Welton, T., Ionic Liquids as Designer Solvents for Nucleophilic Aromatic Substitutions. *Org. Lett.* **2007**, *9*, 5247-5250. https://doi.org/10.1021/ol702435f.
32. Welton, T., Ionic liquids in catalysis. *Coord. Chem. Rev.* **2004**, *248*, 2459-2477. https://doi.org/10.1016/j.ccr.2004.04.015.
33. Brennecke, J.F.; Gurkan, B.E., Ionic Liquids for CO_2 Capture and Emission Reduction. *J. Phys. Chem. Lett.* **2010**, *1*, 3459-3464. https://doi.org/10.1021/jz1014828.
34. Pinto, A.M.; Rodríguez, H.; Colón, Y.J.; Arce, A., Jr.; Arce, A.; Soto, A., Absorption of Carbon Dioxide in Two Binary Mixtures of Ionic Liquids. *Ind. Eng. Chem. Res.* **2013**, *52*, 5975-5984. https://doi.org/10.1021/ie303238h.

35. Borra, E.F.; Seddiki, O.; Angel, R.; Eisenstein, D.; Hickson, P.; Seddon, K.R.; Worden, S.P., Deposition of metal films on an ionic liquid as a basis for a lunar telescope. *Nature* **2007**, *447*, 979-981. https://doi.org/10.1038/nature05909.
36. Hough, W.L.; Smiglak, M.; Rodríguez, H.; Swatloski, R.P.; Spear, S.K.; Daly, D.T.; Pernak, J.; Grisel, J.E.; Carliss, R.D.; Soutullo, M.D.; Davis, J.J.H.; Rogers, R.D., The third evolution of ionic liquids: active pharmaceutical ingredients. *New J. Chem.* **2007**, *31*, 1429-1436. https://doi.org/10.1039/B706677P.
37. Davis Jr, J.H.; Gordon, C.M.; Hilgers, C.; Wasserscheid, P., Synthesis and purification of ionic liquids. In *Ionic Liquids in Synthesis*, Wasserscheid, P.; Welton, T., Eds. Wiley: **2002**; pp 7-40. https://doi.org/10.1002/3527600701.ch2.
38. Palomar, J.; Lemus, J.; Gilarranz, M.A.; Rodriguez, J.J., Adsorption of ionic liquids from aqueous effluents by activated carbon. *Carbon* **2009**, *47*, 1846-1856. https://doi.org/10.1016/j.carbon.2009.03.028.
39. Deng, Y.; Long, T.; Zhang, D.; Chen, J.; Gan, S., Phase Diagram of [Amim]Cl + Salt Aqueous Biphasic Systems and Its Application for [Amim]Cl Recovery. *J. Chem. Eng. Data* **2009**, *54*, 2470-2473. https://doi.org/10.1021/je900009a.
40. Abels, C.; Redepenning, C.; Moll, A.; Melin, T.; Wessling, M., Simple purification of ionic liquid solvents by nanofiltration in biorefining of lignocellulosic substrates. *J. Membr. Sci.* **2012**, *405-406*, 1-10. https://doi.org/10.1016/j.memsci.2011.12.020.
41. Philippi, F.; Quinten, A.; Rauber, D.; Springborg, M.; Hempelmann, R., Density Functional Theory Descriptors for Ionic Liquids and the Introduction of a Coulomb Correction. *J. Phys. Chem. A* **2019**, *123*, 4188-4200. https://doi.org/10.1021/acs.jpca.9b01831.
42. Plechkova, N.V.; Seddon, K.R., Applications of ionic liquids in the chemical industry. *Chem. Soc. Rev.* **2008**, *37*, 123-150. https://doi.org/10.1039/B006677J.
43. Smith, E.L.; Abbott, A.P.; Ryder, K.S., Deep Eutectic Solvents (DESs) and Their Applications. *Chem. Rev.* **2014**, *114*, 11060-11082. https://doi.org/10.1021/cr300162p.
44. Chun, S.; Dzyuba, S.V.; Bartsch, R.A., Influence of Structural Variation in Room-Temperature Ionic Liquids on the Selectivity and Efficiency of Competitive Alkali Metal Salt Extraction by a Crown Ether. *Anal. Chem.* **2001**, *73*, 3737-3741. https://doi.org/10.1021/ac010061v.
45. Giernoth, R., Task-Specific Ionic Liquids. *Angew. Chem. Int. Ed.* **2010**, *49*, 2834-2839. https://doi.org/10.1002/anie.200905981.
46. Schrekker, H.S.; Stracke, M.P.; Schrekker, C.M.L.; Dupont, J., Ether-Functionalized Imidazolium Hexafluorophosphate Ionic Liquids for Improved Water Miscibilities. *Ind. Eng. Chem. Res.* **2007**, *46*, 7389-7392. https://doi.org/10.1021/ie0709685.
47. Greaves, T.L.; Drummond, C.J., Protic Ionic Liquids: Properties and Applications. *Chem. Rev.* **2008**, *108*, 206-237. https://doi.org/10.1021/cr068040u.
48. Koutsoukos, S.; Becker, J.; Dobre, A.; Fan, Z.; Othman, F.; Philippi, F.; Smith, G.J.; Welton, T., Synthesis of aprotic ionic liquids. *Nat Rev Methods Primers* **2022**, *2*, 49. https://doi.org/10.1038/s43586-022-00129-3.
49. Zhang, S.-Y.; Zhuang, Q.; Zhang, M.; Wang, H.; Gao, Z.; Sun, J.-K.; Yuan, J., Poly(ionic liquid) composites. *Chem. Soc. Rev.* **2020**, *49*, 1726-1755. https://doi.org/10.1039/C8CS00938D.
50. Yuan, J.; Mecerreyes, D.; Antonietti, M., Poly(ionic liquid)s: An update. *Prog. Polym. Sci.* **2013**, *38*, 1009-1036. https://doi.org/10.1016/j.progpolymsci.2013.04.002.
51. Kaur, G.; Kumar, H.; Singla, M., Diverse applications of ionic liquids: A comprehensive review. *J. Mol. Liq.* **2022**, *351*, 118556. https://doi.org/10.1016/j.molliq.2022.118556.
52. Pereiro, A.B.; Araújo, J.M.M.; Martinho, S.; Alves, F.; Nunes, S.; Matias, A.; Duarte, C.M.M.; Rebelo, L.P.N.; Marrucho, I.M., Fluorinated Ionic Liquids: Properties and Applications. *ACS. Sustain. Chem. Eng.* **2013**, *1*, 427-439. https://doi.org/10.1021/sc300163n.
53. Korchak, P.A.; Safonova, E.A.; Victorov, A.I., Amino acid ionic liquids as components of aqueous biphasic systems for L-tryptophan extraction: Experiment and thermodynamic modeling with ePC-SAFT equation of state. *J. Mol. Liq.* **2022**, *366*, 120185. https://doi.org/10.1016/j.molliq.2022.120185.
54. Blusztajn, J.K., Choline, a Vital Amine. *Science* **1998**, *281*, 794-795. https://doi.org/10.1126/science.281.5378.794.
55. Zhang, Y.; Ji, X.; Lu, X., Choline-based deep eutectic solvents for CO2 separation: Review and thermodynamic analysis. *Renew. Sustain. Energy Rev* **2018**, *97*, 436-455. https://doi.org/10.1016/j.rser.2018.08.007.
56. Foulet, A.; Ghanem, O.B.; El-Harbawi, M.; Lévêque, J.-M.; Mutalib, M.I.A.; Yin, C.-Y., Understanding the physical properties, toxicities and anti-microbial activities of choline-amino acid-based salts: Low-toxic variants of ionic liquids. *J. Mol. Liq.* **2016**, *221*, 133-138. https://doi.org/10.1016/j.molliq.2016.05.046.
57. Li, Y.; Yang, F.; Li, Y.; Cai, M.; Li, H.; Fan, X.; Zhu, M., Choline amino acid ionic Liquids: A novel green potential lubricant. *J. Mol. Liq.* **2022**, *360*, 119539. https://doi.org/10.1016/j.molliq.2022.119539.
58. Basaiahgari, A.; Priyanka, V.P.; Ijardar, S.P.; Gardas, R.L., Aqueous biphasic systems of amino acid-based ionic liquids: Evaluation of phase behavior and extraction capability for caffeine. *Fluid Phase Equilib.* **2020**, *506*, 112373. https://doi.org/10.1016/j.fluid.2019.112373.
59. Li, Q.; Liu, W.; Zhu, X., Green choline amino acid ionic liquids aqueous two-phase extraction coupled with synchronous fluorescence spectroscopy for analysis naphthalene and pyrene in water samples. *Talanta* **2020**, *219*, 121305. https://doi.org/10.1016/j.talanta.2020.121305.
60. Ramakrishnan, A.; Sadana, A., Economics of bioseparation processes. In *Sep. Sci. Technol.*, Ahuja, S., Ed. Academic Press: **2000**; Vol. 2, pp 667-685. https://doi.org/10.1016/S0149-6395(00)80065-3.
61. Beijerinck, M.W., Über eine Eigentümlichkeit der löslichen Stärke. In *Zentralblatt for Bakteriologie, Parasiten und Infektionskrankheiten*, **1896**; Vol. 2, pp 679-699.
62. Albertsson, P.-Å., Chromatography and partition of cells and cell fragments. *Nature* **1956**, *177*, 771-774. https://doi.org/10.1038/177771a0.
63. Albertsson, P.-Å., Partition of cell particles and macromolecules in polymer two-phase systems. *Adv. Protein Chem.* **1970**, *24*, 309-341. https://doi.org/10.1016/S0065-3233(08)60244-2.
64. Mazzola, P.G.; Lopes, A.M.; Hasmann, F.A.; Jozala, A.F.; Penna, T.C.V.; Magalhães, P.O.; Rangel-Yagui, C.O.; Pessoa, A., Liquid–liquid extraction of biomolecules: an overview and update of the main techniques. *J. Chem. Technol. Biotechnol.* **2008**, *83*, 143-157. https://doi.org/10.1002/jctb.1794.
65. Freire, M.G.; Cláudio, A.F.M.; Araújo, J.M.M.; Coutinho, J.A.P.; Marrucho, I.M.; Lopes, J.N.C.; Rebelo, L.P.N., Aqueous biphasic systems: a boost brought about by using ionic liquids. *Chem. Soc. Rev.* **2012**, *41*, 4966-4995. https://doi.org/10.1039/C2CS35151J.
66. Velho, P.; Rebelo, C.S.; Macedo, E.A., Extraction of Gallic Acid and Ferulic Acid for Application in Hair Supplements. *Molecules* **2023**, *28*, 2369. https://doi.org/10.3390/molecules28052369.
67. Velho, P.; Marques, L.; Macedo, E.A., Extraction of Polyphenols and Vitamins Using Biodegradable ATPS Based on Ethyl Lactate. *Molecules* **2022**, *27*, 7838. https://doi.org/10.3390/molecules27227838.

68. Velho, P.; Barroca, L.R.; Macedo, E.A., Partition of antioxidants available in biowaste using a green aqueous biphasic system. *Sep. Purif. Technol.* **2023**, *307*, 122707. https://doi.org/10.1016/j.seppur.2022.122707.
69. Velho, P.; Oliveira, I.; Gómez, E.; Macedo, E.A., pH Study and Partition of Riboflavin in an Ethyl Lactate-Based Aqueous Two-Phase System with Sodium Citrate. *J. Chem. Eng. Data* **2022**, *67*, 1985-1993. https://doi.org/10.1021/acs.jced.1c00909.
70. Requejo, P.F.; Velho, P.; Gómez, E.; Macedo, E.A., Study of Liquid–Liquid Equilibrium of Aqueous Two-Phase Systems Based on Ethyl Lactate and Partitioning of Rutin and Quercetin. *Ind. Eng. Chem. Res.* **2020**, *59*, 21196-21204. https://doi.org/10.1021/acs.iecr.0c02664.
71. Pereira, J.F.B.; Vicente, F.; Santos-Ebinuma, V.C.; Araújo, J.M.; Pessoa, A.; Freire, M.G.; Coutinho, J.A.P., Extraction of tetracycline from fermentation broth using aqueous two-phase systems composed of polyethylene glycol and cholinium-based salts. *Process Biochem.* **2013**, *48*, 716-722. https://doi.org/10.1016/j.procbio.2013.02.025.
72. Almeida, H.F.D.; Freire, M.G.; Marrucho, I.M., Improved extraction of fluoroquinolones with recyclable ionic-liquid-based aqueous biphasic systems. *Green Chemistry* **2016**, *18*, 2717-2725. https://doi.org/10.1039/C5GC02464A.
73. Passos, H.; Tavares, D.J.P.; Ferreira, A.M.; Freire, M.G.; Coutinho, J.A.P., Are Aqueous Biphasic Systems Composed of Deep Eutectic Solvents Ternary or Quaternary Systems? *ACS. Sustain. Chem. Eng.* **2016**, *4*, 2881-2886. https://doi.org/10.1021/acssuschemeng.6b00485.
74. Wysoczanska, K.; Macedo, E.A., Effect of molecular weight of polyethylene glycol on the partitioning of DNP-amino acids: PEG (4000, 6000) with sodium citrate at 298.15 K. *Fluid Phase Equilib.* **2016**, *428*, 84-91. https://doi.org/10.1016/j.fluid.2016.07.009.
75. Velho, P.; Requejo, P.F.; Gómez, E.; Macedo, E.A., Thermodynamic study of ATPS involving ethyl lactate and different inorganic salts. *Sep. Purif. Technol.* **2021**, *275*, 119155. https://doi.org/10.1016/j.seppur.2021.119155.
76. Velho, P.; Requejo, P.F.; Gómez, E.; Macedo, E.A., Novel ethyl lactate based ATPS for the purification of rutin and quercetin. *Sep. Purif. Technol.* **2020**, *252*, 117447. https://doi.org/10.1016/j.seppur.2020.117447.
77. Arce, A.; Arce, A., Jr.; Rodriguez, O., Revising Concepts on Liquid–Liquid Extraction: Data Treatment and Data Reliability. *J. Chem. Eng. Data* **2022**, *67*, 286-296. https://doi.org/10.1021/acs.jced.1c00778.
78. Li, J.; Sundman, B.; Winkelman, J.G.M.; Vakis, A.I.; Picchioni, F., Implementation of the UNIQUAC model in the OpenCalphad software. *Fluid Phase Equilib.* **2020**, *507*, 112398. https://doi.org/10.1016/j.fluid.2019.112398.
79. Papadopoulos, A.I.; Tsivintzelis, I.; Linke, P.; Seferlis, P., Computer-Aided Molecular Design: Fundamentals, Methods, and Applications. In *Reference Module in Chemistry, Molecular Sciences and Chemical Engineering*, Elsevier: **2018**. https://doi.org/10.1016/B978-0-12-409547-2.14342-2.
80. Van Der Waals, J.D., *On the continuity of the gaseous and liquid states*. Courier Corporation: **1890**. ISBN: 9780486495934.
81. Redlich, O.; Kwong, J.N.S., On the Thermodynamics of Solutions. V. An Equation of State. Fugacities of Gaseous Solutions. *Chem. Rev.* **1949**, *44*, 233-244. https://doi.org/10.1021/cr60137a013.
82. Soave, G., Equilibrium constants from a modified Redlich-Kwong equation of state. *Chem. Eng. Sci.* **1972**, *27*, 1197-1203. https://doi.org/10.1016/0009-2509(72)80096-4.
83. Peng, D.-Y.; Robinson, D.B., A New Two-Constant Equation of State. *Ind. Eng. Chem. Fundam.* **1976**, *15*, 59-64. https://doi.org/10.1021/i160057a011.
84. Fuller, G.G., A Modified Redlich-Kwong-Soave Equation of State Capable of Representing the Liquid State. *Ind. Eng. Chem. Fundam.* **1976**, *15*, 254-257. https://doi.org/10.1021/i160060a005.
85. Gasem, K.A.M.; Gao, W.; Pan, Z.; Robinson, R.L., A modified temperature dependence for the Peng–Robinson equation of state. *Fluid Phase Equilib.* **2001**, *181*, 113-125. https://doi.org/10.1016/S0378-3812(01)00488-5.
86. Chapman, W.G.; Jackson, G.; Gubbins, K.E., Phase equilibria of associating fluids. *Mol. Phys.* **1988**, *65*, 1057-1079. https://doi.org/10.1080/00268978800101601.
87. Beret, S.; Prausnitz, J.M., Perturbed hard-chain theory: An equation of state for fluids containing small or large molecules. *AIChE J.* **1975**, *21*, 1123-1132. https://doi.org/10.1002/aic.690210612.
88. Donohue, M.D.; Prausnitz, J.M., Perturbed hard chain theory for fluid mixtures: Thermodynamic properties for mixtures in natural gas and petroleum technology. *AIChE J.* **1978**, *24*, 849-860. https://doi.org/10.1002/aic.690240511.
89. Gross, J.; Sadowski, G., Perturbed-Chain SAFT: An Equation of State Based on a Perturbation Theory for Chain Molecules. *Ind. Eng. Chem. Res.* **2001**, *40*, 1244-1260. https://doi.org/10.1021/ie0003887.
90. Ji, X.; Held, C.; Sadowski, G., Modeling imidazolium-based ionic liquids with ePC-SAFT. *Fluid Phase Equilib.* **2012**, *335*, 64-73. https://doi.org/10.1016/j.fluid.2012.05.029.
91. Held, C.; Prinz, A.; Wallmeyer, V.; Sadowski, G., Measuring and modeling alcohol/salt systems. *Chem. Eng. Sci.* **2012**, *68*, 328-339. https://doi.org/10.1016/j.ces.2011.09.040.
92. Wysoczanska, K.; Nierhauve, B.; Sadowski, G.; Macedo, E.A.; Held, C., Solubility of DNP-amino acids and their partitioning in biodegradable ATPS: Experimental and ePC-SAFT modeling. *Fluid Phase Equilib.* **2021**, *527*, 112830. https://doi.org/10.1016/j.fluid.2020.112830.
93. Kontogeorgis, G.M.; Voutsas, E.C.; Yakoumis, I.V.; Tassios, D.P., An Equation of State for Associating Fluids. *Ind. Eng. Chem. Res.* **1996**, *35*, 4310-4318. https://doi.org/10.1021/ie9600203.
94. Kontogeorgis, G.M.; Michelsen, M.L.; Folas, G.K.; Derawi, S.; von Solms, N.; Stenby, E.H., Ten Years with the CPA (Cubic-Plus-Association) Equation of State. Part 1. Pure Compounds and Self-Associating Systems. *Ind. Eng. Chem. Res.* **2006**, *45*, 4855-4868. https://doi.org/10.1021/ie051305v.
95. Kontogeorgis, G.M.; Folas, G.K., Applications of CPA to the Oil and Gas Industry. In *Thermodynamic Models for Industrial Applications*, **2010**; pp 299-331. https://doi.org/10.1002/9780470747537.ch10.
96. Kontogeorgis, G.M.; Folas, G.K., Applications of CPA to Chemical Industries. In *Thermodynamic Models for Industrial Applications*, **2010**; pp 333-367. https://doi.org/10.1002/9780470747537.ch11.
97. Velho, P.; Liang, X.; Macedo, E.A.; Gómez, E.; Kontogeorgis, G.M., Towards a predictive Cubic Plus Association equation of state. *Fluid Phase Equilib.* **2021**, *540*, 113045. https://doi.org/10.1016/j.fluid.2021.113045.
98. Maia, F.M.; Tsivintzelis, I.; Rodriguez, O.; Macedo, E.A.; Kontogeorgis, G.M., Equation of state modelling of systems with ionic liquids: Literature review and application with the Cubic Plus Association (CPA) model. *Fluid Phase Equilib.* **2012**, *332*, 128-143. https://doi.org/10.1016/j.fluid.2012.06.026.
99. Wilson, G.M., Vapor-Liquid Equilibrium. XI. A New Expression for the Excess Free Energy of Mixing. *J. Am. Chem. Soc.* **1964**, *86*, 127-130. https://doi.org/10.1021/ja01056a002.
100. Renon, H.; Prausnitz, J.M., Local compositions in thermodynamic excess functions for liquid mixtures. *AIChE J.* **1968**, *14*, 135-144. https://doi.org/10.1002/aic.690140124.
101. Abrams, D.S.; Prausnitz, J.M., Statistical thermodynamics of liquid mixtures: A new expression for the excess Gibbs energy of partly or completely miscible systems. *AIChE J.* **1975**, *21*, 116-128. https://doi.org/10.1002/aic.690210115.

102. Kontogeorgis, G.M.; Folas, G.K., Activity Coefficient Models Part 1: Random-Mixing Models. In *Thermodynamic Models for Industrial Applications*, **2010**; pp 79-107. https://doi.org/10.1002/9780470747537.ch4.
103. Kontogeorgis, G.M.; Folas, G.K., Activity Coefficient Models Part 2: Local Composition Models, from Wilson and NRTL to UNIQUAC and UNIFAC. In *Thermodynamic Models for Industrial Applications*, **2010**; pp 109-157. https://doi.org/10.1002/9780470747537.ch5.
104. Macedo, E.A.; Skovborg, P.; Rasmussen, P., Calculation of phase equilibria for solutions of strong electrolytes in solvent-water mixtures. *Chem. Eng. Sci.* **1990**, *45*, 875-882. https://doi.org/10.1016/0009-2509(90)85009-3.
105. Velho, P.; Gómez, E.; Macedo, E.A., Calculating the closest approach parameter for ethyl lactate-based ATPS. *Fluid Phase Equilib.* **2022**, *556*, 113389. https://doi.org/10.1016/j.fluid.2022.113389.
106. Lopes, C.; Velho, P.; Macedo, E.A., Predicting the ionicity of ionic liquids in binary mixtures based on solubility data. *Fluid Phase Equilib.* **2023**, *567*, 113717. https://doi.org/10.1016/j.fluid.2022.113717.
107. Velho, P.; Lopes, C.; Macedo, E.A., Predicting the ionicity of ionic liquids in binary mixtures based on solubility data: II. *Fluid Phase Equilib.* **2023**, *569*, 113766. https://doi.org/10.1016/j.fluid.2023.113766.
108. Bondi, A., van der Waals Volumes and Radii. *J. Phys. Chem.* **1964**, *68*, 441-451. https://doi.org/10.1021/j100785a001.
109. Joback, K.G.; Reid, R.C., Estimation of Pure-Component Properties from Group-Contributions. *Chem. Eng. Commun.* **1987**, *57*, 233-243. https://doi.org/10.1080/00986448708960487.
110. Marrero, J.; Gani, R., Group-contribution based estimation of pure component properties. *Fluid Phase Equilib.* **2001**, *183-184*, 183-208. https://doi.org/10.1016/S0378-3812(01)00431-9.
111. Zhao, Y.H.; Abraham, M.H.; Zissimos, A.M., Fast Calculation of van der Waals Volume as a Sum of Atomic and Bond Contributions and Its Application to Drug Compounds. *J. Org. Chem.* **2003**, *68*, 7368-7373. https://doi.org/10.1021/jo034808o.
112. Pitzer, K.S., Electrolytes. From dilute solutions to fused salts. *J. Am. Chem. Soc.* **1980**, *102*, 2902-2906. https://doi.org/10.1021/ja00529a006.
113. Marques, H.; Velho, P.; Gómez, E.; Macedo, E.A., Determining the dissociation extent of ionic liquids in water using the PDH + UNIQUAC model. *J. Mol. Liq.* **2022**, *348*, 118403. https://doi.org/10.1016/j.molliq.2021.118403.
114. Pitzer, K.S., *Activity Coefficients in Electrolyte Solutions*. 2nd ed.; CRC Press: Boca Raton, **1991**. ISBN: 978-1-315-89037-1.
115. Balaban, A.; Kuranov, G.; Smirnova, N., Phase equilibria modeling in aqueous systems containing 2-propanol and calcium chloride or/and magnesium chloride. *Fluid Phase Equilib.* **2002**, *194-197*, 717-728. https://doi.org/10.1016/S0378-3812(01)00783-X.
116. Chen, C.C.; Song, Y., Generalized electrolyte-NRTL model for mixed-solvent electrolyte systems. *AlChE J.* **2004**, *50*, 1928-1941. https://doi.org/10.1002/aic.10151.
117. Simoni, L.D.; Lin, Y.; Brennecke, J.F.; Stadtherr, M.A., Modeling Liquid−Liquid Equilibrium of Ionic Liquid Systems with NRTL, Electrolyte-NRTL, and UNIQUAC. *Ind. Eng. Chem. Res.* **2008**, *47*, 256-272. https://doi.org/10.1021/ie070956j.
118. Pitzer, K.S.; Simonson, J.M., Thermodynamics of multicomponent, miscible, ionic systems: theory and equations. *J. Phys. Chem.* **1986**, *90*, 3005-3009. https://doi.org/10.1021/j100404a042.
119. Oster, G., The Dielectric Properties of Liquid Mixtures. *J. Am. Chem. Soc.* **1946**, *68*, 2036-2041. https://doi.org/10.1021/ja01214a050.
120. Kohn, W.; Becke, A.D.; Parr, R.G., Density Functional Theory of Electronic Structure. *J. Phys. Chem.* **1996**, *100*, 12974-12980. https://doi.org/10.1021/jp960669l.
121. Nobel Prize Outreach, A., The nobel prize in chemistry 1998 explore press release. In *Nobelprize.org*, **2021**.
122. Burke, K., Perspective on density functional theory. *J. Chem. Phys.* **2012**, *136*, 150901. https://doi.org/10.1063/1.4704546.
123. Voroshylova, I.V.; Teixeira, F.; Costa, R.; Pereira, C.M.; Cordeiro, M.N.D.S., Interactions in the ionic liquid [EMIM][FAP]: a coupled experimental and computational analysis. *Phys. Chem. Chem. Phys.* **2016**, *18*, 2617-2628. https://doi.org/10.1039/C5CP06027C.
124. Moosavi, M.; Banazadeh, N.; Torkzadeh, M., Structure and Dynamics in Amino Acid Choline-Based Ionic Liquids: A Combined QTAIM, NCI, DFT, and Molecular Dynamics Study. *J. Phys. Chem. B* **2019**, *123*, 4070-4084. https://doi.org/10.1021/acs.jpcb.9b01799.
125. M. J. Frisch, G.W.T., H. B. Schlegel, G. E. Scuseria, M. A. Robb, J. R. Cheeseman, G. Scalmani, V. Barone, B. Mennucci, G. A. Petersson, H. Nakatsuji, M. Caricato, X. Li, H. P. Hratchian, A. F. Izmaylov, J. Bloino, G. Zheng, J. L. Sonnenberg, M. Hada, M. Ehara, K. Toyota, R. Fukuda, J. Hasegawa, M. Ishida, T. Nakajima, Y. Honda, O. Kitao, H. Nakai, T. Vreven, J. A. Montgomery, Jr., J. E. Peralta, F. Ogliaro, M. Bearpark, J. J. Heyd, E. Brothers, K. N. Kudin, V. N. Staroverov, R. Kobayashi, J. Normand, K. Raghavachari, A. Rendell, J. C. Burant, S. S. Iyengar, J. Tomasi, M. Cossi, N. Rega, J. M. Millam, M. Klene, J. E. Knox, J. B. Cross, V. Bakken, C. Adamo, J. Jaramillo, R. Gomperts, R. E. Stratmann, O. Yazyev, A. J. Austin, R. Cammi, C. Pomelli, J. W. Ochterski, R. L. Martin, K. Morokuma, V. G. Zakrzewski, G. A. Voth, P. Salvador, J. J. Dannenberg, S. Dapprich, A. D. Daniels, Ö. Farkas, J. B. Foresman, J. V. Ortiz, J. Cioslowski, and D. J. Fox *Gaussian 09*, Gaussian, Inc.: Wallingford **2009**.
126. Latini, G.; Signorile, M.; Crocellà, V.; Bocchini, S.; Pirri, C.F.; Bordiga, S., Unraveling the CO2 reaction mechanism in bio-based amino-acid ionic liquids by operando ATR-IR spectroscopy. *Catal. Today* **2019**, *336*, 148-160. https://doi.org/10.1016/j.cattod.2018.12.050.
127. Becke, A.D., Density-functional thermochemistry. III. The role of exact exchange. *J. Chem. Phys.* **1993**, *98*, 5648-5652. https://doi.org/10.1063/1.464913.
128. Lee, C.; Yang, W.; Parr, R.G., Development of the Colle-Salvetti correlation-energy formula into a functional of the electron density. *Physical Review B: Condensed Matter* **1988**, *37*, 785-789. https://doi.org/10.1103/physrevb.37.785.
129. Francl, M.M.; Pietro, W.J.; Hehre, W.J.; Binkley, J.S.; Gordon, M.S.; DeFrees, D.J.; Pople, J.A., Self-consistent molecular orbital methods. XXIII. A polarization-type basis set for second-row elements. *J. Chem. Phys.* **1982**, *77*, 3654-3665. https://doi.org/10.1063/1.444267.
130. Merchuk, J.C.; Andrews, B.A.; Asenjo, J.A., Aqueous two-phase systems for protein separation: Studies on phase inversion. *J. Chromatogr. B Biomed. Appl.* **1998**, *711*, 285-293. https://doi.org/10.1016/S0378-4347(97)00594-X.
131. Li, Z.; Pei, Y.; Liu, L.; Wang, J., (Liquid+liquid) equilibria for (acetate-based ionic liquids+inorganic salts) aqueous two-phase systems. *J. Chem. Thermodyn.* **2010**, *42*, 932-937. https://doi.org/10.1016/j.jct.2010.03.010.
132. Yu, C.; Han, J.; Hu, S.; Yan, Y.; Li, Y., Phase Diagrams for Aqueous Two-Phase Systems Containing the 1-Ethyl-3-methylimidazolium Tetrafluoroborate/1-Propyl-3-methylimidazolium Tetrafluoroborate and Trisodium Phosphate/Sodium Sulfite/Sodium Dihydrogen Phosphate at 298.15 K: Experiment and Correlation. *J. Chem. Eng. Data* **2011**, *56*, 3577-3584. https://doi.org/10.1021/je200379r.
133. Othmer, D.F.; Tobias, P.E., Liquid -Liquid Extraction Data -Toluene and Acetaldehyde Systems. *Ind. Eng. Chem.* **1942**, *34*, 690-692. https://doi.org/10.1021/ie50390a011.

134. Bancroft, W.D.; Hubard, S.S., A New Method for Determining Dineric Distribution1. *J. Am. Chem. Soc.* **1942**, *64*, 347-353. https://doi.org/10.1021/ja01254a035.
135. Mourão, T.; Tomé, L.C.; Florindo, C.; Rebelo, L.P.N.; Marrucho, I.M., Understanding the Role of Cholinium Carboxylate Ionic Liquids in PEG-Based Aqueous Biphasic Systems. *ACS. Sustain. Chem. Eng.* **2014**, *2*, 2426-2434. https://doi.org/10.1021/sc500444w.
136. Bicudo, J.G. Novel downstream processes for the purification of monoclonal antibodies based on aqueous two phase partitioning and hydrophobic interaction chromatography. MSc Thesis in Biological Engineering, IST, Lisbon, **2015**.
137. Pereira, J.F.B.; Kurnia, K.A.; Cojocaru, O.A.; Gurau, G.; Rebelo, L.P.N.; Rogers, R.D.; Freire, M.G.; Coutinho, J.A.P., Molecular interactions in aqueous biphasic systems composed of polyethylene glycol and crystalline vs. liquid cholinium-based salts. *Phys. Chem. Chem. Phys.* **2014**, *16*, 5723-5731. https://doi.org/10.1039/C3CP54907K.
138. Klerk, D.L.; Schwarz, C.E., Simplified Approach to Understanding, Evaluating, and Parameterizing the NRTL Model for the Description of Binary VLE: Ττ-VLE Approach. *Ind. Eng. Chem. Res.* **2023**, *XXX*, XXX-XXX. https://doi.org/10.1021/acs.iecr.3c00576.
139. De Santis, S.; Masci, G.; Casciotta, F.; Caminiti, R.; Scarpellini, E.; Campetella, M.; Gontrani, L., Cholinium-amino acid based ionic liquids: a new method of synthesis and physico-chemical characterization. *Phys. Chem. Chem. Phys.* **2015**, *17*, 20687-20698. https://doi.org/10.1039/C5CP01612F.
140. Prankerd, R.J., *Profiles of Drug Substances, Excipients and Related Methodology: Critical Compilation of pKa Values for Pharmaceutical Substances*. Elsevier Science: **2007**. ISBN: 9780080555966.
141. Wróblewska, K.B.; Plewa, S.; Dereziński, P.; Muszalska-Kolos, I., Choline Salicylate Analysis: Chemical Stability and Degradation Product Identification. *Molecules* **2019**, *25*, 51-68. https://doi.org/10.3390/molecules25010051.
142. Sintra, T.E.; Abranches, D.O.; Benfica, J.; Soares, B.P.; Ventura, S.P.M.; Coutinho, J.A.P., Cholinium-based ionic liquids as bioinspired hydrotropes to tackle solubility challenges in drug formulation. *Eur. J. Pharm. Biopharm.* **2021**, *164*, 86-92. https://doi.org/10.1016/j.ejpb.2021.04.013.

Annexes and Appendices

Annex A - Chemicals 53
Annex B - Data used for the modelling approach validation 57
Annex C - Liquid-liquid equilibria (LLE) data of used systems 63
Appendix A - Liquid-liquid equilibria (LLE) data of new systems 65
Appendix B - Thermodynamic modelling 73
Appendix C - Ionic Liquid synthesis 77
Appendix D - Ultraviolet-visible (UV-Vis) absorbance spectra of pure compounds 85
Appendix E - Variation of mean charge with pH 87
Appendix F - Stability of Ultraviolet-Visible (UV-Vis) absorbance spectra 93
Appendix G - Calibration curves 101
Appendix H - Partition coefficients and extraction efficiencies 105

Annex A - Chemicals

A.1 Two-dimensional structures

Table AA.1. Two dimensional structures of chemicals used in this work.

SOLVENTS

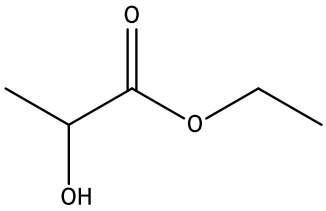

(-)-Ethyl L-lactate

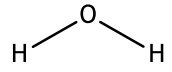

Water

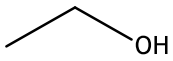

Ethanol

CHOLINE SALTS

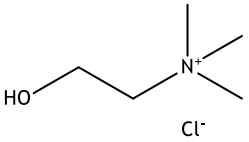

Choline chloride

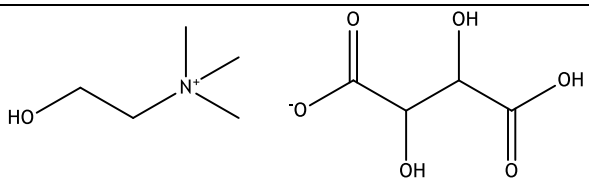

Choline bitartrate

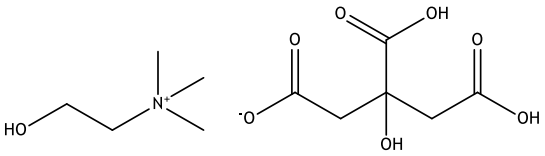

Choline di-hydrogen citrate

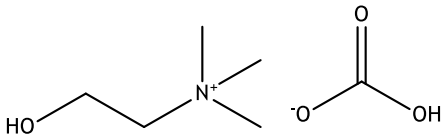

Choline bicarbonate

OTHER SALTS

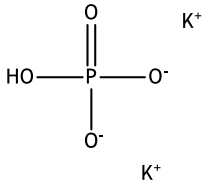

Di-potassium hydrogen phosphate

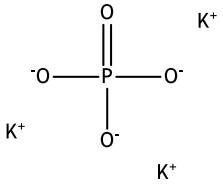

Tri-potassium phosphate

Potassium hydroxide

Table AA.1. Two dimensional structures of chemicals used in this work (cont.).

CHOLINE AMINO-ACID IONIC LIQUIDS

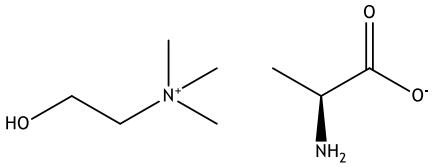

Cholinium L-alaninate

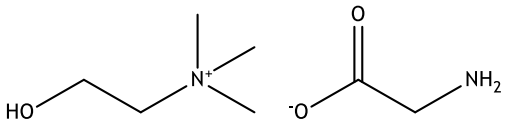

Cholinium glycinate

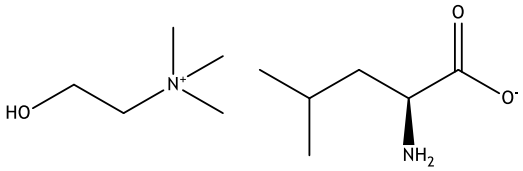

Cholinium leucinate

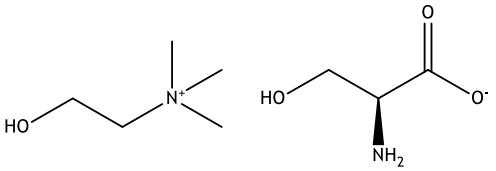

Cholinium L-serinate

AMINO-ACIDS

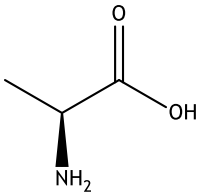

L-alanine

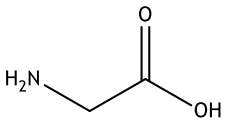

glycine

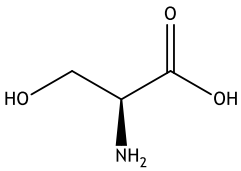

L-serine

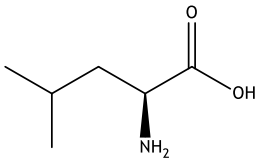

l-leucine

POLYMERS

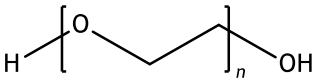

Polyethylene glycol

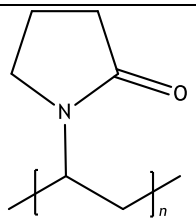

Polyvinylpyrrolidone

A.2 Molar masses and solubilities

Table AA.2. Molar mass (M) of chemicals used in this work.

Species	M / g·mol^{-1}	Species	M / g·mol^{-1}
(-)-Ethyl L-lactate ($C_5H_{10}O_3$)	118.13	Glycine ($C_2H_5NO_2$)	75.07
Acetaminophen ($C_8H_9NO_2$)	151.16	L-alanine ($C_3H_7NO_2$)	89.09
Acetic acid (CH_3CO_2H)	60.05	L-leucine ($C_6H_{13}NO_2$)	131.17
Amoxicillin trihydrate ($C_{16}H_{19}N_3O_5S{\cdot}3(H_2O)$)	419.5	L-serine ($C_3H_7NO_3$)	105.09
Choline bicarbonate ($C_6H_{15}NO_4$)	165.19	Polyethylene-glycol 1500 ($C_{2n}H_{4n+2}O_{n+1}$)	1500
Choline bitartrate ($C_9H_{19}NO_7$)	253.25	Polyethylene-glycol 4000 ($C_{2n}H_{4n+2}O_{n+1}$)	400
Choline chloride ($C_5H_{14}NOCl$)	139.62	Polyethylene-glycol 600 ($C_{2n}H_{4n+2}O_{n+1}$)	600
Choline di-hydrogen citrate ($C_{11}H_{21}NO_8$)	295.29	Polyvinylpyrrolidone 29,000 ($(C_6H_9NO)_n$)	29 000
Cholinium alaninate ($C_8H_{20}N_2O_3$)	192.26	Potassium hydroxide (KOH)	56.11
Cholinium glycinate ($C_7H_{18}N_2O_3$)	178.23	Potassium phosphate (K_3PO_4)	212.27
Cholinium leucinate ($C_{11}H_{26}N_2O_3$)	234.34	Salicylic acid ($C_7H_6O_3$)	138.12
Cholinium serinate ($C_8H_{20}N_2O_4$)	208.26	Sodium hydroxide (NaOH)	40.00
Di-potassium hydrogen phosphate (K_2HPO_4)	174.2	Water (H_2O)	18.02
Ethanol absolute (C_2H_5OH)	46.08		

Table AA.3. Solubility of studied pharmaceutical compounds in water, at 298.15 K and 0.1 MPa.

Species	Solubility / g·mL^{-1}	
Acetaminophen ($C_8H_9NO_2$)	$17.9{\cdot}10^{-2}$	[1]
Amoxicillin trihydrate ($C_{16}H_{19}N_3O_5S{\cdot}3(H_2O)$)	$3.43{\cdot}10^{-3}$	[2]
Salicylic acid ($C_7H_6O_3$)	$1.14{\cdot}10^{-3}$	[3]

References

1. Granberg, R.A.; Rasmuson, Å.C., Solubility of Paracetamol in Pure Solvents. *J. Chem. Eng. Data* **1999**, *44*, 1391-1395. https://doi.org/10.1021/je990124v.

2. Palacio, D.A.; Urbano, B.F.; Rivas, B.L., Water-soluble polymers with the ability to remove amoxicillin as emerging pollutant from water. *Environ. Technol. Innov.* **2021**, *23*, 101589. https://doi.org/10.1016/j.eti.2021.101589.

3. Mota, F.L.; Queimada, A.J.; Pinho, S.P.; Macedo, E.A., Aqueous Solubility of Some Natural Phenolic Compounds. *Ind. Eng. Chem. Res.* **2008**, *47*, 5182-5189. https://doi.org/10.1021/ie071452o.

Annex B - Data used for the modelling approach validation

B.1 Ternary systems used for the modelling approach validation

Table BB1.1. Liquid-liquid equilibria (LLE) data of ternary systems with only neutral species, at 298.15 K and 0.1 MPa, collected from literature. x_1^{I} denotes the mole fraction of component 1 in phase I.

x_1^{I}	x_2^{I}	x_1^{II}	x_2^{II}
{methanol (1) + toluene (2) + *n*-decane (3)} [1]			
0.1633	0.2855	0.7540	0.1459
0.1499	0.2739	0.7850	0.1301
0.1369	0.2377	0.8321	0.1062
0.1336	0.1861	0.8812	0.0759
0.1332	0.1627	0.9056	0.0602
{water (1) + *n*-hexane (2) + methanol (3)} [2]			
0.9435	0.0000	0.0080	0.9779
0.8440	0.0000	0.0093	0.9810
0.6806	0.0000	0.0107	0.9840
0.6352	0.0000	0.0166	0.9693
0.5566	0.0000	0.0115	0.9767
0.5276	0.0000	0.0130	0.9805
0.4953	0.0009	0.0100	0.9827
0.4462	0.0017	0.0117	0.9767
0.4143	0.0032	0.0090	0.9821
0.3606	0.0057	0.0108	0.9812
0.3210	0.0080	0.0189	0.9584
0.2873	0.0105	0.0124	0.9636
0.2578	0.0145	0.0096	0.9726
0.2337	0.0162	0.0065	0.9656
0.2056	0.0217	0.0162	0.9226
0.1717	0.0262	0.0074	0.9491
0.1455	0.0307	0.0155	0.9177
0.1205	0.0368	0.0127	0.9321
0.0936	0.0481	0.0073	0.9246
0.0509	0.0754	0.0124	0.8885
0.0177	0.1143	0.0069	0.8362
0.0109	0.1550	0.0060	0.7825
0.0000	0.2323	0.0000	0.7278

Table BB1.1. Liquid-liquid equilibria (LLE) data of ternary systems with only neutral species, at 298.15 K and 0.1 MPa, collected from literature. x_1^{I} denotes the mole fraction of component 1 in phase I (cont.).

x_1^{I}	x_2^{I}	x_1^{II}	x_2^{II}
{1-butanol (1) + ethanol (2) + water (3)} [3]			
0.4853	0.4853	0.4853	0.4853
0.4650	0.4650	0.4650	0.4650
0.4527	0.4527	0.4527	0.4527
0.4291	0.4291	0.4291	0.4291
0.3936	0.3936	0.3936	0.3936
0.3923	0.3923	0.3923	0.3923
0.3625	0.3625	0.3625	0.3625
0.3385	0.3385	0.3385	0.3385
0.3374	0.3374	0.3374	0.3374
0.2755	0.2755	0.2755	0.2755
0.2644	0.2644	0.2644	0.2644
0.2386	0.2386	0.2386	0.2386
0.2315	0.2315	0.2315	0.2315
0.1904	0.1904	0.1904	0.1904
0.1550	0.1550	0.1550	0.1550
0.1420	0.1420	0.1420	0.1420
0.1275	0.1275	0.1275	0.1275
0.1202	0.1202	0.1202	0.1202
{water (1) + isopropanol (2) + 1-heptanol (3)} [4]			
0.9997	0.9997	0.9997	0.9997
0.9928	0.9928	0.9928	0.9928
0.9884	0.9884	0.9884	0.9884
0.9829	0.9829	0.9829	0.9829
0.9760	0.9760	0.9760	0.9760
0.9664	0.9664	0.9664	0.9664
0.9564	0.9564	0.9564	0.9564
0.9473	0.9473	0.9473	0.9473
0.9407	0.9407	0.9407	0.9407
{dibutyl ether (1) + 1-propanol (2) + water (3)} [5]			
0.9311	0.0292	0.0027	0.0102
0.7867	0.1612	0.0014	0.0333
0.6110	0.2798	0.0010	0.0448
0.4731	0.3696	0.0003	0.0510
0.3157	0.4459	0.0003	0.0579
0.1764	0.4756	0.0004	0.0694
0.0921	0.4401	0.0007	0.0824
0.0467	0.3678	0.0021	0.0973

Table BB1.1. Liquid-liquid equilibria (LLE) data of ternary systems with only neutral species, at 298.15 K and 0.1 MPa, collected from literature. x_1^{I} denotes the mole fraction of component 1 in phase I (cont.).

x_1^{I}	x_2^{I}	x_1^{II}	x_2^{II}
{dibutyl ether (1) + methanol (2) + water (3)} [5]			
0.9694	0.0049	0.0001	0.0329
0.9529	0.0176	0.0001	0.0914
0.9279	0.0409	0.0001	0.1642
0.8965	0.0742	0.0005	0.2839
0.8700	0.0950	0.0011	0.3411
0.8368	0.1285	0.0024	0.4102
0.7598	0.1821	0.0048	0.4766
0.6939	0.2438	0.0104	0.5558
0.6304	0.3056	0.0206	0.6157
0.5562	0.3678	0.0391	0.6613
0.4862	0.4255	0.0556	0.6829

B.2 How to define new solvents for PCM in Gaussian

In order to define new solvents in Gaussian, it was necessary to input a set of properties relative to the solvent, namely:

- the solvent's dielectric constant (specified in the input file with the program's codeword eps),
- the solvent's dynamic or optical dielectric constant (specified with the program's codeword epsinf),
- the solvent's molar volume, in $\mathrm{cm^3 \cdot mol^{-1}}$ (specified with the program's codeword vmol),
- the solvent's density, in $\mathrm{particle \cdot Å^{-3}}$ (specified with the program's codeword density).

The dielectric constant is easily found in literature. epsinf can be estimated from the refractive index, and vmol and density can be calculated from the molar mass and density, according to the following equations:

$$\mathrm{epsinf} = n_{\mathrm{D}}^2 \tag{B2.1}$$

$$\mathrm{vmol} = \frac{M}{\rho} \tag{B2.2}$$

$$\mathrm{density} = \frac{\rho \cdot N_{\mathrm{A}}}{M \cdot 10^{24}} \tag{B2.3}$$

where n_{D} is the refractive index, M is the molar mass, in $\mathrm{g \cdot mol^{-1}}$, ρ is the density, in $\mathrm{g \cdot cm^{-3}}$, and N_{A} is Avogadro's number ($6.022 \cdot 10^{23}\ \mathrm{mol^{-1}}$).

B.3 Physical properties of pure species

Table BB3.1. Physical properties of pure species used in the validation and in the application of the modelling approach.

Species	Dielectric constant, ε		Refractive index, n_D		Density, ρ / g · cm^{-3}		Molar mass, M / g · mol^{-1}
butan-1-ol	17.1	[6]	1.397	[7]	0.8054	[7]	74.121
***n*-decane**	2.00	[8]	1.410	[8]	0.7261	[8]	142.29
di-butyl ether	3.11	[9]	1.397	[9]	0.76397	[9]	130.23
ethanol	24.30	[6]	1.359	[7]	0.7852	[7]	46.07
ethyl lactate	15.70	[10]	1.411	[11]	1.0286	[11]	118.13
heptan-1-ol	12.1	[6]	1.4216	[7]	0.8195	[7]	116.88
***n*-hexane**	1.89	[8]	1.372	[8]	0.6552	[8]	86.18
isopropanol	18.30	[6]	1.3776	[12]	0.786	[12]	60.1
methanol	32.63	[6]	1.327	[7]	0.7864	[7]	32.04
propan-1-ol	20.1	[6]	1.3837	[7]	0.7995	[7]	60.09
toluene	2.38	[13]	1.49415	[14]	0.8623	[13]	92.14
water	78.36	[15]	1.333	[16]	0.9971	[17]	18.02

References

1. Doulabi, F.S.M.; Mohsen-Nia, M.; Rasa, H., Ternary Liquid−Liquid Equilibria for the (Methanol + Methylbenzene + Decane) System at Different Temperatures. *J. Chem. Eng. Data* **2011**, *56*, 1366-1370. https://doi.org/10.1021/je1011554.

2. Liu, J.; Qin, Z.; Wang, J., Liquid−Liquid Equilibria for Methanol + Water + Hexane Ternary Mixtures. *J. Chem. Eng. Data* **2002**, *47*, 1243-1245. https://doi.org/10.1021/je0255269.

3. van Berlo, M.; Gude, M.T.; van der Wielen, L.A.M.; Luyben, K.C.A.M., Partition Coefficients and Solubilities of Glycine in the Ternary Solvent System 1-Butanol + Ethanol + Water. *Ind. Eng. Chem. Res.* **1997**, *36*, 2474-2482. https://doi.org/10.1021/ie960762w.

4. Fan, W.; Han, Y.; Yan, H.; Xu, D.; Huang, H.; Wang, Y., Liquid-liquid equilibrium data for ternary mixtures (water + isopropanol + 1-pentanol/1-hexanol/1-heptanol) at 298.15 K: Measurement, correlation and prediction. *J. Chem. Thermodyn.* **2022**, *174*, 106871. https://doi.org/10.1016/j.jct.2022.106871.

5. Park, S.-J.; Hwang, I.-C.; Kwak, H.-Y., Binary Liquid−Liquid Equilibrium (LLE) for Dibutyl Ether (DBE) + Water from (288.15 to 318.15) K and Ternary LLE for Systems of DBE + C1 ∼ C4 Alcohols + Water at 298.15 K. *J. Chem. Eng. Data* **2008**, *53*, 2089-2094. https://doi.org/10.1021/je800446c.

6. Maryott, A.A.; Smith, E.R., *Table of dielectric constants of pure liquids*. US Government Printing Office: **1951**; Vol. 514.

7. Ortega, J., Densities and refractive indices of pure alcohols as a function of temperature. *J. Chem. Eng. Data* **1982**, *27*, 312-317. https://doi.org/10.1021/je00029a024.

8. de Cominges, B.E.; Pineiro, M.M.; Mascato, E.; Mosteiro, L.; Iglesias, T.P.; Legido, J.L., Relative permittivities of binary mixtures of 1-butanol + n-alkane AT 298.15 K. *J. Therm. Anal. Calorim.* **2003**, *72*, 129-133. https://doi.org/10.1023/A:1023963502038.

9. Alonso, V.; González, J.A.; García de la Fuente, I.; Cobos, J.C., Dielectric and refractive index measurements for the systems 1-pentanol + octane, or + dibutyl ether or for dibutyl ether + octane at different temperatures. *Thermochim. Acta* **2012**, *543*, 246-253. https://doi.org/10.1016/j.tca.2012.05.036.

10. Aparicio, S.; Halajian, S.; Alcalde, R.; García, B.; Leal, J.M., Liquid structure of ethyl lactate, pure and water mixed, as seen by dielectric spectroscopy, solvatochromic and thermophysical studies. *Chem. Phys. Lett.* **2008**, *454*, 49-55. https://doi.org/10.1016/j.cplett.2008.01.068.

11. Cepeda, E.A.; Urbano, C., Isobaric Vapor Liquid Equilibrium of 3-Methyl-1-butanol + Ethyl Lactate and 1-Pentanol + Ethyl Lactate at (13.0 and 101.3) kPa. *J. Chem. Eng. Data* **2011**, 56, 2602-2607. https://doi.org/10.1021/je200111a.

12. Collier, S.J., 2-Propanol. In *Encyclopedia of Reagents for Organic Synthesis (EROS)*, **2016**, 1-15. https://doi.org/10.1002/047084289X.rn01989.

13. Ritzoulis, G.; Papadopoulos, N.; Jannakoudakis, D., Densities, viscosities, and dielectric constants of acetonitrile + toluene at 15, 25, and 35 °C. *J. Chem. Eng. Data* **1986**, 31, 146-148. https://doi.org/10.1021/je00044a004.

14. Singh, R.P.; Sinha, C.P., Viscosities and activation energies of viscous flow of the ternary mixtures of toluene, chlorobenzene, 1-hexanol, and benzyl alcohol. *J. Chem. Eng. Data* **1985**, *30*, 470-474. https://doi.org/10.1021/je00042a031.

15. Owen, B.B.; Miller, R.C.; Milner, C.E.; Cogan, H.L., THE DIELECTRIC CONSTANT OF WATER AS A FUNCTION OF TEMPERATURE AND PRESSURE. *J. Phys. Chem.* **1961**, *65*, 2065-2070. https://doi.org/10.1021/j100828a035.

16. Hale, G.M.; Querry, M.R., Optical Constants of Water in the 200-nm to 200-μm Wavelength Region. *Appl. Opt.* **1973**, *12*, 555-563. https://doi.org/10.1364/AO.12.000555.

17. Tanaka, M.; Girard, G.; Davis, R.; Peuto, A.; Bignell, N., Recommended table for the density of water between 0 °C and 40 °C based on recent experimental reports. *Metrologia* **2001**, *38*, 301. https://doi.org/10.1088/0026-1394/38/4/3.

Annex C - Liquid-liquid equilibria (LLE) data of used systems

In the used ATPS, the longest tie-line (with the highest value of the tie-line length, TLL) always corresponded to the one with the lowest index, except in the system {[Ch][Leu] (1) + K_3PO_4 (2) + water (3)}, in which numbering was changed accordingly.

Table CC.1. Liquid-liquid equilibria (LLE) data (mass fractions), tie-line slope (STL) and length (TLL) for studied ternary systems, at 298.15 K and 0.1 MPa.

Tie-line (TL)	$w_{1,F}$	$w_{2,F}$	$w_{1,T}$	$w_{2,T}$	$w_{1,B}$	$w_{2,B}$	STL	TLL
{[Ch][Ala] (1) + K_3PO_4 (2) + water (3)} [1]								
TL1	0.19764	0.36334	0.64329	0.02376	0.00414	0.51981	-1.288	80.906
TL2	0.25021	0.29529	0.61271	0.02964	0.01065	0.48270	-1.329	75.348
TL3	0.32960	0.20064	0.55931	0.03843	0.02756	0.43098	-1.355	66.095
TL4	0.40200	0.10870	0.49203	0.05570	0.07305	0.35109	-1.418	51.264
{[Ch][Ala] (1) + K_2HPO_4 (2) + water (3)} [1]								
TL1	0.31927	0.30668	0.59007	0.04300	0.04018	0.59670	−0.993	78.036
TL2	0.36098	0.23006	0.54085	0.05917	0.05283	0.55757	−0.979	69.754
TL3	0.40002	0.14046	0.46535	0.08790	0.07204	0.50929	−0.933	57.642
{[Ch][Gly] (1) + K_2HPO_4 (2) + water (3)} [1]								
TL1	0.33104	0.3291	0.61127	0.05076	0.02693	0.66877	−0.946	85.053
TL2	0.36111	0.24979	0.53912	0.07374	0.04038	0.6155	−0.921	73.637
TL3	0.39284	0.16661	0.46376	0.10748	0.06681	0.54274	−0.912	58.908
{[Ch][Ser] (1) + K_2HPO_4 (2) + water (3)} [1]								
TL1	0.39076	0.28915	0.63161	0.07416	0.03447	0.64983	−1.037	82.944
TL2	0.40756	0.22998	0.54695	0.11233	0.05468	0.59622	−1.017	69.028
TL3	0.43071	0.19933	0.5208	0.12512	0.05894	0.58255	−1.010	65.004
{[Ch][Leu] (1) + K_3PO_4 (2) + water (3)} [2]								
TL1	0.2414	0.3388	0.7259	0.0213	0.0131	0.4884	−1.53	85.23
TL2	0.1952	0.3458	0.6779	0.0272	0.0191	0.4620	−1.52	78.93
TL3	0.1511	0.3482	0.6111	0.0375	0.0288	0.4308	−1.48	70.27
TL4	0.1024	0.3495	0.4788	0.0677	0.0450	0.3925	−1.34	54.20
{PEG600 (1) + [Ch]Bic (2) + water (3)} [3]								
TL1	0.4988	0.3493	-	-	-	-	-	117.85
TL2	0.4981	0.2996	-	-	-	-	-	102.38
TL3	0.4987	0.2499	-	-	-	-	-	73.18

References

1. Gómez, E.; Requejo, P.F.; Tojo, E.; Macedo, E.A., Recovery of flavonoids using novel biodegradable choline amino acids ionic liquids based ATPS. *Fluid Phase Equilib.* **2019**, *493*, 1-9. https://doi.org/10.1016/j.fluid.2019.03.024.

2. Wang, R.; Chang, Y.; Tan, Z.; Li, F., Phase behavior of aqueous biphasic systems composed of novel choline amino acid ionic liquids and salts. *J. Mol. Liq.* **2016**, *222*, 836-844. https://doi.org/10.1016/j.molliq.2016.07.079.

3. Pereira, J.F.B.; Vicente, F.; Santos-Ebinuma, V.C.; Araújo, J.M.; Pessoa, A.; Freire, M.G.; Coutinho, J.A.P., Extraction of tetracycline from fermentation broth using aqueous two-phase systems composed of polyethylene glycol and cholinium-based salts. *Process Biochem.* **2013**, *48*, 716-722. https://doi.org/10.1016/j.procbio.2013.02.025.

Appendix A - Liquid-liquid equilibria (LLE) data of new systems

A.1 Experimental

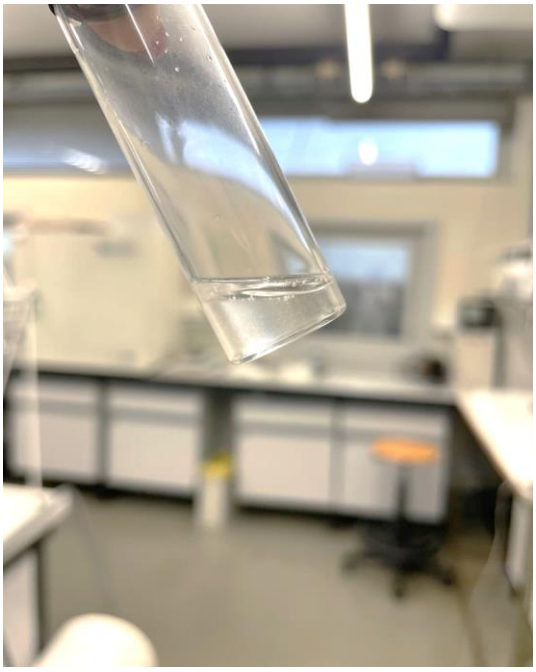

Fig. A1.1. Example of a cloud point.

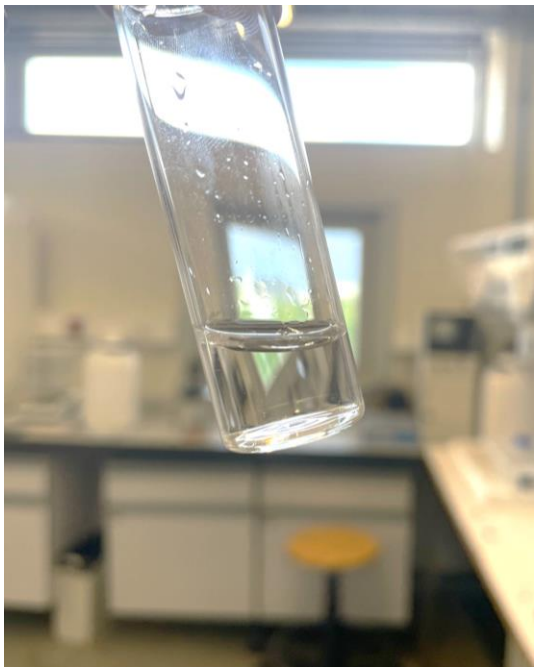

Fig. A1.2. Example of a clear mixture, not in cloud point.

A.2 Binodal data

Table A2.1. List of tested systems and respective range of compositions.

System	No. of points	Range of tested w_1	Range of tested w_2	Immiscible?
{EL (1) + [Ch]Cl (2) + water (3)}	0	0 - 1	0 - 0.32	no
{EL (1) + [Ch]Bit (2) + water (3)}	22	0 - 1	0 - 0.57	yes
{EL (1) + [Ch]DHCit (2) + water (3)}	9	0 - 1	0 - 0.71	yes
{EL (1) + [Ch]Bic (2) + water (3)}	5	0 - 1	0 - 0.80	yes
{PEG1500 (1) + [Ch]DHCit (2) + water (3)}	6	0 - 0.55	0 - 0.78	yes
{PEG1500 (1) + [Ch]Bit (2) + water (3)}	5	0 - 0.66	0 - 0.45	yes
{PEG4000 (1) + [Ch]Cl (2) + water (3)}	0	0.05 - 0.25	0.26 - 0.36	no
{PEG4000 (1) + [Ch]Bit (2) + water (3)}	13	0 - 0.48	0 - 0.60	yes
{PVP29000 (1) + [Ch]Cl (2) + water (3)}	0	0.02 - 0.12	0 - 0.30	no
{PVP29000 (1) + [Ch]Bit (2) + water (3)}	0	0.09 - 0.64	0 - 0.48	no
{PVP29000 (1) + [Ch]DHCit (2) + water (3)}	0	0.09 - 0.64	0 - 0.62	no

Table A2.2. Experimental LLE data (mass fractions) for studied ternary systems, at 298.15 K and 0.1 MPa.

$w_{1,F}$	$w_{2,F}$	$w_{1,F}$	$w_{2,F}$	$w_{1,F}$	$w_{2,F}$
{EL (1) + [Ch]Bit (2) + water (3)}					
0.9292	0.0059	0.5681	0.1460	0.2409	0.3591
0.9268	0.0047	0.5355	0.1624	0.2170	0.3892
0.8183	0.0396	0.4752	0.1966	0.1879	0.4205
0.7677	0.0545	0.4368	0.2182	0.1340	0.4727
0.7174	0.0720	0.4347	0.2175	0.1194	0.5021
0.6776	0.0891	0.3590	0.2678	0.1158	0.5399
0.6526	0.1007	0.2971	0.3160	-	-
0.5975	0.1284	0.2820	0.3313	-	-
{EL (1) + [Ch]DHCit (2) + water (3)}					
0.0907	0.7097	0.2985	0.4550	0.6630	0.1741
0.1282	0.6355	0.4248	0.3492	0.7199	0.1382
0.2569	0.5089	0.5450	0.2559	0.8114	0.0859
{EL (1) + [Ch]Bic (2) + water (3)}					
0.1421	0.6863	0.2155	0.4378	0.5389	0.1812
0.1564	0.5146	0.3700	0.2759	-	-
{PEG1500 (1) + [Ch]DHCit (2) + water (3)}					
0.3812	0.3296	0.0508	0.6538	0.00876	0.7701
0.1994	0.5000	0.00982	0.7667	0.00512	0.7733
{PEG1500 (1) + [Ch]Bit (2) + water (3)}					
0.5566	0.0936	0.2604	0.3246	0.1784	0.4369
0.3513	0.2467	0.1828	0.4103	-	-
{PEG4000 (1) + [Ch]Bit (2) + water (3)}					
0.3235	0.2181	0.1457	0.3561	0.0384	0.4699
0.2509	0.2768	0.1131	0.3847	0.0185	0.5069
0.2143	0.3001	0.0830	0.4134	0.0074	0.5573
0.1985	0.3107	0.0691	0.4280	-	-
0.1673	0.3388	0.0513	0.4468	-	-

A.3 LLE fitting

Table A3.1. Parameters of the Merchuk [1], Li [2] and Yu [3] correlations, for the new ternary systems, at 298.15 K and 0.1 MPa.

	Parameters				Performance Indicators	
{EL (1) + [Ch]Bit (2) + Water (3)}						
Model	A_1	B_1	C_1	D_1	R^2	E_{RMSE} / %
Merchuk	1.074	-1.612	9.917	-	0.9926	2.22
Li	0.973	-0.491	-1.737	-0.850	0.9996	0.524
Yu	0.0299	-1.279	0.01389	-370.9	0.9984	1.02
{EL (1) + [Ch]Bic (2) + Water (3)}						
Model	A_1	B_1	C_1	D_1	R^2	E_{RMSE} / %
Merchuk	3.458	-4.362	-1.128	-	0.9944	1.13
Li	1.334	-1.826	-0.3157	-3.6056	0.9986	0.572
Yu	1.333	-4.642	-0.00277	-370.8	0.9933	1.23
{EL (1) + [Ch]DHCit (2) + Water (3)}						
Model	A_1	B_1	C_1	D_1	R^2	E_{RMSE} / %
Merchuk	1.313	-1.609	3.915	-	0.9994	0.609
Li	1.209	-1.310	-0.0342	0.1367	0.9988	0.849
Yu	0.0836	-0.937	0.00874	-370.9	0.9992	0.726
{PEG4000 (1) + [Ch]Bit (2) + Water (3)}						
Model	A_1	B_1	C_1	D_1	R^2	E_{RMSE} / %
Merchuk	0.501	-0.463	21.6	-	0.9994	0.233
Li	1.243	-2.061	0.0746	10.85	0.9949	0.668
Yu	-2.358	4.395	0.0475	-370.6	0.9988	0.333
{PEG1500 (1) + [Ch]DHCit (2) + water (3)}						
Model	A_1	B_1	C_1	D_1	R^2	E_{RMSE} / %
Merchuk	0.398	0.399	7.682	-	0.9975	0.793
Li	1.292	-1.590	-0.0972	-3.221	0.9999	0.121
Yu	-3.198	5.750	0.0267	-370.9	0.9968	0.897
{PEG1500 (1) + [Ch]Bit (2) + water (3)}						
Model	A_1	B_1	C_1	D_1	R^2	E_{RMSE} / %
Merchuk	1.069	-2.113	4.368	-	0.9977	0.674
Li	0.220	2.986	-6.584	-0.683	0.9995	0.301
Yu	-2.031	10.25	18.94	-0.493	0.9992	0.366

A.4 {EL (1) + [Ch]Bit (2) + water (3)}

A.4.1 Isolines

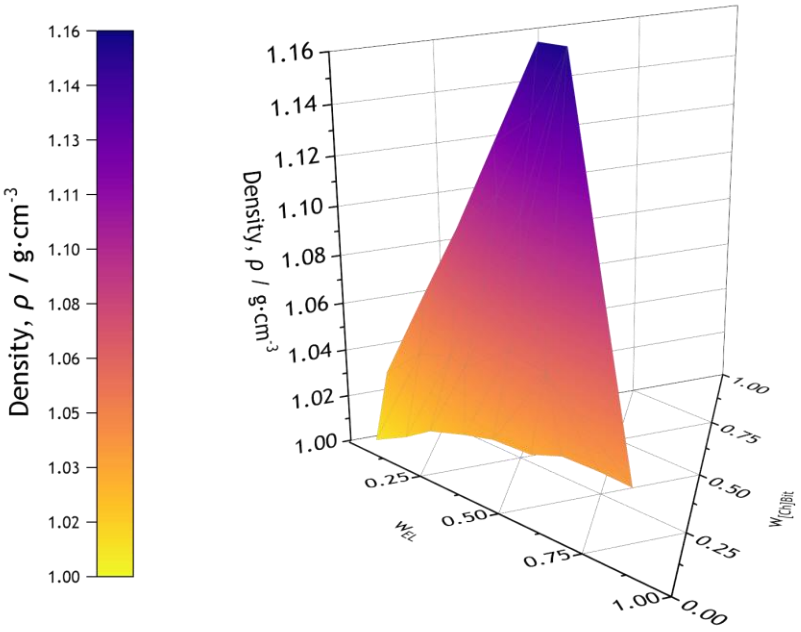

Fig. A4.1. Three-dimensional ternary plot of the density (ρ) as a function of the mass fraction of ethyl lactate (EL) and choline bitartrate ([Ch]Bit).

Table A4.1. Experimental mass fractions and measured density at 298.15 K.

w_{EL}	$w_{[\mathrm{Ch}]\mathrm{Bit}}$	Density, ρ / g · cm^{-3}	w_{EL}	$w_{[\mathrm{Ch}]\mathrm{Bit}}$	Density, ρ / g · cm^{-3}
0.000	0.108	1.02738	0.290	0.086	1.04671
0.000	0.205	1.05795	0.290	0.225	1.08791
0.000	0.293	1.08455	0.400	0.110	1.05899
0.000	0.388	1.11700	0.529	0.093	1.05762
0.000	0.498	1.15477	0.107	0.000	1.00694
0.106	0.115	1.04126	0.196	0.000	1.01460
0.104	0.212	1.07202	0.296	0.000	1.02200
0.107	0.312	1.10236	0.391	0.000	1.02727
0.105	0.397	1.13102	0.488	0.000	1.03064
0.100	0.491	1.15673	0.591	0.000	1.03158
0.217	0.107	1.04672	0.688	0.000	1.03657
0.213	0.203	1.07766	0.776	0.000	1.03710
0.215	0.284	1.10064	0.863	0.000	1.03667

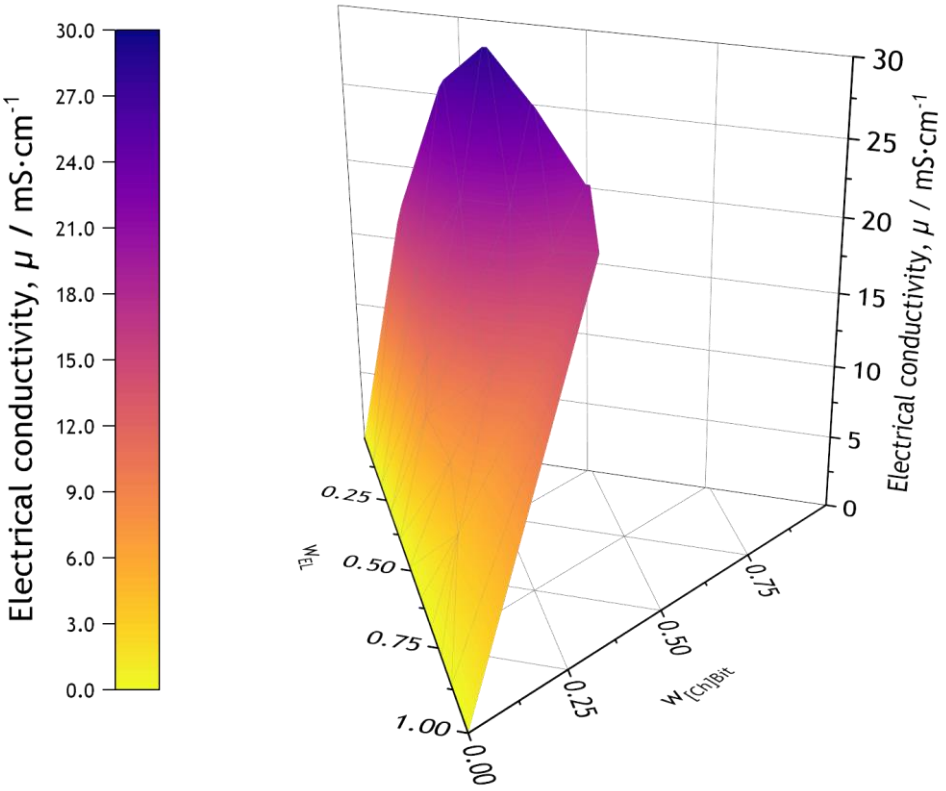

Fig. A4.2. Three-dimensional ternary plot of the electrical conductivity (μ) as a function of the mass fraction of ethyl lactate (EL) and choline bitartrate ([Ch]Bit).

Table A4.2. Experimental mass fractions and measured electrical conductivity at 298.15 K.

w_{EL}	$w_{[Ch]Bit}$	Electrical conductivity, μ / $mS \cdot cm^{-1}$	w_{EL}	$w_{[Ch]Bit}$	Electrical conductivity, μ / $mS \cdot cm^{-1}$
0.000	0.108	17.70	0.290	0.225	11.10
0.000	0.205	26.66	0.400	0.110	6.42
0.000	0.293	29.24	0.529	0.093	3.80
0.000	0.388	25.69	0.104	0.000	$2.610 \cdot 10^{-2}$
0.000	0.498	20.58	0.208	0.000	$3.095 \cdot 10^{-2}$
0.106	0.115	14.14	0.287	0.000	$2.647 \cdot 10^{-2}$
0.104	0.212	19.61	0.399	0.000	$1.765 \cdot 10^{-2}$
0.107	0.312	19.62	0.487	0.000	$1.117 \cdot 10^{-2}$
0.105	0.397	16.85	0.600	0.000	$5.130 \cdot 10^{-2}$
0.100	0.491	17.06	0.691	0.000	$2.400 \cdot 10^{-2}$
0.217	0.107	10.22	0.797	0.000	$7.950 \cdot 10^{-2}$
0.213	0.203	13.91	0.889	0.000	$2.800 \cdot 10^{-2}$
0.215	0.284	13.78	0.000	0.000	$8.000 \cdot 10^{-4}$
0.290	0.086	7.45	1.000	0.000	$1.950 \cdot 10^{-4}$

Table A4.3. Results of the *F*-test performed to the density and electrical conductivity isolines.

Density			Electrical conductivity		
	Experimental values	Predicted values		Experimental values	Predicted values
Mean	1.064	1.064	**Mean**	9.782	9.714
Variance	0.001758	0.001757	**Variance**	94.37	93.73
Observations	26	26	**Observations**	28	28
F	1.0005		***F***	1.007	
***F* Critical one-tail**	1.9554		***F* Critical one-tail**	1.9048	

A.4.2 Critical point

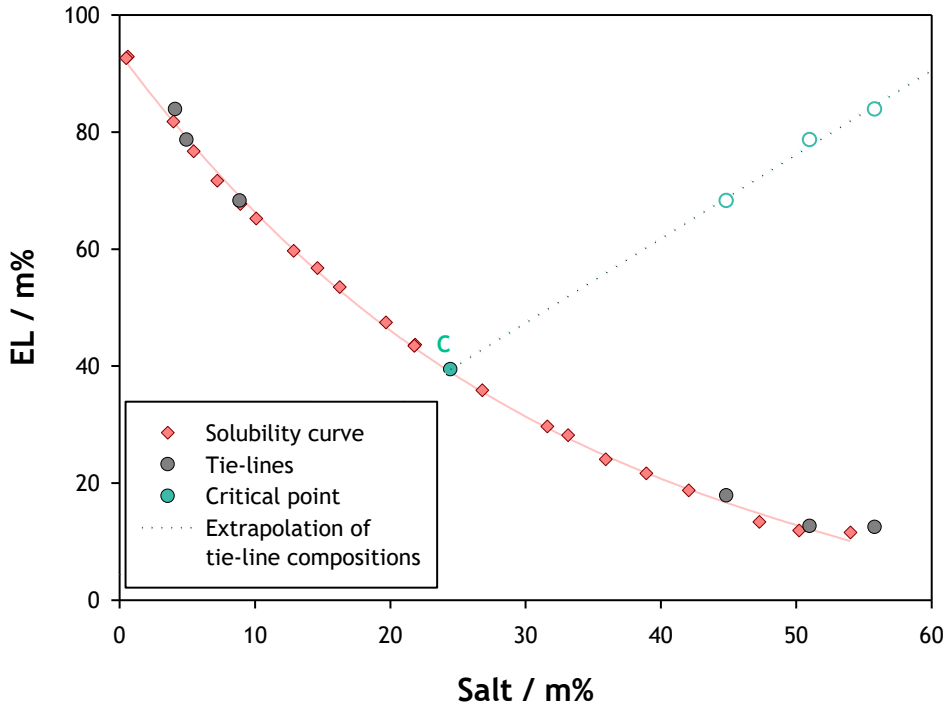

Fig. A4.3. Phase diagram of the system {EL (1) + [Ch]Bit (2) + water (3)} used for the critical point determination. The extrapolation of tie-line compositions follows equation $w_{\mathrm{EL}} \cdot 100 = 1.4381 \cdot w_{\mathrm{Salt}} + 4.3019 \cdot 10^{-2}$ with R^2 =0.9860.

References

1. Merchuk, J.C.; Andrews, B.A.; Asenjo, J.A., Aqueous two-phase systems for protein separation: Studies on phase inversion. *J. Chromatogr. B Biomed. Appl.* **1998**, *711*, 285-293. https://doi.org/10.1016/S0378-4347(97)00594-X.

2. Li, Z.; Pei, Y.; Liu, L.; Wang, J., (Liquid+liquid) equilibria for (acetate-based ionic liquids+inorganic salts) aqueous two-phase systems. *J. Chem. Thermodyn.* **2010**, *42*, 932-937. https://doi.org/10.1016/j.jct.2010.03.010.

3. Yu, C.; Han, J.; Hu, S.; Yan, Y.; Li, Y., Phase Diagrams for Aqueous Two-Phase Systems Containing the 1- Ethyl-3-methylimidazolium Tetrafluoroborate/1-Propyl-3-methylimidazolium Tetrafluoroborate and Trisodium Phosphate/Sodium Sulfite/Sodium Dihydrogen Phosphate at 298.15 K: Experiment and Correlation. *J. Chem. Eng. Data* **2011**, *56*, 3577-3584. https://doi.org/10.1021/je200379r.

Appendix B - Thermodynamic modelling

B.1 Calculated van der Waals volumes and surface areas

Table B1.1. van der Waals volumes and surface areas calculated using Bondi's method [1] for pure neutral compounds.

Species	V_w / $cm^3 \cdot mol^{-1}$	A_w / $cm^2 \cdot mol^{-1}$	Species	V_w / $cm^3 \cdot mol^{-1}$	A_w / $cm^2 \cdot mol^{-1}$
butan-1-ol	52.402	$7.630 \cdot 10^9$	***n*-hexane**	68.262	$9.640 \cdot 10^9$
***n*-decane**	109.185	$1.504 \cdot 10^{10}$	**isopropanol**	42.159	$6.270 \cdot 10^9$
dibutyl ether	92.423	$1.294 \cdot 10^{10}$	**methanol**	21.710	$3.580 \cdot 10^9$
ethanol	31.940	$4.930 \cdot 10^9$	**propan-1-ol**	42.171	$6.280 \cdot 10^9$
ethyl lactate	67.591	$1.003 \cdot 10^{10}$	**toluene**	59.509	$7.420 \cdot 10^9$
heptan-1-ol	83.094	$1.168 \cdot 10^{10}$	**water**	13.956	$3.500 \cdot 10^9$

Table B1.2. van der Waals volumes and surface areas calculated using Bondi's method [1] for ions.

Cations	V_w / $cm^3 \cdot mol^{-1}$	A_w / $cm^2 \cdot mol^{-1}$	Anions	V_w / $cm^3 \cdot mol^{-1}$	A_w / $cm^2 \cdot mol^{-1}$
cholinium	73.840	$1.075 \cdot 10^{10}$	**bitartrate**	65.671	$9.610 \cdot 10^9$
			di-hydrogen citrate	87.604	$1.277 \cdot 10^{10}$
			fumarate (1-)	52.972	$7.718 \cdot 10^9$
			malonate (1-)	46.262	$6.900 \cdot 10^9$
			succinate (1-)	56.493	$8.250 \cdot 10^9$

B.2 Calculated non-randomness factors

Table B2.1. Non-randomness factors (α) calculated for pure neutral compounds.

Species	α	Species	α
butan-1-ol	0.27171	***n*-hexane**	$1.0254 \cdot 10^{-5}$
***n*-decane**	$9.3757 \cdot 10^{-6}$	**isopropanol**	0.22336
dibutyl ether	0.10044	**methanol**	0.40430
ethanol	0.50558	**propan-1-ol**	0.25622
ethyl lactate	0.16434	**toluene**	0.042803
heptan-1-ol	0.24821	**water**	0.57735

Table B2.2. Non-randomness factors (α) calculated for ions.

Cations	α	Anions	α
cholinium	0.12888	**bitartrate**	0.11009
		di-hydrogen citrate	0.037857
		fumarate (1-)	0.37657
		malonate (1-)	0.066132
		succinate (1-)	0.068831

B.3 Validation of the novel approach for the non-randomness factor

Table B3.1. Average value of the non-randomness factor in phases I and II, and overall in each system, at 298.15 K and 0.1 MPa.

System	Average value of α [a]		
	Phase I	Phase II	Overall
{methanol (1) + toluene (2) + *n*-decane (3)}	0.0678	0.3406	0.2042
{water (1) + *n*-hexane (2) + methanol (3)}	0.4491	0.0276	0.2383
{butan-1-ol (1) + ethanol (2) + water (3)}	0.4812	0.5660	0.5236
{water (1) + isopropanol (2) + heptan-1-ol (3)}	0.5676	0.3909	0.4792
{dibutyl ether (1) + propan-1-ol (2) + water (3)}	0.2696	0.5589	0.4142
{dibutyl ether (1) + methanol (2) + water (3)}	0.1757	0.5036	0.3396

[a] The average value of α was calculated following equation (3.29) for each phase and all points. The overall value indicated the average of the α of both phases.

Table B3.2. Optimised interaction energies with UNIQUAC (with $Z = 10$ and $Z = f(\alpha)$), for the system {methanol (1) + toluene (2) + *n*-decane (3)}, at 298.15 K and 0.1 MPa, and standard deviation from the tie-line data.

{methanol (1) + toluene (2) + *n*-decane (3)}							
UNIQUAC with $Z = 10$				UNIQUAC with $Z = f(\alpha)$			
$u_{ij} \cdot 10^{-3}$ / J·mol^{-1}	methanol	toluene	*n*-decane	$u_{ij} \cdot 10^{-3}$ / J·mol^{-1}	methanol	toluene	*n*-decane
methanol	0	-3.5742	5.4313	methanol	0	-5.3878	0.3326
toluene	2.4881	0	1.5861	toluene	2.6072	0	1.5995
n-decane	3.5423	-2.5548	0	*n*-decane	2.5123	1.5995	0
σ		$2.8666 \cdot 10^{-17}$		σ		$2.8666 \cdot 10^{-17}$	

Table B3.3. Optimised interaction energies with UNIQUAC (with $Z = 10$ and $Z = f(\alpha)$), for the system {water (1) + *n*-hexane (2) + methanol (3)}, at 298.15 K and 0.1 MPa, and standard deviation from the tie-line data.

{water (1) + *n*-hexane (2) + methanol (3)}							
UNIQUAC with $Z = 10$				UNIQUAC with $Z = f(\alpha)$			
$u_{ij} \cdot 10^{-3}$ / J·mol^{-1}	water	*n*-hexane	methanol	$u_{ij} \cdot 10^{-3}$ / J·mol^{-1}	water	*n*-hexane	methanol
water	0	-5.5000	5.4968	water	0	-5.4580	2.6488
n-hexane	5.2110	0	5.1076	*n*-hexane	5.5000	0	5.4998
methanol	5.2454	4.9112	0	methanol	5.4999	5.4990	0
σ		0.029389		σ		0.029389	

Table B3.4. Optimised interaction energies with UNIQUAC (with $Z = 10$ and $Z = f(\alpha)$), for the system {butan-1-ol (1) + ethanol (2) + water (3)}, at 298.15 K and 0.1 MPa, and standard deviation from the tie-line data.

{butan-1-ol (1) + ethanol (2) + water (3)}							
UNIQUAC with $Z = 10$				UNIQUAC with $Z = f(\alpha)$			
$u_{ij} \cdot 10^{-3}$ / J·mol^{-1}	butan-1-ol	ethanol	water	$u_{ij} \cdot 10^{-3}$ / J·mol^{-1}	butan-1-ol	ethanol	water
butan-1-ol	0	1.0017	-5.4675	butan-1-ol	0	2.5876	-5.4995
ethanol	1.0000	0	0.9567	ethanol	0.1992	0	-5.2266
water	1.0476	1.0415	0	water	-5.3428	1.0499	0
σ	1.3608·10^{-7}			σ	2.8666·10^{-17}		

Table B3.5. Optimised interaction energies with UNIQUAC (with $Z = 10$ and $Z = f(\alpha)$), for the system {water (1) + isopropanol (2) + heptan-1-ol (3)}, at 298.15 K and 0.1 MPa, and standard deviation from the tie-line data.

{water (1) + isopropanol (2) + heptan-1-ol (3)}							
UNIQUAC with $Z = 10$				UNIQUAC with $Z = f(\alpha)$			
$u_{ij} \cdot 10^{-3}$ / J·mol^{-1}	water	isopropanol	heptan-1-ol	$u_{ij} \cdot 10^{-3}$ / J·mol^{-1}	water	isopropanol	heptan-1-ol
water	0	-0.6533	-5.3380	water	0	-0.9724	-5.4275
isopropanol	-0.6550	0	-0.6580	isopropanol	-0.5325	0	-0.5480
heptan-1-ol	-0.6369	-0.6550	0	heptan-1-ol	-0.5224	-0.5345	0
σ	1.9245·10^{-7}			σ	1.9245·10^{-7}		

Table B3.6. Optimised interaction energies with UNIQUAC (with $Z = 10$ and $Z = f(\alpha)$), for the system {dibutyl ether (1) + methanol (2) + water (3)}, at 298.15 K and 0.1 MPa, and standard deviation from the tie-line data.

{dibutyl ether (1) + methanol (2) + water (3)}							
UNIQUAC with $Z = 10$				UNIQUAC with $Z = f(\alpha)$			
$u_{ij} \cdot 10^{-3}$ / J·mol^{-1}	dibutyl ether	methanol	water	$u_{ij} \cdot 10^{-3}$ / J·mol^{-1}	dibutyl ether	methanol	water
dibutyl ether	0	-0.6418	-5.2622	dibutyl ether	0	-0.0135	-5.0520
methanol	-0.4752	0	-0.4752	methanol	0.1786	0	0.1596
water	-0.4752	-0.4752	0	water	0.3068	0.1733	0
σ	1.9350·10^{-17}			σ	1.9350·10^{-17}		

Table B3.7. Optimised interaction energies with UNIQUAC (with $Z = 10$ and $Z = f(\alpha)$), for the system {dibutyl ether (1) + propan-1-ol (2) + water (3)}, at 298.15 K and 0.1 MPa, and standard deviation from the tie-line data.

{dibutyl ether (1) + propan-1-ol (2) + water (3)}							
UNIQUAC with $Z = 10$				UNIQUAC with $Z = f(\alpha)$			
$u_{ij} \cdot 10^{-3}$ / J·mol^{-1}	dibutyl ether	propan-1-ol	water	$u_{ij} \cdot 10^{-3}$ / J·mol^{-1}	dibutyl ether	propan-1-ol	water
dibutyl ether	0	-0.9187	-5.4766	dibutyl ether	0	0.2231	-3.8214
propan-1-ol	-0.8325	0	-0.8326	propan-1-ol	0.1401	0	-0.9244
water	-0.8325	-0.8325	0	water	0.4118	0.1037	0
σ	3.5832·10^{-17}			σ	3.5832·10^{-17}		

B.4 Modelling with PDH-UNIQUAC

Table B4.1. Average value of the non-randomness factor in phases I and II, and overall for the system {ethyl lactate (1) + [Ch]Bit (2) + water (3)}, at 298.15 K and 0.1 MPa.

System	Average value of α a		
	Phase I	Phase II	Overall
{ethyl lactate (1) + [Ch]Bit (2) + water (3)}	0.2333	0.2794	0.2564

Table B4.2. Optimised interaction energies with PDH+UNIQUAC (with $Z = 10$ and $Z = f(\alpha)$), for the system {EL (1) + [Ch]Bit (2) + water (3)}, at 298.15 K and 0.1 MPa, and standard deviation from the tie-line data.

{ethyl lactate (1) + [Ch]Bit (2) + water (3)}									
UNIQUAC with $Z = 10$					**UNIQUAC with $Z = f(\alpha)$**				
$u_{ij} \cdot 10^{-3}$ / J·mol^{-1}	**ethyl lactate**	**[Ch]$^+$**	**Bit$^-$**	**water**	$u_{ij} \cdot 10^{-3}$ / J·mol^{-1}	**ethyl lactate**	**[Ch]$^+$**	**Bit$^-$**	**water**
ethyl lactate	0	-0.9260	-0.3149	-5.3770	**ethyl lactate**	0	0.8224	0.8602	-5.4675
[Ch]$^+$	2.0197	0	0.9607	-3.7779	**[Ch]$^+$**	1.1308	0	0.9974	-1.7644
Bit$^-$	1.9115	0.5087	0	0.4739	**Bit$^-$**	1.0902	0.9790	0	0.2372
water	5.4775	-1.4084	0.8282	0	**water**	4.9032	-0.3619	0.8635	0
σ	3.2049·10^{-17}				σ	3.2049·10^{-17}			

References

1. Bondi, A., van der Waals Volumes and Radii. *J. Phys. Chem.* **1964**, *68*, 441-451. https://doi.org/10.1021/j100785a001.

Appendix C - Ionic Liquid synthesis

C.1 Experimental apparatus

Fig. C1.1. Experimental setup of the ionic liquid synthesis.

Fig. C1.2. Drying of the ionic liquid by reduced-pression distillation, at 323.15 K, in a rotary evaporator.

Fig. C1.3. Drying of the ionic liquid by reduced-pression filtration.

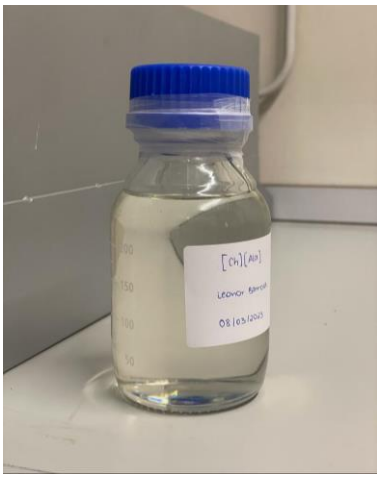

Fig. C1.4. Aspect of the ionic liquid [Ch][Ala] (cholinium alaninate) after purification.

C.2 FTIR spectra

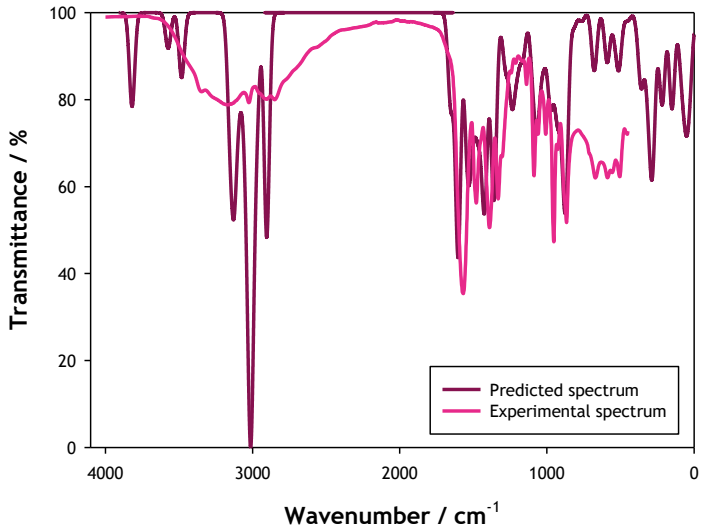

Fig. C2.1. Experimental and predicted infrared spectra of cholinium glycinate ([Ch][Gly]).

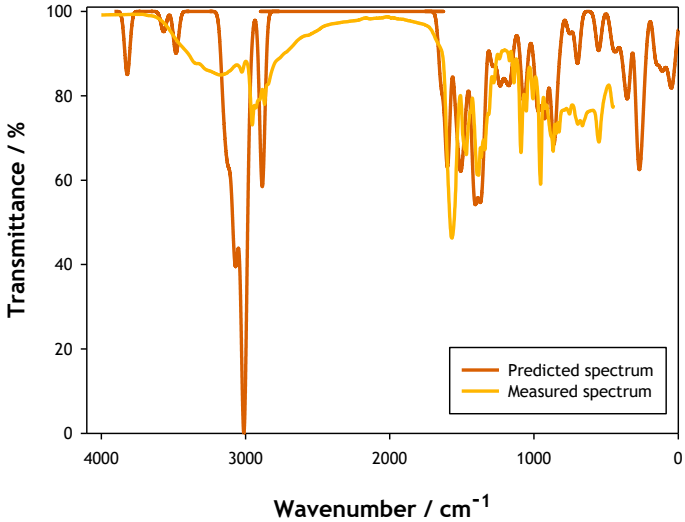

Fig. C2.2. Experimental and predicted infrared spectra of cholinium leucinate ([Ch][Leu]).

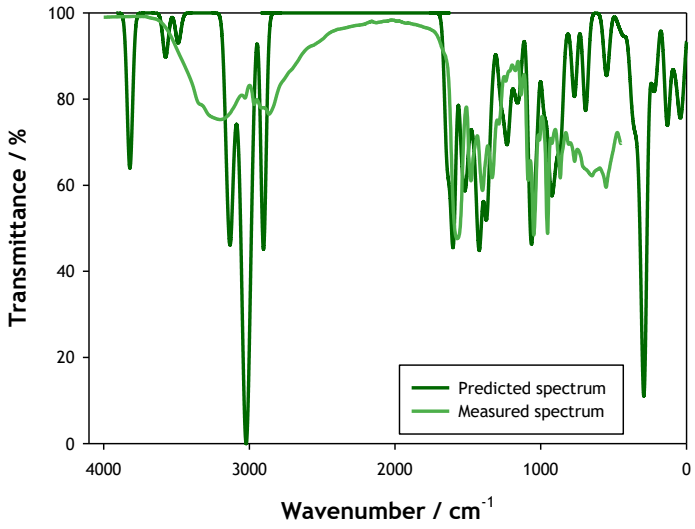

Fig. C2.3. Experimental and predicted infrared spectra of cholinium serinate ([Ch][Ser]).

Table C2.1. Predicted wavenumbers (WN, in cm^{-1}) and normalised intensities of absorption (*I*, in arbitrary units) for [Ch][Ala].

WN	*I*	WN	*I*	WN	*I*	WN	*I*	WN	*I*
19	7.78	373	5.55	1069	39.31	1444	15.82	3013	53.52
23	5.48	379	6.95	1085	18.52	1463	12.12	3021	81.75
43	19.21	390	2.92	1091	1.42	1468	11.73	3030	20.42
50	11.04	449	2.13	1097	1.19	1476	2.62	3051	25.40
60	15.75	464	2.38	1158	15.05	1480	9.16	3065	32.94
80	1.70	534	21.66	1160	17.04	1492	11.48	3077	16.80
91	10.91	538	2.32	1183	3.59	1498	10.85	3088	28.51
139	27.04	658	26.19	1199	21.70	1499	21.38	3097	18.45
144	10.86	763	3.78	1229	10.77	1510	15.74	3118	5.50
231	18.80	777	12.89	1241	22.93	1512	11.23	3127	47.71
246	20.27	816	5.66	1276	20.28	1522	8.45	3129	13.12
250	6.68	835	40.51	1295	2.98	1532	8.33	3144	16.30
272	30.77	877	49.96	1303	2.98	1541	20.80	3154	13.69
276	8.80	920	31.91	1346	35.54	1546	16.64	3159	18.18
292	52.58	925	19.55	1358	12.34	1601	94.23	3476	24.64
308	14.03	941	19.55	1360	46.03	1644	49.42	3560	12.69
333	3.97	977	36.32	1385	16.38	2893	100.00	3821	39.18
335	3.92	1025	16.17	1386	11.31	3003	29.25		
365	30.31	1043	13.31	1419	67.87	3005	38.04		

Table C2.2. Predicted wavenumbers (WN, in cm^{-1}) and normalised intensities of absorption (I, in arbitrary units) for [Ch][Gly].

WN	*I*	WN	*I*	WN	*I*	WN	*I*	WN	*I*
14	5.42	374	1.99	1069	38.76	1461	8.02	3011	66.77
32	14.89	381	3.37	1091	0.60	1466	19.48	3017	72.85
41	16.52	448	2.59	1097	2.27	1475	0.82	3038	28.62
58	16.67	463	0.98	1098	15.76	1479	13.88	3050	25.08
64	10.66	510	21.30	1160	16.02	1494	5.96	3077	16.58
79	5.95	538	7.40	1183	3.79	1498	7.59	3097	18.94
89	13.69	590	20.46	1202	17.27	1510	16.91	3115	3.63
143	10.11	678	23.93	1229	8.85	1512	1.03	3124	46.72
152	30.34	763	3.44	1238	23.85	1522	19.18	3128	10.11
214	31.47	816	5.62	1240	3.05	1532	8.99	3143	16.38
230	8.66	871	64.68	1276	19.18	1542	19.95	3153	13.01
270	9.78	891	26.49	1295	2.93	1545	22.35	3158	18.68
284	51.47	921	29.21	1301	3.18	1603	100.00	3482	26.81
307	14.75	941	19.16	1359	74.03	1653	38.19	3574	14.68
317	13.99	976	35.19	1388	10.80	2904	92.73	3819	38.73
331	1.07	1016	14.75	1422	69.21	2970	35.37		
358	26.65	1043	13.45	1443	16.56	2996	38.54		

Table C2.3. Predicted wavenumbers (WN, in cm^{-1}) and normalised intensities of absorption (I, in arbitrary units) for [Ch][Leu].

WN	*I*	WN	*I*	WN	*I*	WN	*I*	WN	*I*
14	7.65	382	6.97	1045	13.99	1415	66.19	2997	32.01
21	5.22	386	9.55	1069	34.72	1422	12.23	3007	29.74
35	5.64	398	1.89	1083	12.11	1446	12.85	3012	53.84
43	12.69	424	15.07	1092	0.96	1465	11.27	3015	68.74
50	15.74	450	4.76	1100	4.14	1469	8.90	3016	43.05
62	5.35	454	9.00	1132	8.88	1476	4.28	3033	9.15
74	9.32	461	3.13	1164	29.97	1477	2.22	3049	29.89
89	10.16	544	8.23	1183	5.24	1488	12.13	3050	19.94
108	13.59	556	15.19	1189	6.71	1491	3.43	3063	8.19
122	15.25	698	29.49	1202	19.96	1493	9.61	3071	41.71
152	13.29	751	10.39	1230	11.41	1495	8.09	3073	31.63
159	12.33	764	2.44	1239	24.83	1504	11.22	3076	17.01
224	7.80	816	4.65	1262	5.54	1510	13.45	3091	24.96
227	1.91	829	14.42	1277	13.35	1513	16.13	3097	15.55
245	14.72	855	28.00	1295	8.36	1514	15.57	3113	3.88
248	12.22	867	47.28	1296	5.89	1529	9.01	3122	44.63
261	30.44	907	21.45	1302	4.99	1533	6.04	3128	15.23
275	15.09	925	25.76	1345	22.43	1542	13.68	3147	8.66
282	45.10	930	7.91	1356	13.44	1548	18.78	3151	16.78
318	2.10	939	15.86	1358	25.19	1599	86.07	3158	17.09
334	4.68	964	8.55	1371	41.36	1643	38.84	3482	23.89
342	15.80	966	7.45	1385	22.86	2884	100.00	3568	11.58
346	6.01	976	35.71	1389	6.93	2972	20.59	3820	36.01
359	25.31	1006	12.93	1401	18.17	2995	18.41		

Table C2.4. Predicted wavenumbers (WN, in cm^{-1}) and normalised intensities of absorption (I, in arbitrary units) for [Ch][Ser].

WN	*I*	WN	*I*	WN	*I*	WN	*I*	WN	*I*
15	7.40	352	27.76	1029	38.45	1371	62.37	2903	100.00
20	7.62	372	11.43	1043	13.63	1386	13.10	2980	33.61
38	8.43	376	8.91	1067	49.72	1413	50.97	3002	56.17
42	20.47	386	7.37	1069	36.25	1429	45.37	3013	38.92
58	12.26	427	7.53	1091	0.50	1444	16.78	3026	82.08
80	6.74	449	2.20	1097	1.91	1463	12.63	3032	15.56
89	10.42	465	3.18	1142	19.44	1468	12.00	3049	37.65
128	21.89	537	7.54	1159	16.13	1477	2.49	3051	26.87
130	17.13	552	20.63	1182	16.58	1480	9.54	3077	17.49
144	10.21	692	41.25	1183	3.65	1498	8.09	3098	19.33
211	23.53	763	6.28	1219	25.82	1509	12.42	3119	11.11
237	18.56	770	29.21	1229	11.07	1510	14.17	3129	60.92
278	9.47	816	5.55	1241	23.84	1513	13.39	3144	16.70
286	39.27	862	48.34	1266	10.39	1521	10.26	3155	12.46
291	49.56	896	39.24	1276	20.71	1532	8.75	3159	19.38
292	47.50	921	33.45	1295	3.15	1541	21.12	3488	12.68
309	18.55	934	20.52	1303	3.08	1547	19.25	3575	18.68
321	27.62	941	20.96	1335	19.22	1600	94.09	3818	25.35
333	5.65	977	37.29	1358	11.23	1642	58.77	3821	40.53

C.3 Density measurements

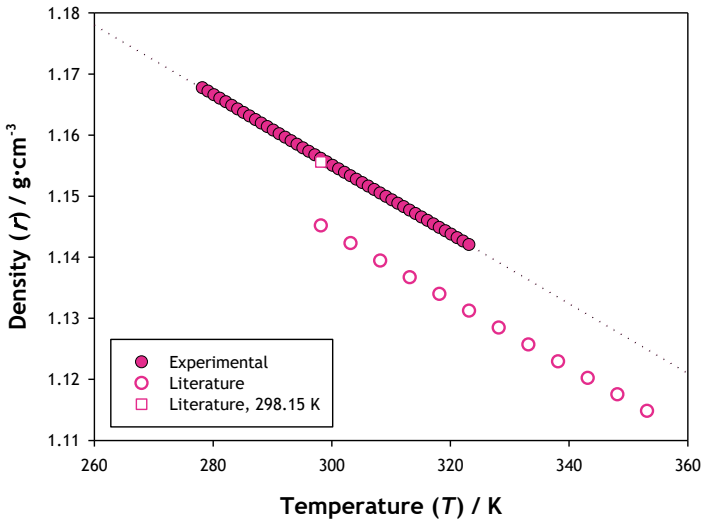

Fig. C3.1. Measured and literature density of cholinium glycinate ([Ch][Gly]). Literature data were collected from [1] and [2] (measurement at 298.15 K). The linear regression of experimental density data follows equation: $\rho = 1.326 - 5.702 \cdot 10^{-4} \cdot T$ with $R^2 = 0.9999$.

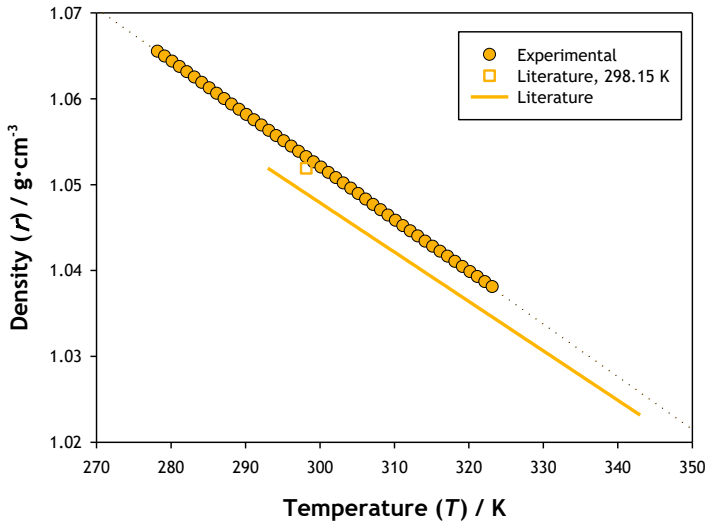

Fig. C3.2. Measured and literature density of cholinium leucinate ([Ch][Leu]). Literature data of [Ch][Leu] density is a correlation obtained between 293.15 and 343.15 K, with the equation: $\rho = 1.2205 - 5.7533 \cdot 10^{-4} \cdot T$, with $R = 0.99997$[2]. The linear regression of experimental density data follows equation: $\rho = 1.236 - 6.128 \cdot 10^{-4} \cdot T$ with $R^2 = 0.9999$.

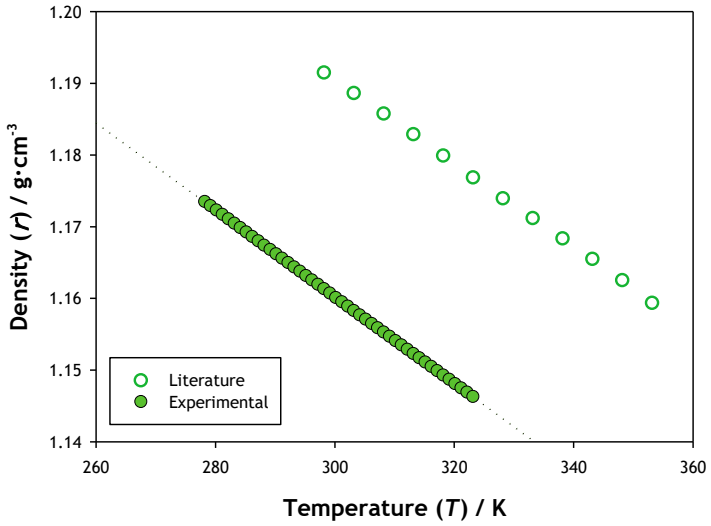

Fig. C3.3. Measured and literature density of cholinium serinate ([Ch][Ser]). Literature data was collected from [1]. The linear regression of experimental density data follows equation: $\rho = 1.342 - 6.052 \cdot 10^{-4} \cdot T$ with $R^2 = 0.9999$.

References

1. Tao, D.-J.; Cheng, Z.; Chen, F.-F.; Li, Z.-M.; Hu, N.; Chen, X.-S., Synthesis and Thermophysical Properties of Biocompatible Cholinium-Based Amino Acid Ionic Liquids. *J. Chem. Eng. Data* **2013**, *58* (6), 1542-1548. https://doi.org/10.1021/je301103d.

2. De Santis, S.; Masci, G.; Casciotta, F.; Caminiti, R.; Scarpellini, E.; Campetella, M.; Gontrani, L., Cholinium-amino acid based ionic liquids: a new method of synthesis and physico-chemical characterization. *Phys. Chem. Chem. Phys.* **2015**, *17*, 20687-20698. https://doi.org/10.1039/C5CP01612F.

Appendix D - Ultraviolet-visible (UV-Vis) absorbance spectra of pure compounds

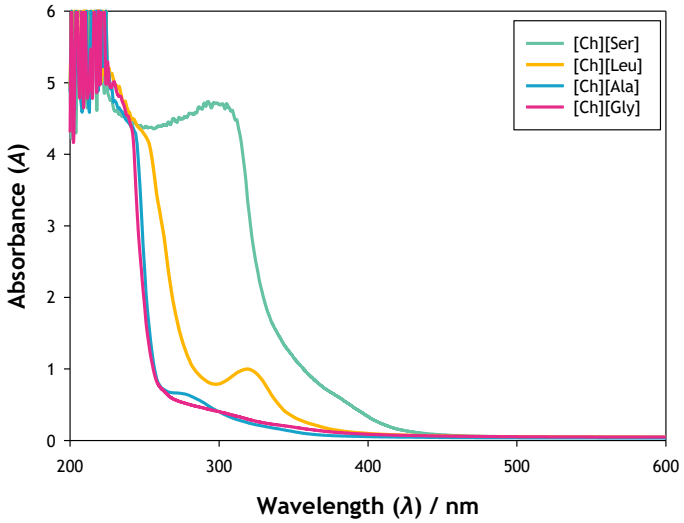

Fig. D.1. UV-Vis absorbance spectra of the four Choline Amino Acid Ionic Liquids (CAAILs) used: cholinium alaninate ([Ch][Ala]), cholinium glycinate ([Ch][Gly]), cholinium leucinate ([Ch][Leu]) and cholinium serinate ([Ch][Ser]).

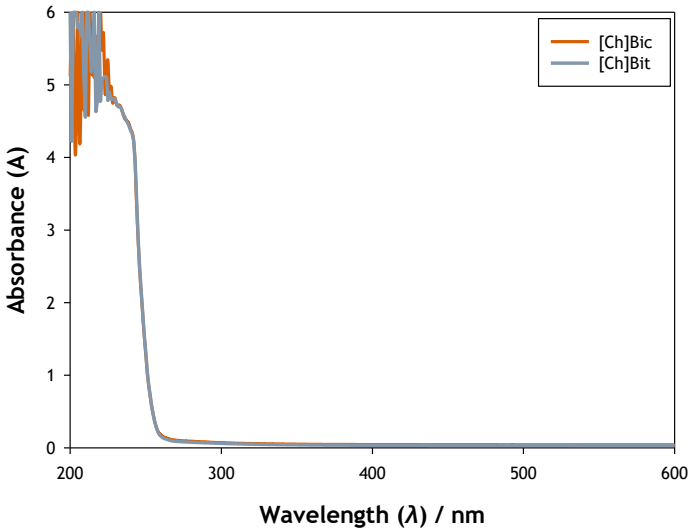

Fig. D.2. UV-Vis absorbance spectra of aqueous solutions of the choline salts used: choline bicarbonate ([Ch]Bic, $w = 0.80$) and choline bitartrate ([Ch]Bit, $w = 0.62$).

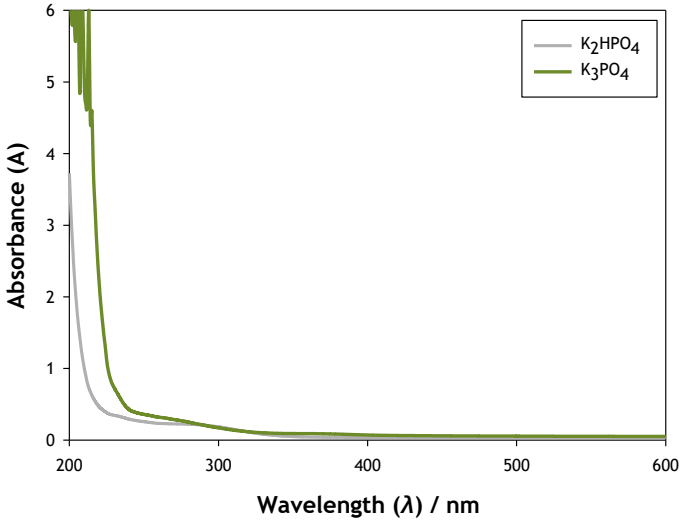

Fig. D.3. UV-Vis absorbance spectra of aqueous solutions of the other salts used: K_2HPO_4 ($w = 0.59$) and K_3PO_4 ($w = 0.47$).

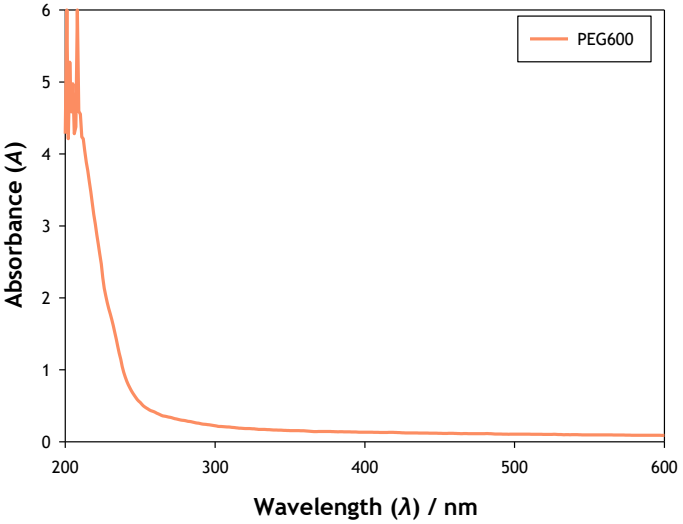

Fig. D.4. UV-Vis absorbance spectra of pure polyethylene glycol 600 (PEG600) and aqueous solutions of polyethylene glycol 4000 (PEG4000, $w = 0.50$).

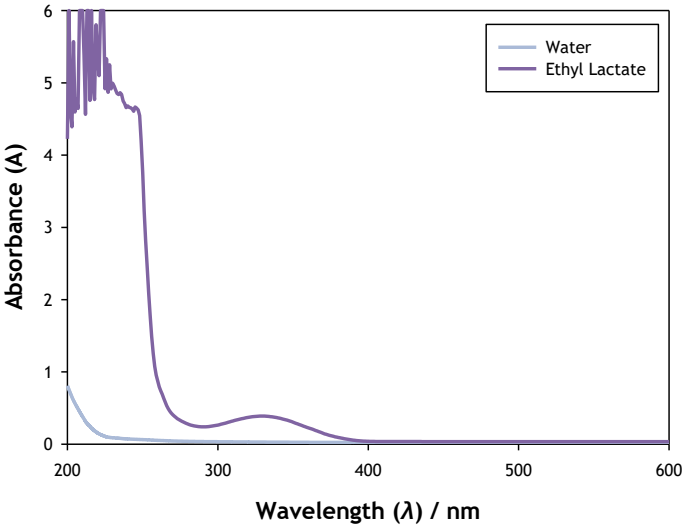

Fig. D.5. UV-Vis absorbance spectra of pure solvents: water and ethyl lactate.

Appendix E - Variation of mean charge with pH

E.1 Acetaminophen

Table E1.1. Calculated fractions of each stage and mean charge ($\bar{q}$) for acetaminophen at different pH values.

pH	x_{Ac^0} [a]	$x_{Ac^{-1}}$	$\bar{q}$ / e [b]
0.00	1.00	0.00	0.00
0.25	1.00	0.00	0.00
0.50	1.00	0.00	0.00
0.75	1.00	0.00	0.00
1.00	1.00	0.00	0.00
1.25	1.00	0.00	0.00
1.50	1.00	0.00	0.00
1.75	1.00	0.00	0.00
2.00	1.00	0.00	0.00
2.25	1.00	0.00	0.00
2.50	1.00	0.00	0.00
2.75	1.00	0.00	0.00
3.00	1.00	0.00	0.00
3.25	1.00	0.00	0.00
3.50	1.00	0.00	0.00
3.75	1.00	0.00	0.00
4.00	1.00	0.00	0.00
4.25	1.00	0.00	0.00
4.50	1.00	0.00	0.00
4.75	1.00	0.00	0.00
5.00	1.00	0.00	0.00
5.25	1.00	0.00	0.00
5.50	1.00	0.00	0.00
5.75	1.00	0.00	0.00
6.00	1.00	0.00	0.00
6.25	1.00	0.00	0.00
6.50	1.00	0.00	0.00
6.75	1.00	0.00	0.00
7.00	1.00	0.00	0.00
7.25	1.00	0.00	0.00
7.50	0.99	0.01	-0.01
7.75	0.98	0.02	-0.02
8.00	0.97	0.03	-0.03

[a] x_{Ac^0} and $x_{Ac^{-1}}$ are the fractions of acetaminophen with electrical charges equal to 0 and -1 e, respectively.
[b] e stands for the elementary charge, equal to $1.602 \cdot 10^{-19}$C.

Table E1.1. Calculated fractions of each stage and mean charge ($\bar{q}$) for acetaminophen at different pH values (cont.).

pH	x_{Ac^0}	$x_{Ac^{-1}}$	$\bar{q}$ / e
8.25	0.95	0.05	-0.05
8.50	0.92	0.08	-0.08
8.75	0.86	0.14	-0.14
9.00	0.78	0.22	-0.22
9.25	0.67	0.33	-0.33
9.50	0.53	0.47	-0.47
9.75	0.39	0.61	-0.61
10.00	0.26	0.74	-0.74
10.25	0.17	0.83	-0.83
10.50	0.10	0.90	-0.90
10.75	0.06	0.94	-0.94
11.00	0.03	0.97	-0.97
11.25	0.02	0.98	-0.98
11.50	0.01	0.99	-0.99
11.75	0.01	0.99	-0.99
12.00	0.00	1.00	-1.00
12.25	0.00	1.00	-1.00
12.50	0.00	1.00	-1.00
12.75	0.00	1.00	-1.00
13.00	0.00	1.00	-1.00
13.25	0.00	1.00	-1.00
13.50	0.00	1.00	-1.00
13.75	0.00	1.00	-1.00
14.00	0.00	1.00	-1.00

[a] x_{Ac^0} and $x_{Ac^{-1}}$ are the fractions of acetaminophen with electrical charges equal to 0 and -1 e, respectively.
[b] e stands for the elementary charge, equal to $1.602 \cdot 10^{-19}$C.

E.2 Amoxicillin

Table E2.1. Calculated fractions of each stage and mean charge ($\bar{q}$) for amoxicillin at different pH values.

pH	x_{Amox^0} [a]	$x_{Amox^{-1}}$	$x_{Amox^{-2}}$	$x_{Amox^{-3}}$	$\bar{q}$ / e [b]
0.00	1.00	0.00	0.00	0.00	0.00
0.25	1.00	0.00	0.00	0.00	0.00
0.50	0.99	0.01	0.00	0.00	-0.01
0.75	0.99	0.01	0.00	0.00	-0.01
1.00	0.98	0.02	0.00	0.00	-0.02
1.25	0.96	0.04	0.00	0.00	-0.04
1.50	0.93	0.07	0.00	0.00	-0.07
1.75	0.88	0.12	0.00	0.00	-0.12
2.00	0.80	0.20	0.00	0.00	-0.20

[a] x_{Amox^0}, $x_{Amox^{-1}}$, $x_{Amox^{-2}}$ and $x_{Amox^{-3}}$ are the fractions of amoxicillin with electrical charges equal to 0, -1, -2 and -3 e, respectively.
[b] e stands for the elementary charge, equal to $1.602 \cdot 10^{-19}$ C.

Table E2.1. Calculated fractions of each stage and mean charge ($\bar{q}$) for amoxicillin at different pH values (cont.).

pH	x_{Amox^0} [a]	$x_{\mathrm{Amox}^{-1}}$	$x_{\mathrm{Amox}^{-2}}$	$x_{\mathrm{Amox}^{-3}}$	$\bar{q}$ / e [b]
2.25	0.69	0.31	0.00	0.00	-0.31
2.50	0.56	0.44	0.00	0.00	-0.44
2.75	0.41	0.59	0.00	0.00	-0.59
3.00	0.28	0.72	0.00	0.00	-0.72
3.25	0.18	0.82	0.00	0.00	-0.82
3.50	0.11	0.89	0.00	0.00	-0.89
3.75	0.07	0.93	0.00	0.00	-0.93
4.00	0.04	0.96	0.00	0.00	-0.96
4.25	0.02	0.98	0.00	0.00	-0.98
4.50	0.01	0.99	0.00	0.00	-0.99
4.75	0.01	0.99	0.00	0.00	-1.00
5.00	0.00	0.99	0.00	0.00	-1.00
5.25	0.00	0.99	0.01	0.00	-1.01
5.50	0.00	0.98	0.02	0.00	-1.01
5.75	0.00	0.97	0.03	0.00	-1.03
6.00	0.00	0.95	0.05	0.00	-1.05
6.25	0.00	0.92	0.08	0.00	-1.08
6.50	0.00	0.87	0.13	0.00	-1.13
6.75	0.00	0.78	0.22	0.00	-1.22
7.00	0.00	0.67	0.33	0.00	-1.33
7.25	0.00	0.53	0.46	0.00	-1.47
7.50	0.00	0.39	0.60	0.01	-1.62
7.75	0.00	0.26	0.72	0.01	-1.75
8.00	0.00	0.17	0.81	0.02	-1.86
8.25	0.00	0.10	0.86	0.04	-1.95
8.50	0.00	0.06	0.86	0.08	-2.02
8.75	0.00	0.03	0.83	0.14	-2.11
9.00	0.00	0.02	0.76	0.22	-2.21
9.25	0.00	0.01	0.65	0.34	-2.33
9.50	0.00	0.00	0.52	0.48	-2.48
9.75	0.00	0.00	0.38	0.62	-2.62
10.00	0.00	0.00	0.25	0.75	-2.75
10.25	0.00	0.00	0.16	0.84	-2.84
10.50	0.00	0.00	0.10	0.90	-2.90
10.75	0.00	0.00	0.06	0.94	-2.94
11.00	0.00	0.00	0.03	0.97	-2.97
11.25	0.00	0.00	0.02	0.98	-2.98

[a] x_{Amox^0}, $x_{\mathrm{Amox}^{-1}}$, $x_{\mathrm{Amox}^{-2}}$ and $x_{\mathrm{Amox}^{-3}}$ are the fractions of amoxicillin with electrical charges equal to 0, -1, -2 and -3 e, respectively.

[b] e stands for the elementary charge, equal to $1.602 \cdot 10^{-19}$ C.

Table E2.1. Calculated fractions of each stage and mean charge ($\bar{q}$) for amoxicillin at different pH values (cont.).

pH	x_{Amox^0} [a]	$x_{\mathrm{Amox}^{-1}}$	$x_{\mathrm{Amox}^{-2}}$	$x_{\mathrm{Amox}^{-3}}$	$\bar{q}$ / e [b]
11.50	0.00	0.00	0.01	0.99	-2.99
11.75	0.00	0.00	0.01	0.99	-2.99
12.00	0.00	0.00	0.00	1.00	-3.00
12.25	0.00	0.00	0.00	1.00	-3.00
12.50	0.00	0.00	0.00	1.00	-3.00
12.75	0.00	0.00	0.00	1.00	-3.00
13.00	0.00	0.00	0.00	1.00	-3.00
13.25	0.00	0.00	0.00	1.00	-3.00
13.50	0.00	0.00	0.00	1.00	-3.00
13.75	0.00	0.00	0.00	1.00	-3.00
14.00	0.00	0.00	0.00	1.00	-3.00

[a] x_{Amox^0}, $x_{\mathrm{Amox}^{-1}}$, $x_{\mathrm{Amox}^{-2}}$ and $x_{\mathrm{Amox}^{-3}}$ are the fractions of amoxicillin with electrical charges equal to 0, -1, -2 and -3 e, respectively.
[b] e stands for the elementary charge, equal to $1.602 \cdot 10^{-19}$ C.

E.3 Salicylic acid

Table E3.1. Calculated fractions of each stage and mean charge ($\bar{q}$) for salicylic acid at different pH values.

pH	x_{SA^0} [a]	$x_{\mathrm{SA}^{-1}}$	$x_{\mathrm{SA}^{-2}}$	$\bar{q}$ / e [b]
0.00	1.00	0.00	0.00	0.00
0.25	1.00	0.00	0.00	0.00
0.50	0.99	0.01	0.00	-0.01
0.75	0.99	0.01	0.00	-0.01
1.00	0.98	0.02	0.00	-0.02
1.25	0.97	0.03	0.00	-0.03
1.50	0.95	0.05	0.00	-0.05
1.75	0.91	0.09	0.00	-0.09
2.00	0.86	0.14	0.00	-0.14
2.25	0.77	0.23	0.00	-0.23
2.50	0.66	0.34	0.00	-0.34
2.75	0.52	0.48	0.00	-0.48
3.00	0.38	0.62	0.00	-0.62
3.25	0.25	0.75	0.00	-0.75
3.50	0.16	0.84	0.00	-0.84
3.75	0.10	0.90	0.00	-0.90
4.00	0.06	0.94	0.00	-0.94
4.25	0.03	0.97	0.00	-0.97
4.50	0.02	0.98	0.00	-0.98
4.75	0.01	0.99	0.00	-0.99
5.00	0.01	0.99	0.00	-0.99

[a] x_{SA^0}, $x_{\mathrm{SA}^{-1}}$, and $x_{\mathrm{SA}^{-2}}$ are the fractions of salicylic acid with electrical charges equal to 0, -1, and -2 e, respectively.
[b] e stands for the elementary charge, equal to $1.602 \cdot 10^{-19}$ C.

Table E3.1. Calculated fractions of each stage and mean charge ($\bar{q}$) for salicylic acid at different pH values (cont.).

pH	x_{SA^0} [a]	$x_{SA^{-1}}$	$x_{SA^{-2}}$	$\bar{q}$ / e [b]
5.25	0.00	1.00	0.00	-1.00
5.50	0.00	1.00	0.00	-1.00
5.75	0.00	1.00	0.00	-1.00
6.00	0.00	1.00	0.00	-1.00
6.25	0.00	1.00	0.00	-1.00
6.50	0.00	1.00	0.00	-1.00
6.75	0.00	1.00	0.00	-1.00
7.00	0.00	1.00	0.00	-1.00
7.25	0.00	1.00	0.00	-1.00
7.50	0.00	1.00	0.00	-1.00
7.75	0.00	1.00	0.00	-1.00
8.00	0.00	1.00	0.00	-1.00
8.25	0.00	1.00	0.00	-1.00
8.50	0.00	1.00	0.00	-1.00
8.75	0.00	1.00	0.00	-1.00
9.00	0.00	1.00	0.00	-1.00
9.25	0.00	1.00	0.00	-1.00
9.50	0.00	1.00	0.00	-1.00
9.75	0.00	1.00	0.00	-1.00
10.00	0.00	1.00	0.00	-1.00
10.25	0.00	1.00	0.00	-1.00
10.50	0.00	1.00	0.00	-1.00
10.75	0.00	1.00	0.00	-1.00
11.00	0.00	1.00	0.00	-1.00
11.25	0.00	1.00	0.00	-1.00
11.50	0.00	0.99	0.01	-1.01
11.75	0.00	0.99	0.01	-1.01
12.00	0.00	0.98	0.02	-1.02
12.25	0.00	0.97	0.03	-1.03
12.50	0.00	0.95	0.05	-1.05
12.75	0.00	0.91	0.09	-1.09
13.00	0.00	0.85	0.15	-1.15
13.25	0.00	0.77	0.23	-1.23
13.50	0.00	0.65	0.35	-1.35
13.75	0.00	0.51	0.49	-1.49
14.00	0.00	0.37	0.63	-1.63

[a] x_{SA^0}, $x_{SA^{-1}}$, and $x_{SA^{-2}}$ are the fractions of salicylic acid with electrical charges equal to 0, -1, and -2 e, respectively.
[b] e stands for the elementary charge, equal to $1.602 \cdot 10^{-19}$ C.

Appendix F - Stability of Ultraviolet-Visible (UV-Vis) absorbance spectra

F.1 Acetaminophen

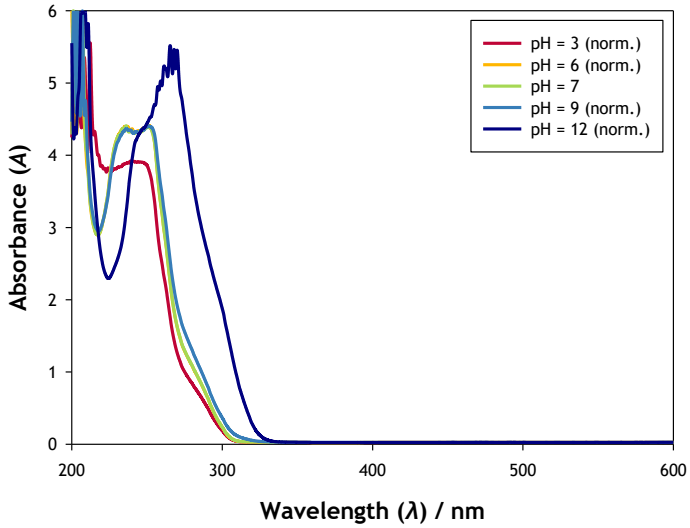

Fig. F1.1. Influence of pH on the UV-Vis absorbance spectra of an aqueous solution of acetaminophen ($\sim 1.5 \cdot 10^{-4}\ \mathrm{g \cdot mL^{-1}}$) at 298.15 K and 0.1 MPa.

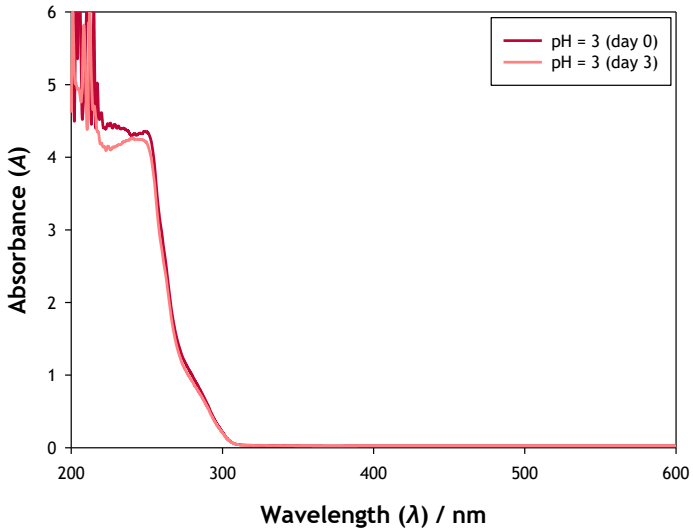

Fig. F1.2. UV-Vis absorbance spectra of an aqueous solution of acetaminophen ($\sim 1.5 \cdot 10^{-4}\ \mathrm{g \cdot mL^{-1}}$, pH = 3) in the moment of preparation and after 72 h of settling, at 298.15 K and 0.1 MPa.

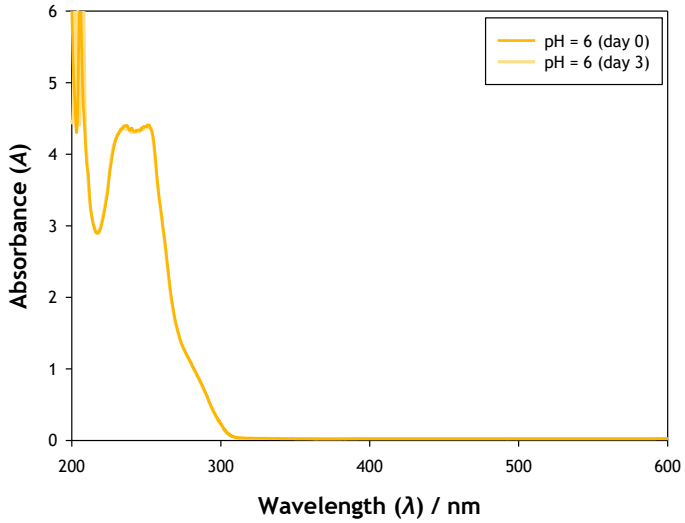

Fig. F1.3. UV-Vis absorbance spectra of an aqueous solution of acetaminophen (~$1.5 \cdot 10^{-4}$ g · mL^{-1}, pH = 6) in the moment of preparation and after 72 h of settling, at 298.15 K and 0.1 MPa.

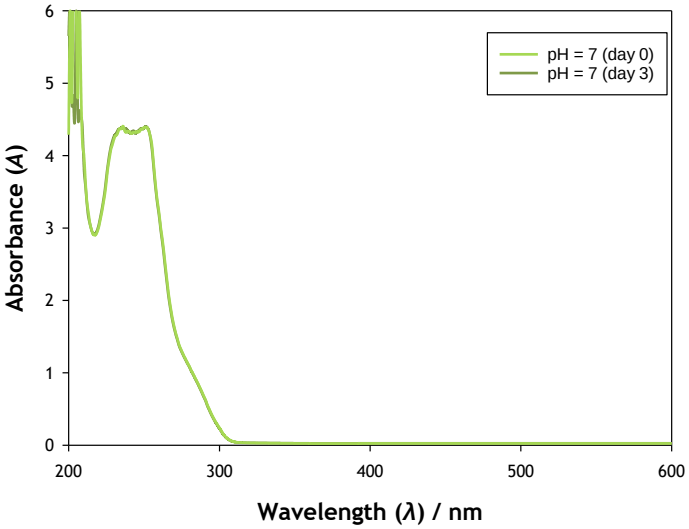

Fig. F1.4. UV-Vis absorbance spectra of an aqueous solution of acetaminophen (~$1.5 \cdot 10^{-4}$ g · mL^{-1}, pH = 7) in the moment of preparation and after 72 h of settling, at 298.15 K and 0.1 MPa.

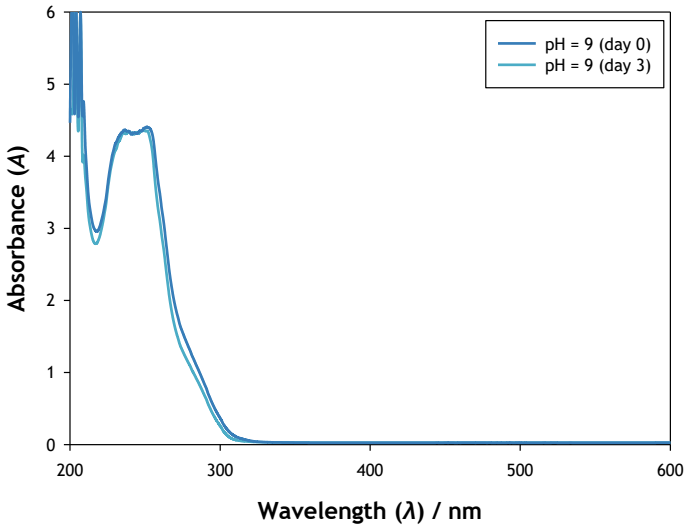

Fig. F1.5. UV-Vis absorbance spectra of an aqueous solution of acetaminophen (~$1.5 \cdot 10^{-4}$ g · mL^{-1}, pH = 9) in the moment of preparation and after 72 h of settling, at 298.15 K and 0.1 MPa.

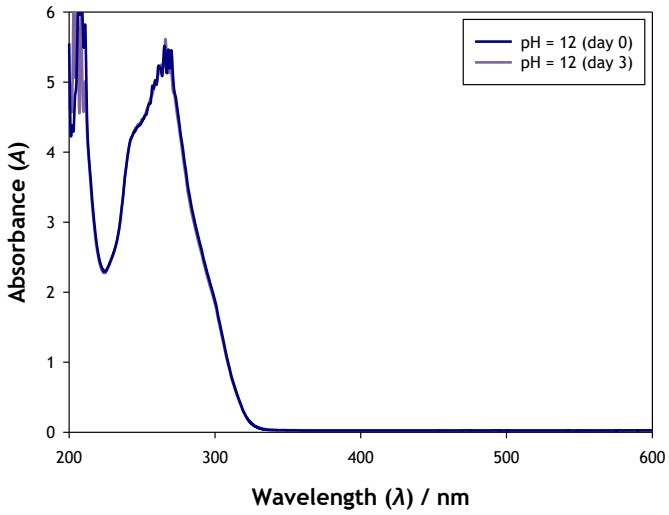

Fig. F1.6. UV-Vis absorbance spectra of an aqueous solution of acetaminophen ($\sim 1.5 \cdot 10^{-4}\ \mathrm{g \cdot mL^{-1}}$, pH = 12) in the moment of preparation and after 72 h of settling, at 298.15 K and 0.1 MPa.

F.2 Amoxicillin

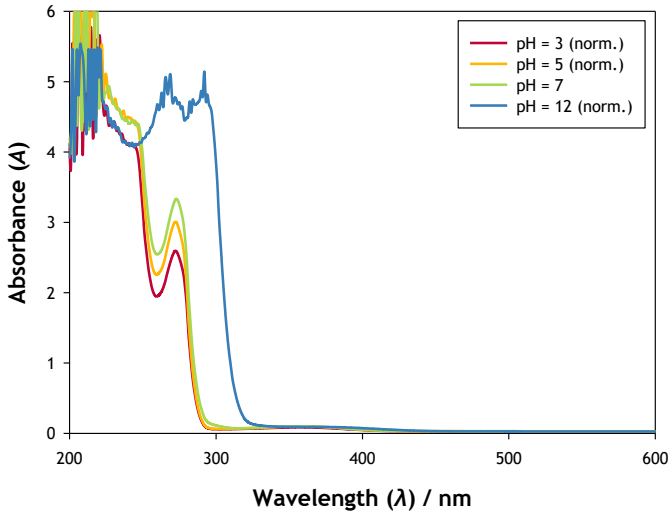

Fig. F2.1. Influence of pH on the UV-Vis absorbance spectra of an aqueous solution of amoxicillin ($\sim 1.8 \cdot 10^{-3}\ \mathrm{g \cdot mL^{-1}}$) at 298.15 K and 0.1 MPa.

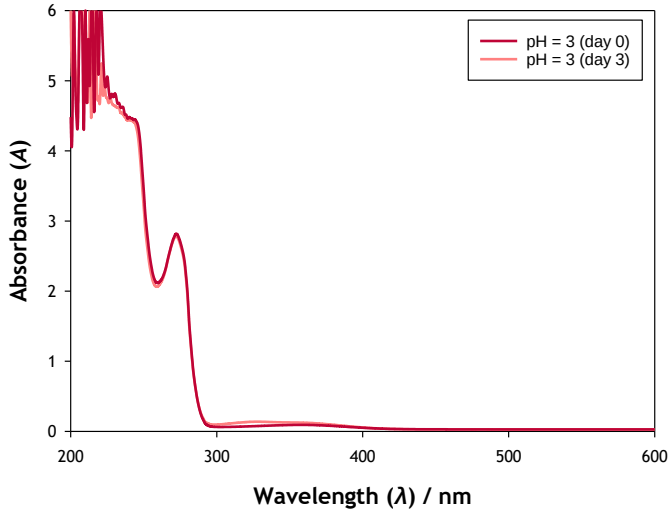

Fig. F2.2. UV-Vis absorbance spectra of an aqueous solution of amoxicillin ($\sim 1.8 \cdot 10^{-3}\ \mathrm{g \cdot mL^{-1}}$, pH = 3) in the moment of preparation and after 72 h of settling, at 298.15 K and 0.1 MPa.

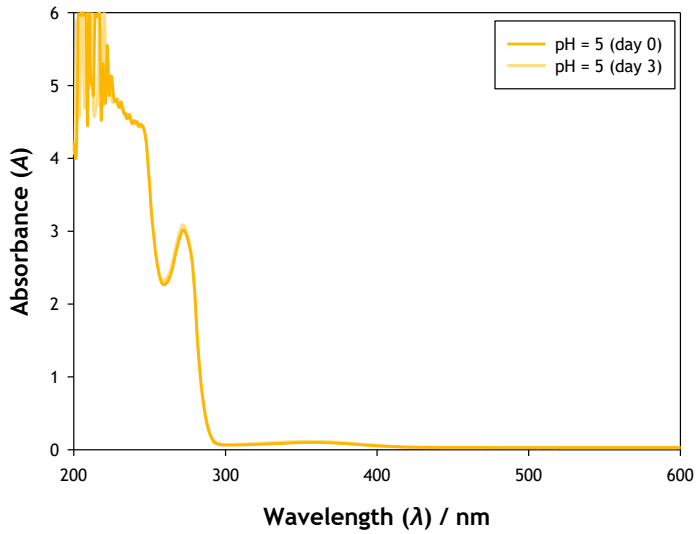

Fig. F2.3. UV-Vis absorbance spectra of an aqueous solution of amoxicillin (~$1.8 \cdot 10^{-3}\ \mathrm{g \cdot mL^{-1}}$, pH = 5) in the moment of preparation and after 72 h of settling, at 298.15 K and 0.1 MPa.

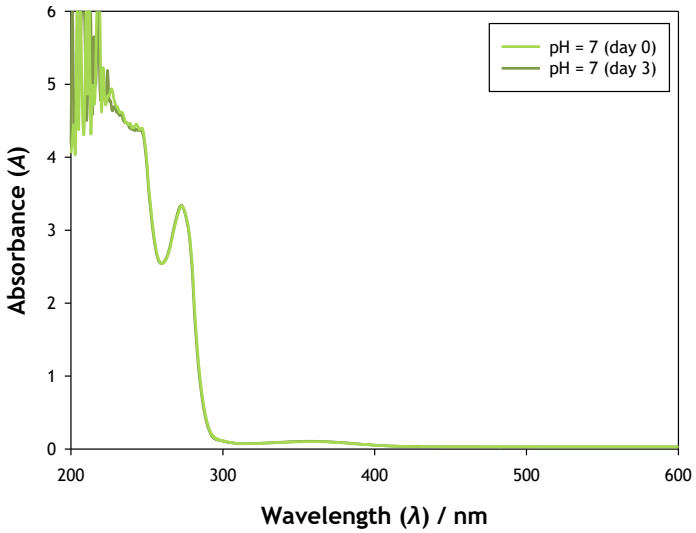

Fig. F2.4. UV-Vis absorbance spectra of an aqueous solution of amoxicillin (~$1.8 \cdot 10^{-3}\ \mathrm{g \cdot mL^{-1}}$, pH = 7) in the moment of preparation and after 72 h of settling, at 298.15 K and 0.1 MPa.

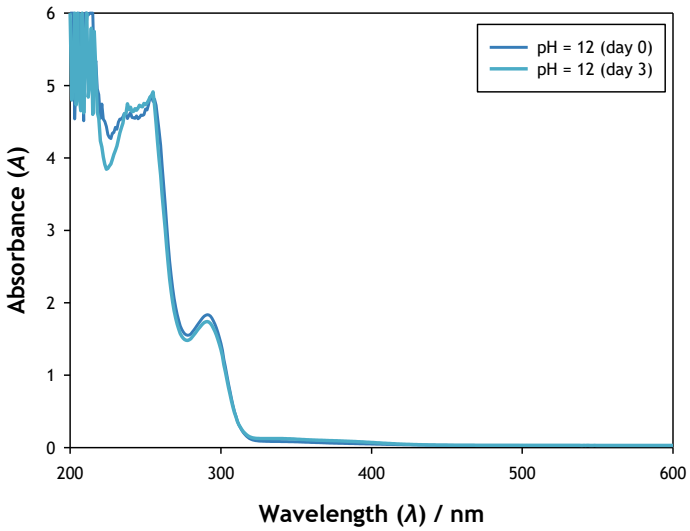

Fig. F2.5. UV-Vis absorbance spectra of an aqueous solution of amoxicillin (~$4.9 \cdot 10^{-4}$ g · mL^{-1}, pH = 12) in the moment of preparation and after 72 h of settling, at 298.15 K and 0.1 MPa.

F.3 Salicylic acid

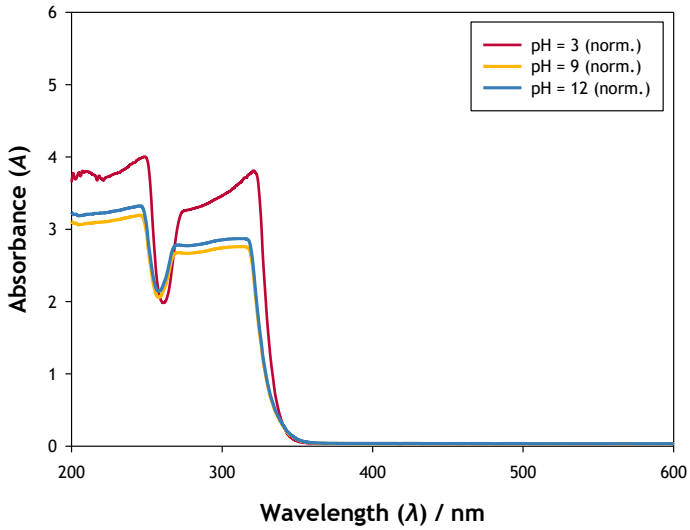

Fig. F3.1. Influence of pH on the UV-Vis absorbance spectra of an aqueous solution of salicylic acid (~$1.8 \cdot 10^{-3}$ g · mL^{-1}) at 298.15 K and 0.1 MPa.

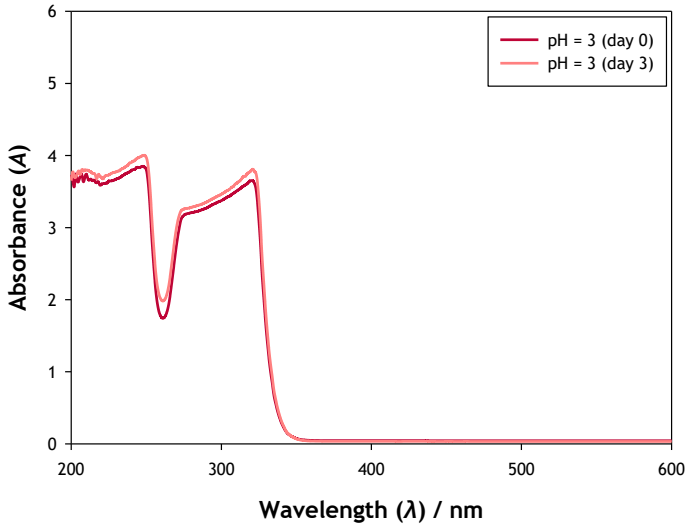

Fig. F3.2. UV-Vis absorbance spectra of an aqueous solution of salicylic acid (~$1.8 \cdot 10^{-3}$ g · mL^{-1}, pH = 3) in the moment of preparation and after 72 h of settling, at 298.15 K and 0.1 MPa.

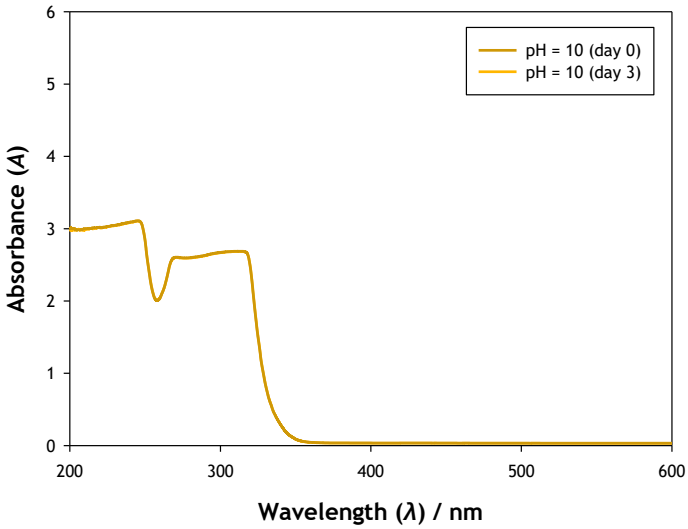

Fig. F3.3. UV-Vis absorbance spectra of an aqueous solution of salicylic acid (~$1.8 \cdot 10^{-3}$ g · mL^{-1}, pH = 10) in the moment of preparation and after 72 h of settling, at 298.15 K and 0.1 MPa.

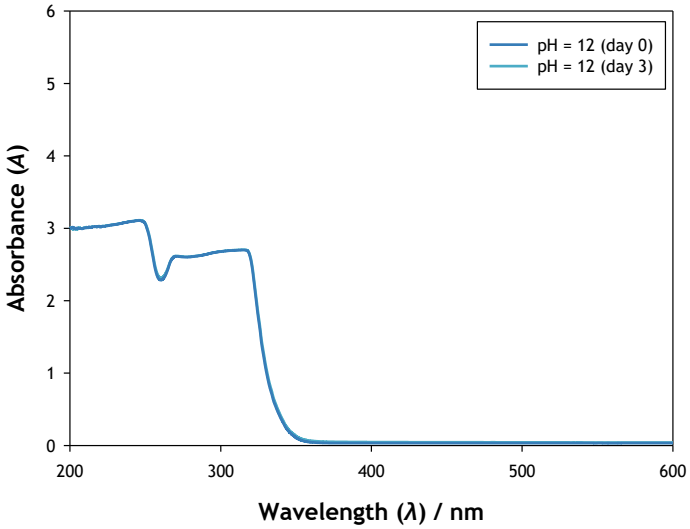

Fig. F3.4. UV-Vis absorbance spectra of an aqueous solution of salicylic acid (~$1.8 \cdot 10^{-3}$ g · mL^{-1}, pH = 12) in the moment of preparation and after 72 h of settling, at 298.15 K and 0.1 MPa.

Appendix G - Calibration curves

Limits of detection and quantification were calculated as indicated in Skoog [1].

G.1 Acetaminophen

Table G1.1. Concentration and UV-Vis absorbances at λ_{max} of the solutions prepared for the calibration curves of acetaminophen, at pH = 3 and 12.

pH = 3			pH = 12		
Concentration / g·mL^{-1}	**Absorbance (A) at λ_{max} = 259 nm**	**Absorbance without blanks**	**Concentration / g·mL^{-1}**	**Absorbance (A) at λ_{max} = 267 nm**	**Absorbance without blanks**
$1.27 \cdot 10^{-4}$	2.17551	2.10371	$1.33 \cdot 10^{-4}$	3.27334	3.23022
$1.19 \cdot 10^{-4}$	2.05033	1.97853	$1.30 \cdot 10^{-4}$	3.20362	3.16050
$1.15 \cdot 10^{-4}$	1.97438	1.90258	$1.25 \cdot 10^{-4}$	3.07283	3.02971
$1.01 \cdot 10^{-4}$	1.78223	1.71043	$1.21 \cdot 10^{-4}$	2.95617	2.91305
$8.74 \cdot 10^{-5}$	1.46951	1.39771	$1.05 \cdot 10^{-4}$	2.58836	2.54524
$7.48 \cdot 10^{-5}$	1.26510	1.19330	$9.25 \cdot 10^{-5}$	2.28667	2.24355
$6.33 \cdot 10^{-5}$	1.13814	1.06634	$8.06 \cdot 10^{-5}$	2.00732	1.96420
$5.06 \cdot 10^{-5}$	0.90441	0.83261	$6.67 \cdot 10^{-5}$	1.67802	1.63490
$3.96 \cdot 10^{-5}$	0.72025	0.64845	$5.40 \cdot 10^{-5}$	1.36132	1.31820
$2.57 \cdot 10^{-5}$	0.50787	0.43607	$4.09 \cdot 10^{-5}$	1.04244	0.99932
$1.63 \cdot 10^{-5}$	0.35601	0.28421	$2.82 \cdot 10^{-5}$	0.72575	0.68262
$5.16 \cdot 10^{-6}$	0.16349	0.09169	$1.53 \cdot 10^{-5}$	0.40316	0.36003
$2.55 \cdot 10^{-6}$	0.12012	0.04831	$7.47 \cdot 10^{-6}$	0.20542	0.16229
			$2.60 \cdot 10^{-6}$	0.08698	0.04386

Table G1.2. Calculated detection and quantification limits for the calibration curves of acetaminophen.

	Value for the calibration curve at pH = 5	**Value for the calibration curve at pH = 12**
Detection limit / g·mL^{-1}	$1.900 \cdot 10^{-6}$	$6.609 \cdot 10^{-7}$
Quantification limit / g·mL^{-1}	$6.335 \cdot 10^{-6}$	$2.203 \cdot 10^{-6}$

G.2 Amoxicillin

Table G2.1. Concentration and UV-Vis absorbances at λ_{max} of the solutions prepared for the calibration curves of amoxicillin, at pH = 3 and 12.

pH = 3			pH = 12		
Concentration / g·mL^{-1}	**Absorbance (A) at λ_{max} = 272 nm**	**Absorbance without blanks**	**Concentration / g·mL^{-1}**	**Absorbance (A) at λ_{max} = 290 nm**	**Absorbance without blanks**
8.67·10^{-4}	1.49539	1.45300	4.93·10^{-4}	1.84566	1.80087
8.39·10^{-4}	1.43344	1.39105	4.64·10^{-4}	1.72228	1.67749
7.99·10^{-4}	1.35933	1.31694	4.39·10^{-4}	1.63573	1.59094
7.66·10^{-4}	1.29581	1.25342	4.16·10^{-4}	1.55661	1.51182
6.88·10^{-4}	1.21223	1.16984	3.95·10^{-4}	1.47304	1.42825
6.14·10^{-4}	1.07267	1.03028	3.67·10^{-4}	1.36499	1.32020
5.38·10^{-4}	0.92576	0.88337	3.27·10^{-4}	1.19791	1.15312
4.40·10^{-4}	0.81168	0.76929	2.48·10^{-4}	0.93090	0.88611
3.56·10^{-4}	0.63887	0.59648	2.20·10^{-4}	0.83324	0.78845
2.48·10^{-4}	0.47517	0.43278	1.96·10^{-4}	0.76423	0.71944
1.81·10^{-4}	0.36334	0.32094	1.78·10^{-4}	0.68084	0.63605
4.55·10^{-5}	0.17240	0.13001	1.46·10^{-4}	0.56717	0.52238
1.40·10^{-5}	0.08870	0.04630	1.23·10^{-4}	0.48549	0.44070
			1.03·10^{-4}	0.41788	0.37309
			7.94·10^{-5}	0.33906	0.29427
			5.52·10^{-5}	0.24102	0.19622
			3.20·10^{-5}	0.14639	0.10160
			9.96·10^{-6}	0.07783	0.03304

Table G2.2. Calculated detection and quantification limits for the calibration curves of amoxicillin.

	Value for the calibration curve at pH = 5	**Value for the calibration curve at pH = 12**
Detection limit / g·mL^{-1}	1.690·10^{-5}	3.748 ·10^{-5}
Quantification limit / g·mL^{-1}	5.634·10^{-5}	1.249·10^{-4}

G.3 Salicylic acid

Table G3.1. Concentration and UV-Vis absorbances at λ_{max} of the solutions prepared for the calibration curves of salicylic acid, at pH = 3 and 12.

pH = 3			pH = 12		
Concentration / g·mL^{-1}	**Absorbance (A) at λ_{max} = 272 nm**	**Absorbance without blanks**	**Concentration / g·mL^{-1}**	**Absorbance (A) at λ_{max} = 322 nm**	**Absorbance without blanks**
$5.50 \cdot 10^{-4}$	1.81668	1.77455	$1.48 \cdot 10^{-3}$	2.02360	1.98884
$5.40 \cdot 10^{-4}$	1.76555	1.72342	$1.32 \cdot 10^{-3}$	1.91744	1.88268
$5.29 \cdot 10^{-4}$	1.72156	1.67943	$1.18 \cdot 10^{-3}$	1.65364	1.61888
$5.02 \cdot 10^{-4}$	1.63725	1.59512	$1.00 \cdot 10^{-3}$	1.43024	1.39548
$4.42 \cdot 10^{-4}$	1.44701	1.40488	$8.99 \cdot 10^{-4}$	1.31915	1.28439
$3.87 \cdot 10^{-4}$	1.26532	1.22319	$7.32 \cdot 10^{-4}$	1.10303	1.06827
$3.43 \cdot 10^{-4}$	1.12483	1.08270	$5.88 \cdot 10^{-4}$	0.89956	0.86480
$2.82 \cdot 10^{-4}$	0.92273	0.88060	$4.28 \cdot 10^{-4}$	0.68538	0.65062
$2.26 \cdot 10^{-4}$	0.76288	0.72074	$3.00 \cdot 10^{-4}$	0.50672	0.47195
$1.96 \cdot 10^{-4}$	0.64345	0.60132	$1.56 \cdot 10^{-4}$	0.29001	0.25524
$1.32 \cdot 10^{-4}$	0.42824	0.38611	$6.84 \cdot 10^{-5}$	0.15325	0.11848
$7.85 \cdot 10^{-4}$	0.26131	0.21918	$1.45 \cdot 10^{-5}$	0.06480	0.03004
$4.04 \cdot 10^{-4}$	0.14419	0.10205			
$1.17 \cdot 10^{-4}$	0.06800	0.02587			

Table G3.2. Calculated detection and quantification limits for the calibration curves of salicylic acid.

	Value for the calibration curve at pH = 5	**Value for the calibration curve at pH = 12**
Detection limit / g·mL^{-1}	$4.858 \cdot 10^{-6}$	$3.826 \cdot 10^{-5}$
Quantification limit / g·mL^{-1}	$1.619 \cdot 10^{-5}$	$1.275 \cdot 10^{-4}$

References

1. Skoog, D.A., *Fundamentals of Analytical Chemistry*. 9th ed.; **2014**.

Appendix H - Partition coefficients and extraction efficiencies

Plots and tables with the results of the partitions are grouped by ATPS.

H.1 {[Ch][Ala] (1) + K_2HPO_4 (2) + water (3)}

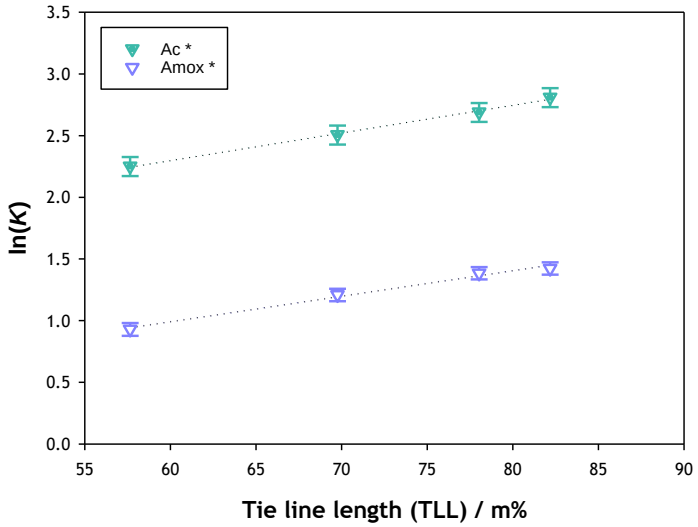

Fig. H1.1. Relation of the tie-line length (TLL) with the natural logarithm of the experimental partition coefficients (K) for acetaminophen (Ac) and amoxicillin (Amox) and respective linear regressions (···), in the system {[Ch][Ala] (1) + K_2HPO_4 (2) + water (3)} at 298.15 K and 0.1 MPa.

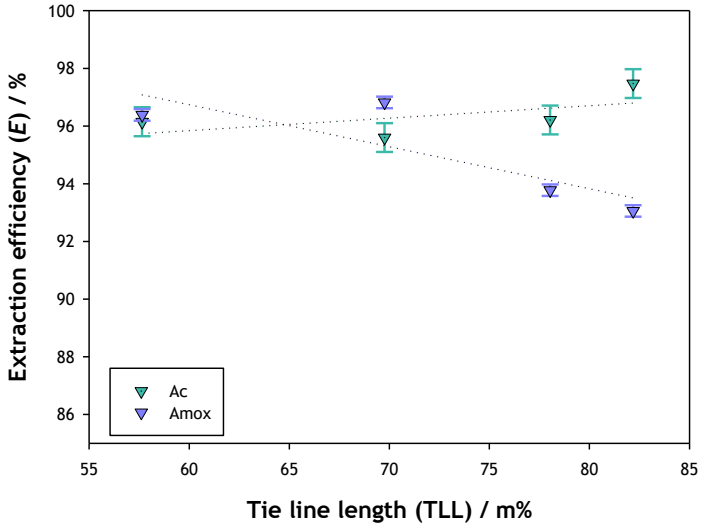

Fig. H1.2. Relation of the tie-line length (TLL) with the extraction efficiencies (E) for acetaminophen (Ac) and amoxicillin (Amox) and respective linear regressions (···), in the system {[Ch][Ala] (1) + K_2HPO_4 (2) + water (3)} at 298.15 K and 0.1 MPa.

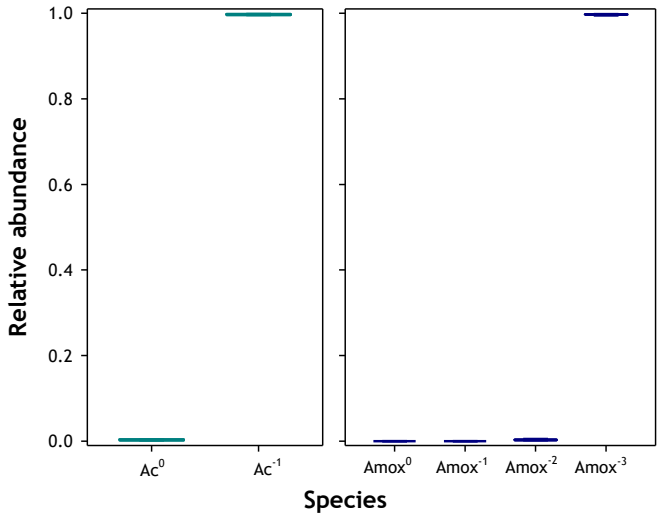

Fig. H1.3. Influence of the tie-line compositions in the relative abundance (fraction) of the stages of the studied pharmaceuticals, in the ATPS {[Ch][Ala] (1) + K_2HPO_4 (2) + water (3)} at 298.15 K and 0.1 MPa.
Ac^0 and Ac^{-1} stand for the stages of acetaminophen with electrical charges equal to 0 and −1 e, respectively. $Amox^0$, $Amox^{-1}$, $Amox^{-2}$ and $Amox^{-3}$ stand for the stages of amoxicillin with electrical charges equal to 0, - 1, -2 and −3 e, respectively. e stands for the elementary charge ($1.602 \cdot 10^{-19}$ C).

Table H1.1. Experimental mass of each phase, mass losses in the phase separation (L_m), solute concentration, phase density (ρ) and phase pH for the top and bottom phases in the extraction of acetaminophen and amoxicillin in the ATPS {[Ch][Ala] (1) + K_2HPO_4 (2) + water (3)}, at 298.15 K and 0.1 MPa.

Tie-line	Phase	Mass of phase / g	Mass losses, L_m / %	Solute concentration / g·mL^{-1}	Phase density, ρ / g·cm^{-3}	pH
Acetaminophen						
TL1	top	4.8308	-0.4	$3.577 \cdot 10^{-5}$	1.12353	12.33
	bottom	5.2182		< $2.152 \cdot 10^{-4}$ (n.d.) [a]	1.70402	12.05
TL2	top	5.3706	-0.8	$3.173 \cdot 10^{-5}$	1.12154	12.23
	bottom	4.6739		< $2.152 \cdot 10^{-4}$ (n.d.)	1.67665	11.92
TL3	top	6.4225	-0.4	$2.641 \cdot 10^{-5}$	1.12409	12.17
	bottom	3.6306		< $2.152 \cdot 10^{-4}$ (n.d.)	1.62119	11.94
TL4	top	8.3735	-0.8	$2.048 \cdot 10^{-5}$	1.13335	12.06
	bottom	1.5948		< $2.152 \cdot 10^{-4}$	1.53810	-
Amoxicillin						
TL1	top	4.6105	-1.1	$5.186 \cdot 10^{-4}$	1.11541	12.03
	bottom	5.4295		< $1.249 \cdot 10^{-4}$ (n.d.)	1.64431	12.02
TL2	top	5.0048	-0.7	$4.990 \cdot 10^{-4}$	1.11441	12.27
	bottom	4.9643		< $1.249 \cdot 10^{-4}$ (n.d.)	1.65594	12.10
TL3	top	6.1902	-0.9	$4.186 \cdot 10^{-4}$	1.11552	12.13
	bottom	3.8163		< $1.249 \cdot 10^{-4}$ (n.d.)	1.58374	12.14
TL4	top	8.2897	-1.1	$3.166 \cdot 10^{-4}$	1.12605	12.07
	bottom	1.7403		< $1.249 \cdot 10^{-4}$ (n.d.)	1.50115	11.81

Table H1.2. Calculated solute losses (L_S), extraction efficiency (E) intervals, partition coefficients (K) and literature values of tie-line lengths (TLL) for the partition of acetaminophen and amoxicillin in the ATPS {[Ch][Ala] (1) + K_2HPO_4 (2) + water (3)}, at 298.15 K and 0.1 MPa.

Tie-line	Solute losses, L_S / %	Partition coefficient, K	Extraction efficiencies, E / %	Tie-line length, TLL / m%[a]
		Acetaminophen		
TL1	-	> 17 ± 2	97.5 ± 0.5	82.18
TL2	-	> 15 ± 2	96.2 ±0.5	78.04
TL3	-	> 13 ±1	95.6 ±0.5	69.75
TL4	-	> 9.5 ± 0.8	96.2 ±0.5	57.64
		Amoxicillin		
TL1	-	> 4.2 ± 0.3	93.1 ± 0.2	82.18
TL2	-	> 4.0 ± 0.3	93.8 ± 0.2	78.04
TL3	-	> 3.4 ± 0.2	96.8 ± 0.2	69.75
TL4	-	> 2.5 ± 0.2	96.4 ± 0.2	57.64

[a] m% denotes mass percentage.

H.2 {[Ch][Ala] (1) + K_3PO_4 (2) + water (3)}

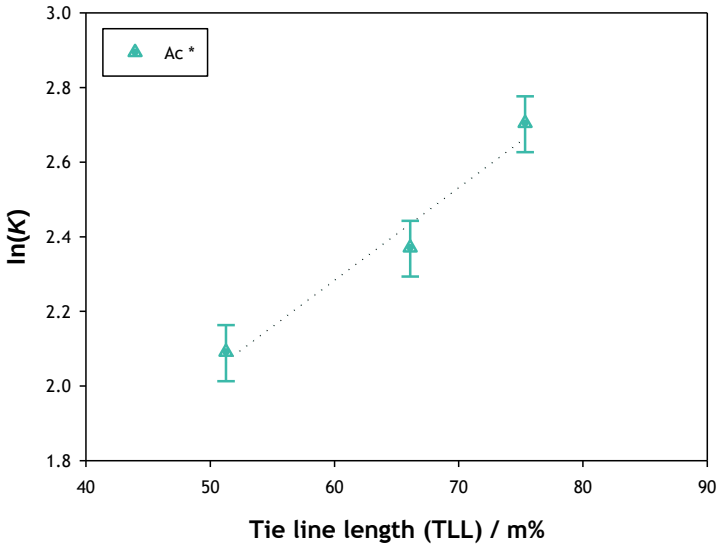

Fig. H2.1. Relation of the tie-line length (TLL) with the natural logarithm of the experimental partition coefficients (K) for acetaminophen (Ac) and linear regression (···), in the system {[Ch][Ala] (1) + K_3PO_4 (2) + water (3)} at 298.15 K and 0.1 MPa.

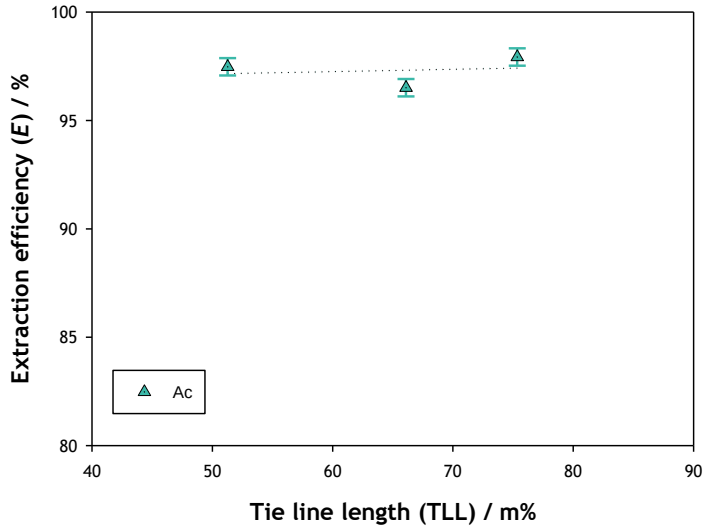

Fig. H2.2. Relation of the tie-line length (TLL) with the extraction efficiencies (E) for acetaminophen (Ac) and linear regression (⋯), in the system {[Ch][Ala] (1) + K_3PO_4 (2) + water (3)} at 298.15 K and 0.1 MPa.

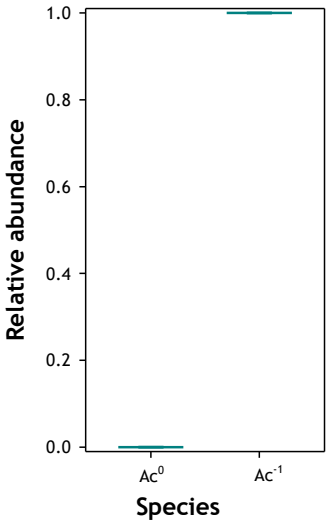

Fig. H2.3. Influence of the tie-line compositions in the relative abundance (fraction) of the stages of the studied pharmaceuticals, in the ATPS {[Ch][Ala] (1) + K_3PO_4 (2) + water (3)} at 298.15 K and 0.1 MPa.
Ac^0 and Ac^{-1} stand for the stages of acetaminophen with electrical charges equal to 0 and −1 e, respectively. e stands for the elementary charge ($1.602 \cdot 10^{-19}$ C).

Table H2.1. Experimental mass of each phase, mass losses in the phase separation (L_m), solute concentration, phase density (ρ) and phase pH for the top and bottom phases in the extraction of acetaminophen and amoxicillin in the ATPS {[Ch][Ala] (1) + K_3PO_4 (2) + water (3)}, at 298.15 K and 0.1 MPa.

Tie-line	Phase	Mass of phase / g	Mass losses, L_m / %	Solute concentration / g·mL^{-1}	Phase density, ρ / g·cm^{-3}	pH
			Acetaminophen			
TL1	top	4.6201	-1.5	$3.299 \cdot 10^{-5}$	1.10866	>14
	bottom	5.2822		$< 2.203 \cdot 10^{-6}$	1.61171	13.99
TL2	top	6.3777	-1.1	$2.363 \cdot 10^{-5}$	1.11068	13.98
	bottom	3.5416		$< 2.203 \cdot 10^{-6}$	1.58138	13.82
TL3	top	8.6042	-1.3	$1.786 \cdot 10^{-5}$	1.12064	13.58
	bottom	1.2520		$< 2.203 \cdot 10^{-6}$	1.49152	-

Table H3.2. Calculated solute losses (L_S), extraction efficiency (E) intervals, partition coefficients (K) and literature values of tie-line lengths (TLL) for the partition of acetaminophen and amoxicillin in the ATPS {[Ch][Gly] (1) + K_2HPO_4 (2) + water (3)}, at 298.15 K and 0.1 MPa.

Tie-line	Solute losses, L_S / %	Partition coefficient, K	Extraction efficiencies, E / %	Tie-line length, TLL / m% [a]
		Acetaminophen		
TL1	-	> 15 ± 2	97.9 ± 0.4	75.348
TL2	-	> 10.7 ± 0.9	96.5 ± 0.4	66.095
TL3	-	> 8.1 ± 0.7	97.5 ± 0.4	51.264

[a] m% denotes mass percentage.

H.3 {[Ch][Gly] (1) + K_2HPO_4 (2) + water (3)}

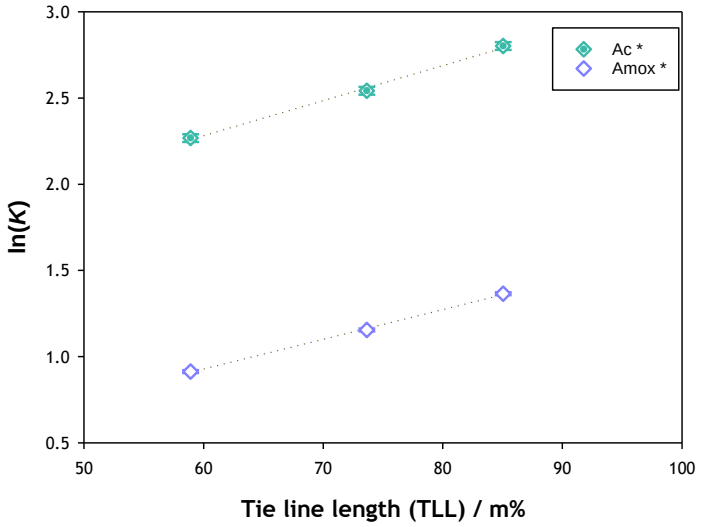

Fig. H3.1. Relation of the tie-line length (TLL) with the natural logarithm of the experimental partition coefficients (K) for acetaminophen (Ac) and amoxicillin (Amox) and respective linear regressions (···), in the system {[Ch][Gly] (1) + K_2HPO_4 (2) + water (3)} at 298.15 K and 0.1 MPa.

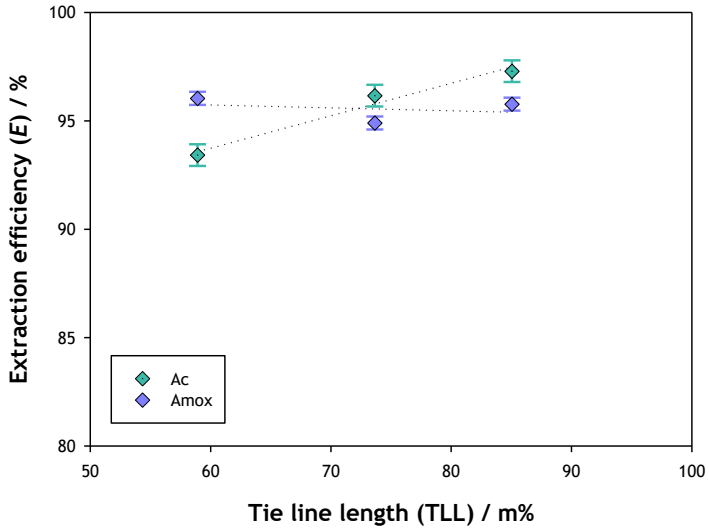

Fig. H3.2. Relation of the tie-line length (TLL) with the extraction efficiencies (E) for acetaminophen (Ac) and amoxicillin (Amox) and respective linear regressions (···), in the system {[Ch][Gly] (1) + K_2HPO_4 (2) + water (3)} at 298.15 K and 0.1 MPa.

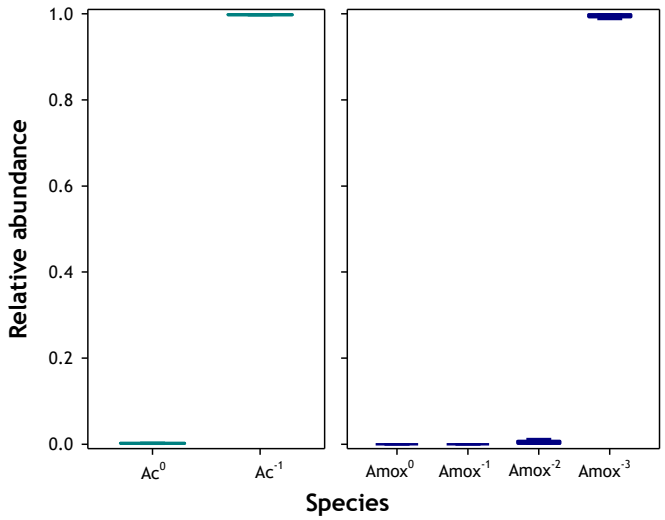

Fig. H3.3. Influence of the tie-line compositions in the relative abundance (fraction) of the stages of the studied pharmaceuticals, in the ATPS {[Ch][Gly] (1) + K_2HPO_4 (2) + water (3)} at 298.15 K and 0.1 MPa.
Ac^0 and Ac^{-1} stand for the stages of acetaminophen with electrical charges equal to 0 and −1 e, respectively. $Amox^0$, $Amox^{-1}$, $Amox^{-2}$ and $Amox^{-3}$ stand for the stages of amoxicillin with electrical charges equal to 0, - 1, -2 and −3 e, respectively. e stands for the elementary charge ($1.602 \cdot 10^{-19}$ C).

Table H3.1. Experimental mass of each phase, mass losses in the phase separation (L_m), solute concentration, phase density (ρ) and phase pH for the top and bottom phases in the extraction of acetaminophen and amoxicillin in the ATPS {[Ch][Gly] (1) + K_2HPO_4 (2) + water (3)} at 298.15 K and 0.1 MPa.

Tie-line	Phase	Mass of phase / g	Mass losses, L_m / %	Solute concentration / g·mL^{-1}	Phase density, ρ / g·cm^{-3}	pH
Acetaminophen						
TL1	top	4.8030	-1.5	$3.631 \cdot 10^{-5}$	1.14154	12.46
	bottom	5.0508		< $2.203 \cdot 10^{-6}$ (n.d.) [a]	1.68256	12.19
TL2	top	6.1877	-1.6	$2.800 \cdot 10^{-5}$	1.14388	12.28
	bottom	3.6638		< $2.203 \cdot 10^{-6}$ (n.d.)	1.61332	12.01
TL3	top	8.0015	-1.0	$1.085 \cdot 10^{-4}$	1.16049	12.18
	bottom	1.8612		< $2.203 \cdot 10^{-6}$ (n.d.)	1.50164	-
Amoxicillin						
TL1	top	4.9009	-0.4	$4.891 \cdot 10^{-4}$	1.13861	11.76
	bottom	5.1312		< $1.249 \cdot 10^{-4}$ (n.d.)	1.70652	12.38
TL2	top	5.9771	-0.7	$3.962 \cdot 10^{-4}$	1.13865	12.32
	bottom	3.9199		< $1.249 \cdot 10^{-4}$ (n.d.)	1.63063	12.05
TL3	top	7.8568	-0.8	$3.113 \cdot 10^{-4}$	1.15364	12.21
	bottom	2.0584		< $1.249 \cdot 10^{-4}$ (n.d.)	1.53901	11.45

[a] (n.d.): not detected.

Table H3.2. Calculated solute losses (L_s), extraction efficiency (E) intervals, partition coefficients (K) and literature values of tie-line lengths (TLL) for the partition of acetaminophen and amoxicillin in the ATPS {[Ch][Gly] (1) + K_2HPO_4 (2) + water (3)}, at 298.15 K and 0.1 MPa.

Tie-line	Solute losses, L_s / %	Partition coefficient, K	Extraction efficiencies, E / %	Tie-line length, TLL / m% [a]
		Acetaminophen		
TL1	-	> 16.5 ± 0.4	97.3 ± 0.5	85.053
TL2	-	> 12.7 ± 0.3	96.2 ± 0.5	73.637
TL3	-	> 9.7 ± 0.3	93.4 ± 0.5	58.908
		Amoxicillin		
TL1	-	> 3.91 ± 0.04	95.8 ± 0.3	85.05
TL2	-	> 3.17 ± 0.03	94.9 ± 0.3	73.64
TL3	-	> 2.49 ± 0.03	96.0 ± 0.3	58.91

[a] m% denotes mass percentage.

H.4 {[Ch][Ser] (1) + K_2HPO_4 (2) + water (3)}

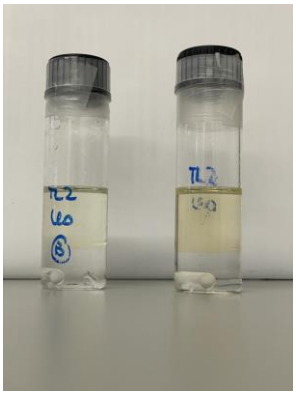

Fig. H4.1. Blank (left) and partition of salicylic acid (right) in the system {[Ch][Ser] (1) + K_2HPO_4 (2) + water (3)}, where a difference in colour of the top phases can be observed.

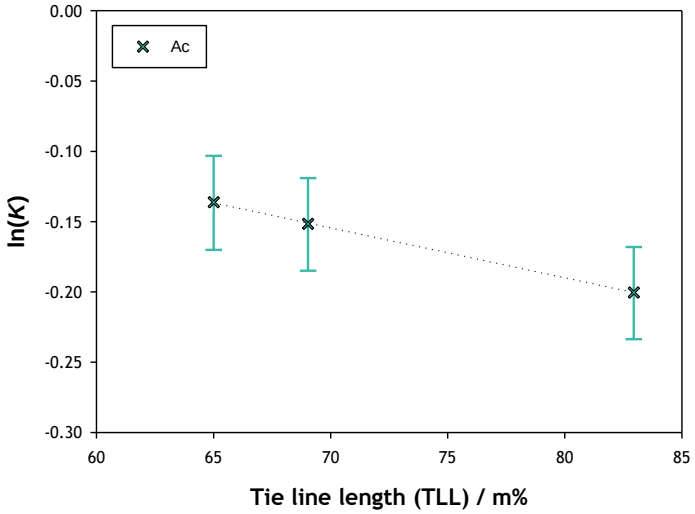

Fig. H4.2. Relation of the tie-line length (TLL) with the natural logarithm of the experimental partition coefficients (K) for acetaminophen (Ac) and linear regression (···), in the system {[Ch][Ser] (1) + K_2HPO_4 (2) + water (3)} at 298.15 K and 0.1 MPa.

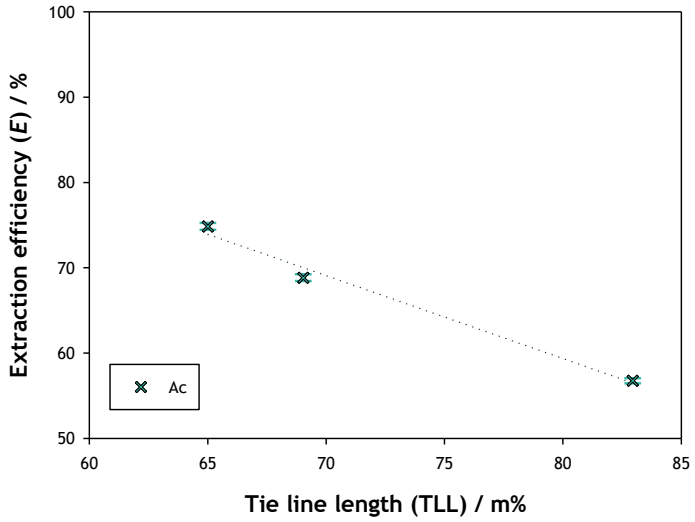

Fig. H4.3. Relation of the tie-line length (TLL) with the extraction efficiencies (E) for acetaminophen (Ac) and linear regression (···), in the system {[Ch][Ser] (1) + K_2HPO_4 (2) + water (3)} at 298.15 K and 0.1 MPa.

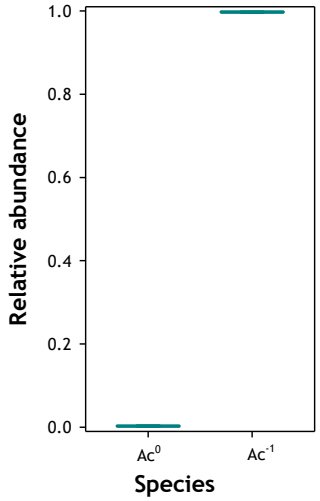

Fig. H4.4. Influence of the tie-line compositions in the relative abundance (fraction) of the stages of the studied pharmaceuticals, in the ATPS {[Ch][Ser] (1) + K_2HPO_4 (2) + water (3)} at 298.15 K and 0.1 MPa.
Ac^0 and Ac^{-1} stand for the stages of acetaminophen with electrical charges equal to 0 and −1 e, respectively, and e stands for the elementary charge ($1.602 \cdot 10^{-19}$ C).

Table H4.1. Experimental mass of each phase, mass losses in the phase separation (L_m), solute concentration, phase density (ρ) and phase pH for the top and bottom phases in the extraction of acetaminophen in the ATPS {[Ch][Ser] (1) + K_2HPO_4 (2) + water (3)} at 298.15 K and 0.1 MPa.

Tie-line	Phase	Mass of phase / g	Mass losses, L_m / %	Solute concentration / g·mL^{-1}	Phase density, ρ / g·cm^{-3}	pH
			Acetaminophen			
TL1	top	5.4722	-0.6	$1.887 \cdot 10^{-5}$	1.14926	12.37
	bottom	4.5524		$2.305 \cdot 10^{-5}$	1.67293	11.92
TL2	top	6.5475	-0.7	$1.914 \cdot 10^{-5}$	1.15576	12.18
	bottom	3.3459		$2.227 \cdot 10^{-5}$	1.59840	12.14
TL3	top	7.1898	-0.9	$1.898 \cdot 10^{-5}$	1.15804	12.17
	bottom	2.7202		$2.175 \cdot 10^{-5}$	1.58217	11.92

Table H4.2. Calculated solute losses (L_s), extraction efficiency (E) intervals, partition coefficients (K) and literature values of tie-line lengths (TLL) for the partition of acetaminophen in the ATPS {[Ch][Ser] (1) + K_2HPO_4 (2) + water (3)}, at 298.15 K and 0.1 MPa.

Tie-line	Solute losses, L_s / %	Partition coefficient, K	Extraction efficiencies, E / %	Tie-line length, TLL / m% [a]
		Acetaminophen		
TL1	-3.6	0.82 ± 0.03	(56.8-60.4) ± 0.3	82.944
TL2	-1.6	0.86 ± 0.03	(68.9-70.4) ± 0.4	69.028
TL3	-1.4	0.87 ± 0.03	(74.9-76.3) ± 0.4	65.004

[a] m% denotes mass percentage.

H.5 {[Ch][Leu] (1) + K_3PO_4 (2) + water (3)}

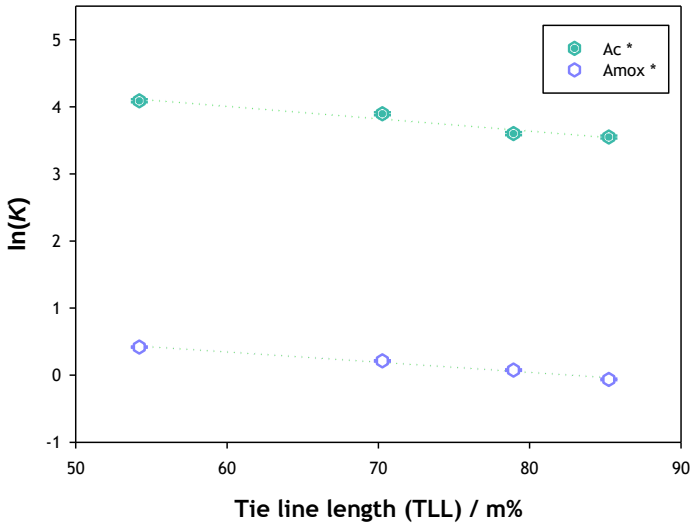

Fig. H5.1. Relation of the tie-line length (TLL) with the natural logarithm of the experimental partition coefficients (K) for acetaminophen (Ac) and amoxicillin (Amox) and respective linear regressions (···), in the system {[Ch][Leu] (1) + K_3PO_4 (2) + water (3)} at 298.15 K and 0.1 MPa.

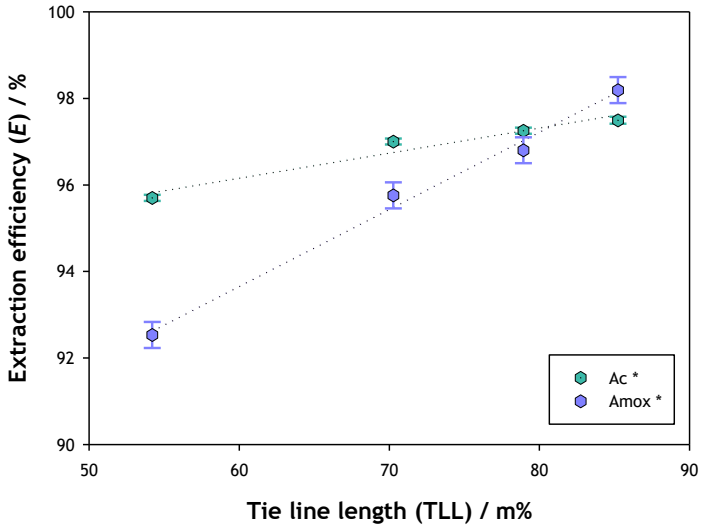

Fig. H5.2. Relation of the tie-line length (TLL) with the extraction efficiencies (E) for acetaminophen (Ac) and amoxicillin (Amox) and respective linear regressions (···), in the system {[Ch][Leu] (1) + K_3PO_4 (2) + water (3)} at 298.15 K and 0.1 MPa.

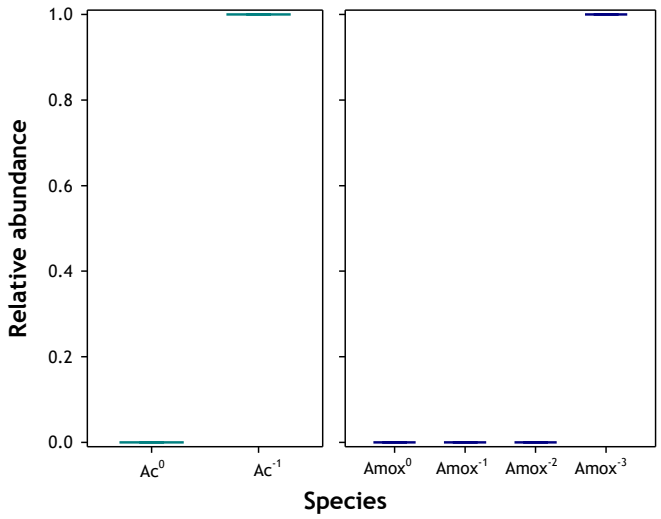

Fig. H5.3. Influence of the tie-line compositions in the relative abundance (fraction) of the stages of the studied pharmaceuticals, in the ATPS {[Ch][Leu] (1) + K_3PO_4 (2) + water (3)} at 298.15 K and 0.1 MPa.
Ac^0 and Ac^{-1} stand for the stages of acetaminophen with electrical charges equal to 0 and −1 e, respectively. $Amox^0$, $Amox^{-1}$, $Amox^{-2}$ and $Amox^{-3}$ stand for the stages of amoxicillin with electrical charges equal to 0, - 1, -2 and −3 e, respectively. e stands for the elementary charge ($1.602 \cdot 10^{-19}$ C).

Table H5.1. Experimental mass of each phase, mass losses in the phase separation (L_m), solute concentration, phase density (ρ) and phase pH for the top and bottom phases in the extraction of acetaminophen and amoxicillin in the ATPS {[Ch][Leu] (1) + K_3PO_4 (2) + water (3)} at 298.15 K and 0.1 MPa.

Tie-line	Phase	Mass of phase / g	Mass losses, L_m / %	Solute concentration / g·mL^{-1}	Phase density, ρ / g·cm^{-3}	pH
Acetaminophen						
TL1	top	3.8361	-1.1	$7.677 \cdot 10^{-5}$	1.06451	>14
	bottom	6.1848		$< 2.203 \cdot 10^{-6}$	1.63231	>14
TL2	top	3.7057	-1.0	$8.705 \cdot 10^{-5}$	1.08744	>14
	bottom	6.3980		$< 2.203 \cdot 10^{-6}$	1.59517	>14
TL3	top	2.7045	-0.9	$1.085 \cdot 10^{-4}$	1.06954	13.86
	bottom	7.2232		$< 2.203 \cdot 10^{-6}$	1.54837	>14
TL4	top	2.3180	-0.5	$1.317 \cdot 10^{-4}$	1.12284	>14
	bottom	7.6425		$< 2.203 \cdot 10^{-6}$	1.49303	>14
Amoxicillin						
TL1	top	3.8046	-1.2	$1.173 \cdot 10^{-4}$	1.06598	>14
	bottom	6.1298		$< 1.249 \cdot 10^{-4}$ (n.d.) [a]	1.63776	>14
TL2	top	3.2581	-1.1	$1.348 \cdot 10^{-4}$	1.06614	>14
	bottom	6.6716		$< 1.249 \cdot 10^{-4}$ (n.d.)	1.59221	>14
TL3	top	2.8121	-0.9	$1.546 \cdot 10^{-4}$	1.06789	>14
	bottom	7.1030		$< 1.249 \cdot 10^{-4}$ (n.d.)	1.54377	>14
TL4	top	2.2375	-1.0	$1.900 \cdot 10^{-4}$	1.07985	>14
	bottom	7.7505		$< 1.249 \cdot 10^{-4}$ (n.d.)	1.48911	>14

[a] (n.d.): not detected.

Table H5.2. Calculated solute losses (L_S), extraction efficiency (E) intervals, partition coefficients (K) and literature values of tie-line lengths (TLL) for the partition of acetaminophen and amoxicillin in the ATPS {[Ch][Leu] (1) + K_3PO_4 (2) + water (3)}, at 298.15 K and 0.1 MPa.

Tie-line	Solute losses, L_S / %	Partition coefficient, K	Extraction efficiencies, E / %	Tie-line length, TLL / m% [a]
		Acetaminophen		
TL1	-	> 34.9 ± 0.8	97.50 ± 0.08	85.23
TL2	-	> 36.7 ± 0.9	97.26 ± 0.07	78.93
TL3	-	> 49 ± 2	97.00 ± 0.07	70.27
TL4	-	> 60 ± 2	95.70 ± 0.07	54.20
		Amoxicillin		
TL1	-	> 0.94 ± 0.02	98.2 ± 0.3	85.23
TL2	-	> 1.08 ± 0.02	96.9 ± 0.3	78.93
TL3	-	> 1.24 ± 0.02	95.8 ± 0.3	70.27
TL4	-	> 1.52 ± 0.02	92.5 ± 0.3	54.20

[a] m% denotes mass percentage.

H.6 {PEG600 (1) + [Ch]Bic (2) + water (3)}

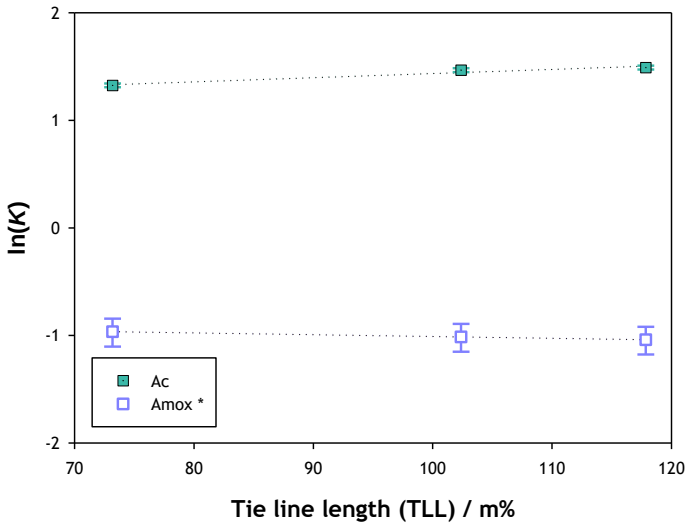

Fig. H6.1. Relation of the tie-line length (TLL) with the natural logarithm of the experimental partition coefficients (K) for acetaminophen (Ac) and amoxicillin (Amox) and respective linear regressions (···), in the system {PEG600 (1) + [Ch]Bic (2) + water (3)} at 298.15 K and 0.1 MPa.

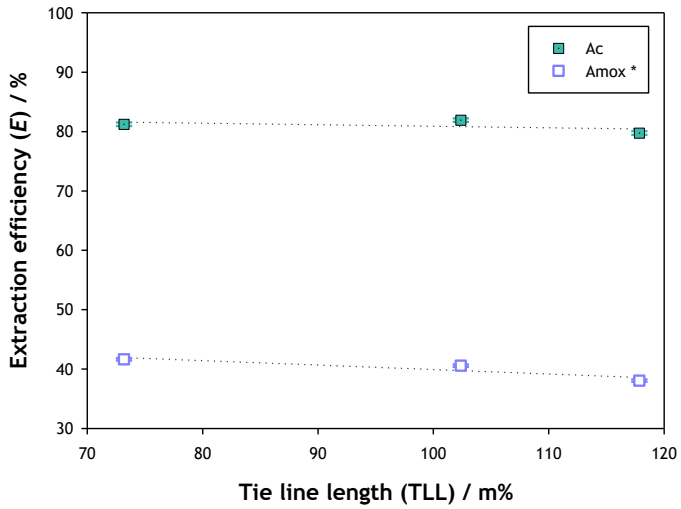

Fig. H6.2. Relation of the tie-line length (TLL) with the extraction efficiencies (E) for acetaminophen (Ac) and amoxicillin (Amox) and respective linear regressions (⋯), in the system {PEG600 (1) + [Ch]Bic (2) + water (3)} at 298.15 K and 0.1 MPa.

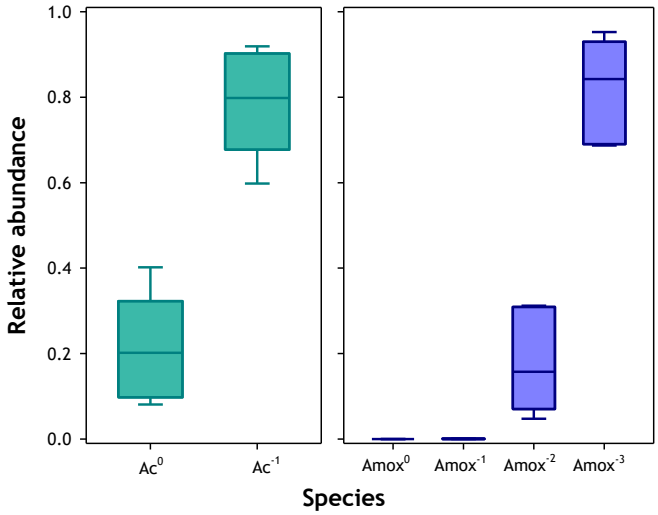

Fig. H6.3. Influence of the tie-line compositions in the relative abundance (fraction) of the stages of the studied pharmaceuticals, in the ATPS {PEG600 (1) + [Ch]Bic (2) + water (3)} at 298.15 K and 0.1 MPa.
Ac^0 and Ac^{-1} stand for the stages of acetaminophen with electrical charges equal to 0 and −1 e, respectively. $Amox^0$, $Amox^{-1}$, $Amox^{-2}$ and $Amox^{-3}$ stand for the stages of amoxicillin with electrical charges equal to 0, - 1, -2 and −3 e, respectively. e stands for the elementary charge ($1.602 \cdot 10^{-19}$ C).

Table H6.1. Experimental mass of each phase, mass losses in the phase separation (L_m), solute concentration, phase density (ρ) and phase pH for the top and bottom phases in the extraction of acetaminophen and amoxicillin in the ATPS {PEG600 (1) + [Ch]Bic (2) + water (3)} at 298.15 K and 0.1 MPa.

Tie-line	Phase	Mass of phase / g	Mass losses, L_m / %	Solute concentration / g·mL^{-1}	Phase density, ρ / g·cm^{-3}	pH
			Acetaminophen			
TL1	top	5.0179	-0.9	$1.270 \cdot 10^{-4}$	1.12406	10.61
	bottom	4.7391		$2.856 \cdot 10^{-5}$	1.15737	10.49
TL2	top	5.5115	-0.7	$1.187 \cdot 10^{-4}$	1.12324	10.28
	bottom	4.4448		$2.737 \cdot 10^{-5}$	1.14378	10.04
TL3	top	5.8431	-0.6	$1.117 \cdot 10^{-4}$	1.12457	9.93
	bottom	4.1231		$2.967 \cdot 10^{-5}$	1.13158	9.72

Table H6.1. Experimental mass of each phase, mass losses in the phase separation (L_m), solute concentration, phase density (ρ) and phase pH for the top and bottom phases in the extraction of acetaminophen and amoxicillin in the ATPS {PEG600 (1) + [Ch]Bic (2) + water (3)} at 298.15 K and 0.1 MPa (cont.).

Tie-line	Phase	Mass of phase / g	Mass losses, L_m / %	Solute concentration / g·mL^{-1}	Phase density, ρ / g·cm^{-3}	pH
Acetaminophen						
TL1	top	5.3608	-1.4	< $1.249 \cdot 10^{-4}$	1.12387	10.83
	bottom	4.5697		$3.536 \cdot 10^{-4}$	1.15823	10.37
TL2	top	5.6892	-0.8	< $1.249 \cdot 10^{-4}$	1.12194	10.61
	bottom	4.3030		$3.445 \cdot 10^{-4}$	1.14338	10.17
TL3	top	5.8527	-1.2	< $1.249 \cdot 10^{-4}$	1.12316	9.88
	bottom	4.1426		$3.281 \cdot 10^{-4}$	1.13128	9.87

Table H6.2. Calculated solute losses (L_s), extraction efficiency (E) intervals, partition coefficients (K) and literature values of tie-line lengths (TLL) for the partition of acetaminophen and amoxicillin in the ATPS {PEG600 (1) + [Ch]Bic (2) + water (3)}, at 298.15 K and 0.1 MPa.

Tie-line	Solute losses, L_s / %	Partition coefficient, K	Extraction efficiencies, E / %	Tie-line length, TLL / m% [a]
Acetaminophen				
TL1	-3.8	4.44 ± 0.08	(79.8–83.5) ± 0.3	117.85
TL2	-3.1	4.34 ± 0.09	(81.9–85.0) ± 0.3	102.38
TL3	-3.7	3.77 ± 0.07	(81.2–84.9) ± 0.3	73.18
Amoxicillin				
TL1	-	< 0.35 ± 0.05	< 38.1 ± 0.2	117.85
TL2	-	< 0.36 ± 0.05	< 40.6 ± 0.2	102.38
TL3	-	< 0.38 ± 0.05	< 41.7 ± 0.2	73.18

[a] m% denotes mass percentage.

H.7 {EL (1) + [Ch]Bit (2) + water (3)}

Table H7.1. Experimental mass of each phase, mass losses in the phase separation (L_m), solute concentration, phase density (ρ) and phase pH for the top and bottom phases in the extraction of acetaminophen, amoxicillin and salicylic acid in the ATPS {EL (1) + [Ch]Bit (2) + water (3)}, at 298.15 K and 0.1 MPa.

Tie-line	Phase	Mass of phase / g	Mass losses, L_m / %	Solute concentration / g·mL^{-1}	Phase density, ρ / g·cm^{-3}	pH
Acetaminophen						
TL1	top	7.8125	-1.0	$5.031 \cdot 10^{-5}$	1.04565	4.92
	bottom	2.1214		$2.987 \cdot 10^{-5}$	1.18948	3.81
TL2	top	5.4209	-0.7	$5.993 \cdot 10^{-5}$	1.04972	4.76
	bottom	4.3617		$2.985 \cdot 10^{-5}$	1.16867	3.98
TL3	top	2.1392	-0.6	$8.476 \cdot 10^{-5}$	1.05093	4.68
	bottom	7.8248		$3.790 \cdot 10^{-5}$	1.14934	4.06

Table H7.1. Experimental mass of each phase, mass losses in the phase separation (L_m), solute concentration, phase density (ρ) and phase pH for the top and bottom phases in the extraction of acetaminophen, amoxicillin and salicylic acid in the ATPS {EL (1) + [Ch]Bit (2) + water (3)}, at 298.15 K and 0.1 MPa (cont.).

Tie-line	Phase	Mass of phase / g	Mass losses, L_m / %	Solute concentration / g·mL^{-1}	Phase density, ρ / g·cm^{-3}	pH
Amoxicillin						
TL1	top	7.8186	-0.9	< 5.635·10^{-5}	1.04347	4.81
	bottom	2.1025		4.969·10^{-4}	1.18177	4.65
TL2	top	5.5814	-1.0	< 5.635·10^{-5}	1.04842	4.59
	bottom	4.2201		2.691·10^{-4}	1.16394	3.98
TL3	top	2.0776	-1.0	< 5.635·10^{-5}	1.05327	4.37
	bottom	7.8334		1.522·10^{-4}	1.14821	3.93
Salicylic acid						
TL1	top	7.7359	-0.4	1.605·10^{-4}	1.04473	4.74
	bottom	2.2264		1.798·10^{-5}	1.18352	4.24
TL2	top	5.4863	-0.9	2.052·10^{-4}	1.04831	4.62
	bottom	4.4861		3.226·10^{-5}	1.16745	4.19
TL3	top	2.0441	-1.0	3.833·10^{-4}	1.05367	4.46
	bottom	7.9252		6.830·10^{-5}	1.14836	4.33

Table H7.2. Calculated solute losses (L_s), extraction efficiency (E) intervals, partition coefficients (K) and values of tie-line lengths (TLL) for the partition of acetaminophen, amoxicillin and salicylic acid in the ATPS {EL (1) + [Ch]Bit (2) + water (3)}, at 298.15 K and 0.1 MPa.

Tie-line	Solute losses, L_s / %	Partition coefficient, K	Extraction efficiencies, E / %	Tie-line length, TLL / m% [a]
Acetaminophen				
TL1	-3.6	1.7 ± 0.1	(84.5–88.0) ± 0.2	115.08
TL2	-4.9	2.0 ± 0.1	(70.0–74.8) ± 0.2	107.11
TL3	-2.8	2.2 ± 0.1	(39.09–41.7) ± 0.1	101.25
Amoxicillin				
TL1	-	< 0.11 ± 0.03	< 35.27 ± 0.04	115.08
TL2	-	< 0.21 ± 0.05	< 25.81 ± 0.03	107.11
TL3	-	< 0.37 ± 0.09	< 9.60 ± 0.02	101.25
Salicylic acid				
TL1	-2.2	9 ± 2	(95.1–97.3) ± 0.1	115.08
TL2	-3.9	6.4 ± 0.7	(86.13–90.06) ± 0.09	107.11
TL3	-2.9	5.6 ± 0.3	(59.42–62.33) ± 0.07	101.25

[a] m% denotes mass percentage.